MECHANISTIC KINETIC MODELING OF THE HYDROCRACKING OF COMPLEX FEEDSTOCKS

A Dissertation

by

HANS KUMAR

Submitted to the Office of Graduate Studies of
Texas A&M University
in partial fulfillment of the requirements for the degree of

DOCTOR OF PHILOSOPHY

December 2006

Major Subject: Chemical Engineering

MECHANISTIC KINETIC MODELING OF THE HYDROCRACKING OF COMPLEX FEEDSTOCKS

A Dissertation

by

HANS KUMAR

Submitted to the Office of Graduate Studies of
Texas A&M University
in partial fulfillment of the requirements for the degree of

DOCTOR OF PHILOSOPHY

Approved by:

Co-Chairs of Committee,	Gilbert F. Froment
	Rayford G. Anthony
Committee Members,	Perla B. Balbuena
	Abraham Clearfield
Head of Department,	N. K. Anand

December 2006

Major Subject: Chemical Engineering

ABSTRACT

Mechanistic Kinetic Modeling of the Hydrocracking of Complex Feedstocks.

(December 2006)

Hans Kumar, B.E., Indian Institute of Technology, Roorkee;

M.S., Texas A&M University, College Station.

Co-Chairs of Advisory Committee: Dr. Gilbert F. Froment
Dr. Rayford G. Anthony

Two separate mechanistic kinetic models have been developed for the hydrocracking of complex feedstocks. The first model is targeted for the hydrocracking of vacuum gas oil. The second one addresses specifically the hydrocracking of long-chain paraffins, but at a more fundamental level as compared to the first one. Both models are based on an exhaustive computer generated reaction network of elementary steps.

In the first model, the dehydrogenation/hydrogenation steps occurring on the metal sites to generate/consume the reactive olefinic intermediates are assumed to be very fast so that the acid site steps are considered as the rate determining steps. The frequency factors for acid site steps are modeled using the single-event concept and the activation energies based on the nature of the reactant and product carbenium ions.

This model utilizes a detailed composition of the vacuum gas oil characterized by 16 different molecular classes up to carbon number 40. These classes are divided into 45 subclasses by distinguishing the isomers of a class according to the number of methyl branches. The kinetic model is plugged into an adiabatic multi-bed trickle flow reactor model. The model contains 33 feedstock and temperature independent parameters which have been estimated from the experimental data.

The model has been used to study the effect of the operating conditions on the yield and composition of various products. A sensitivity analysis of the distribution of isomers of a

class among its different subclasses has been performed showing that the total conversion increases when the content of isomers with a higher degree of branching is increased in the feed.

In the second model, the dehydrogenation/hydrogenation steps on the metal sites are also assumed to be rate determining. The rate coefficients for the dehydrogenation steps are modeled depending on the nature of the carbon atoms forming the double bond. The frequency factors for the acid site steps are modeled using the single-event concept. A more rigorous approach has been selected to model the activation energies of the acid site steps by implementing the Evans-Polanyi relationship. The 14 model parameters, which are independent of the temperature and feedstock composition, have been estimated from the experimental data. The model elucidates the effect of the relative metal/acid activity of the catalyst on the isomerization/cracking selectivities and on the carbon number distribution of the products.

DEDICATION

To my parents

ACKNOWLEDGMENTS

I would like to express my sincere gratitude to Dr. Gilbert F. Froment and Dr. Rayford G. Anthony for serving as the co-chairs of my committee and for their continued guidance and support in this research. The scientific discussions with Dr. Froment have always been very insightful and I will always be indebted to him for all the knowledge he shared with me. His prompt responses to all my email queries are truly appreciated. Dr. Anthony always assisted me with all the technical and non-technical issues during this research. His encouragement and interest led this project to be completed successfully in a timely manner. This research would not have been completed without the generosity of Dr. Anthony providing financial support from the C. D. Holland Professorship for this project. I am truly thankful to my advisors for the trust they showed in my capabilities to complete this research.

I would also like to thank Dr. Perla Balbuena and Dr. Abraham Clearfield for being on my committee and for their time, efforts and ideas they contributed during our meetings. I am also grateful to Dr. R. E. Galiasso for various stimulating discussions and knowledge.

My special thanks go to my friend and mentor, Dr. J. Govindhakannan. I had a wonderful time with him discussing different aspects of research and life. His previous contribution in this field is highly appreciated.

I am also grateful to the faculty of the Department of Chemical Engineering for being extremely cooperative and friendly at all times during my stay at Texas A&M University. I would especially like to thank Dr. K. R. Hall, Dr. D. M. Ford, Dr. D. F. Shantz and Dr. M. El- Halwagi. The help that I received from our wonderful staff, especially Towanna Hubacek, Missy Newton, Valerie Green, Ninette Portales, Barbara Prout and Jeff Polasek, is simply unforgettable.

Many thanks to my friends and my group members for making my research at Texas A&M University a pleasant and exciting experience. I am fortunate to have good friends

like Arnab, Faisal, Amit, Vipin, Srini, Ashwini, Manish, Sanjay, Jyoti, Nishant, Hemendra, Greg and Nitin who were always there for me in good and bad times.

Finally, I would like to express my warmest regards to my parents and family members for their unconditional love and support without which I could have never completed this dissertation.

TABLE OF CONTENTS

Page

CHAPTER Page

CHAPTER Page

LIST OF TABLES

TABLE Page

LIST OF FIGURES

FIGURE Page

FIGURE Page

FIGURE Page

FIGURE Page

CHAPTER I

INTRODUCTION

Hydrocracking at high hydrogen pressures is commonly used to upgrade the heavier fractions like vacuum gas oils (VGO) obtained from crude oil distillation. Hydrocracking of residues and several products obtained from other refining processes, i.e., coker gas oil, deasphalted oil, fluid catalytic cracking (FCC) cycle oils and decant oils etc. is also carried out for getting high value products. Hydrocracking is also applied in the production of superior quality middle distillates from Fischer-Tropsch waxes and in the production of lube oil bases from middle distillates by removing long chain paraffins (dewaxing). Very heavy hydrocarbons such as those extracted from tar sands and shale can also be upgraded by hydrocracking.

A typical VGO feedstock consists of paraffinic, naphthenic, aromatic and naphtheno-aromatic species, along with heteroatom impurities like sulfur, nitrogen, oxygen compounds. Significant amount of metals may also be present. Based on the atmospheric equivalent boiling points[1] (AEBP), vacuum gas oils (VGO) can be classified as light vacuum gas oils (LVGO) and heavy vacuum gas oils (HVGO). LVGOs have a boiling range of about 345-430 ^{o}C. Typically, saturates in this range account for 40-60 wt% of the fraction, consisting mainly of paraffins, and alkylnaphthenes with 1-4 rings. They have carbon numbers between 15 and 30. The aromatic content of LVGO may be as high as 50 wt%. Most compound types in this fraction are alkylbenzenes, naphthalenes and phenanthrenes, with or without naphthenic rings. Sulfur compounds like benzo-, dibenzo-, naphthobenzo-thiophenes and other derivatives are also present. The elemental sulfur, oxygen and nitrogen content is of the order 3 wt%, 0.2 wt% and 1500 ppm respectively[1].

This dissertation follows the style of *Industrial & Engineering Chemistry Research*.

The polar compounds in LVGOs may range from 1-10 wt%, consisting of compounds containing nitrogen, oxygen, or both. Snyder[2] identified the polar compounds in the LVGO range of a California crude oil and reported 3.4 wt% carbazoles, 0.6% indoles, 0.5% benzocarbazoles, 0.66% pyridines, 1.74% quonolines, 0.26% benzoquonolines, and 1.2% of pyridones etc. Furthermore, they found 1.74% aliphatic carboxylic acids, 0.97% phenols, 1.2% benzoaromatic and higher aromatic furanes, and 0.7% aliphatic esters, ketones, and other carbonyl derivatives. The atmospheric equivalent boiling range of HVGO is about 430–540 ^{o}C with a carbon number ranging from 20 to 50. Compared to LVGO there is a dramatic decrease in the amount of saturates and a corresponding increase in aromatics and polar compounds. Most aromatic and naphthenic molecules in this range primarily contain 1-4 rings. Compounds with more than 4 rings are present at much lower concentrations. Elemental sulfur, oxygen and nitrogen content can be about 4 wt%, 0.3 wt% and 2000 ppm respectively. Snyder[2] identified polar compounds in the HVGO fraction of a California crude oil with 0.75 wt% indoles, 4.1% carbazoles, 1.3% benzocarbazoles, 1.3% pyridines, 2.0% quonolines, 1.6% benzoquonolines, 2.0% pyridones, 0.4% azaindoles, 0.85% dibenzofuranes, 0.8% benzonaphthofuranes, 0.15% dinaphthofuranes, 0.08% dihydrobenzofuranes, 1.35% phenols, 1.35% aliphatic carboxylic acids, and 2.3% aliphatic esters, ketones, and other carbonyl derivatives. Significant differences can be found in the compositional analysis of different VGOs depending upon the source or the origin of the feedstock.

Typically the products obtained from fractionation of the hydrocracker effluent are defined based on their boiling point range as follows: light ends (C_4^-), light naphtha (C_5 – 80 ^{o}C), heavy naphtha (80 ^{o}C – 150 ^{o}C), jet fuel/kerosene (150 ^{o}C – 290 ^{o}C), diesel fuel (290 ^{o}C – 370 ^{o}C) and the unconverted fractionator bottoms (370 ^{o}C +). The products obtained from hydrocracking are generally of high quality. The light naphtha with a research octane number between 78 and 85 can be used for the blending stock in the gasoline pool. The heavy naphtha is a good quality reformer feedstock for the production of high octane gasoline. The jet fuel obtained is low in aromatics and has a high smoke point. The diesel fraction has a relatively high cetane number and very low

sulfur content. High quality lube oils and FCC and thermal cracking feedstocks are also obtained from the hydrocracking process[3].

Environmental concern in recent years has set the agenda for the development of hydrocracking and hydrotreatment processes to get high quality fuels with low aromatics, sulfur and nitrogen content. Global hydrocracking capacity has increased consistently over the last two decades[3] and is expected to increase further, given the ability of this process to upgrade heavier feedstocks. Significant developments have been made in the hydrocracking process technologies like single-stage once through, single-stage with recycle, two-stage process, two-stage with recycle etc. in an effort to gain higher flexibility in the unit's operation and maximize the financial returns. At the same time, different catalysts have been commercialized for processing the feedstocks of vastly different compositions under less severe operating conditions. The development of the fundamental kinetic models, on the other hand, for this kind of complex conversion processes had been rather limited, with most of the kinetic models still based on a very simplified lumped scheme for describing the product distribution. Therefore, development of reliable mechanistic kinetic models for the hydrocracking process is an important activity from a commercial as well as a research viewpoint.[5] The design and optimization of the hydrocracking units require a detailed kinetic model that can take into account the complexity of the feedstock while following the rules of the underlying carbenium ion chemistry.[6] The use of comprehensive process models with an accurate representation of hydrocracking kinetics at the elementary step level can be used to reduce expensive experimentation in pilot plants. This kind of mathematical models can be used for process design to predict the detailed product distribution and optimum operating conditions for a range of feedstocks as well as for simulation and optimization of the existing units.

1.1. Hydrocracking Process Description

Many different flow schemes have been developed for the hydrocracking process so that various feedstocks can be processed to produce a full range of products. All of the

processes are vendor specific with respect to the reactor design and catalyst selection. The three major schemes for hydrocracking processes can be classified as follows:

(a) Single-stage recycle hydrocracking

(b) Two-stage recycle hydrocracking

(c) Once through hydrocracking

In general, the commercial hydrocracking plants are operated at the following conditions:[3]

Catalyst bed temperature	300-450^{o} C
Pressure	85-200 bars
Liquid hourly space velocity	0.5-2.5 hr^{-1}
H_2/HC ratio	10-30 mole/mole (~3,000-10,000 Std. ft^3/barrel)

Due to high hydrogen partial pressures and the use of dual function catalysts, the rate of catalyst coking and deactivation is very low, resulting in on-stream cycle lengths of several years.

The typical feedstocks used in hydrocracking process contain sulfur, nitrogen, and in the case of resid feedstock, metals such as nickel and vanadium. Because such compounds have a deleterious effect on hydrocracking catalysts, the feedstock typically requires hydrotreatment prior to contact with the hydrocracking catalyst. For this reason, most of the hydrocracking processes consist of two stages involving both hydrotreatment and hydrocracking.

Figure 1-1 shows the simplified flow diagram for a two stage hydrocracking process with recycle. The vacuum gas oil is sent to the first stage of the hydrocracker and is severely hydrotreated. Most of the sulfur and nitrogen compounds are removed from the oil and many of the aromatics are saturated. In addition, significant conversion to light products occurs in the first stage. The liquid products from the first stage are sent to a common fractionation section. To prevent overcracking, lighter products are removed by

distillation. The unconverted oil from the bottom of the fractionator is routed to the second stage reactor section. The second reaction stage saturates almost all the aromatics and cracks the oil feed to light products. Due to the saturation of aromatics, the second stage produces excellent quality products. The liquid product from the second stage is sent to the common fractionator where light products are distilled. The second stage operates in a recycle to extinction mode with per-pass conversions ranging from 50 to 80%. The following products are obtained from fractionation: light ends, light naphtha, heavy naphtha, jet fuel/kerosene, and diesel fuel. The fractionator bottoms containing the unconverted feed is recycled to the second stage reactor so that it can be converted into commercial products.

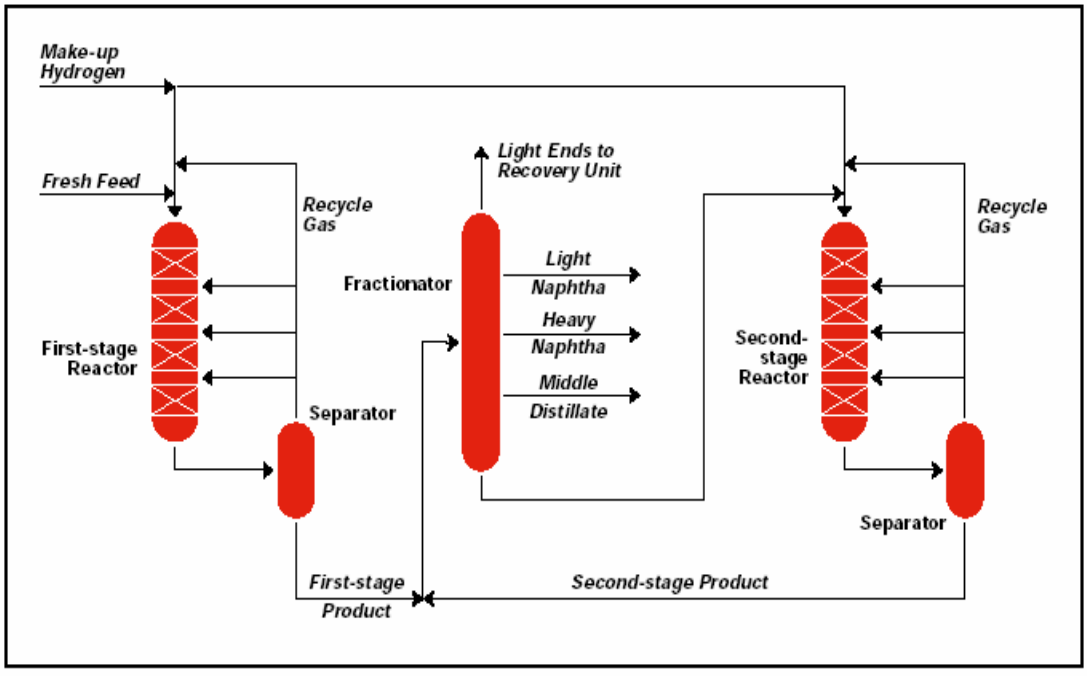

Figure 1-1. Simplified process flow diagram of a two stage hydrocracker. (source: www.abb.com).

The overhead liquid and vapor from the hydrocracker fractionator is further processed in a light ends recovery unit where fuel gas, liquefied petroleum gas (LPG) and, naphtha are separated. The hydrogen supplied to the reactor sections of the hydrocracker comes from steam reformers. The hydrogen is compressed in stages until it reaches system pressure of the reactor sections.

The catalyst in the first reactor is designed to eliminate the hetero compounds in the feedstock and to convert the organic sulfur and nitrogen to hydrogen sulfide and ammonia, respectively. Such catalysts typically comprise sulfided molybdenum or tungsten and nickel or cobalt on an alumina support. The deleterious effect of H_2S and NH_3 on hydrocracking catalyst is considerably lower than those of the corresponding organic hetero compounds. The hydrotreating catalyst also facilitates the hydrogenation of aromatics.

The hydrocracking catalyst in the second stage is designed to optimize the yields and quality of the desired products. Various reactions such as hydrogenation, dehydrogenation, isomerization, cracking, alkylation, dealkylation, etc. predominately take place in the second stage reactor. Hydrogenation reactions are highly exothermic, whereas the cracking reactions are endothermic. The amount of heat liberated in the hydrogenation reactions is greater than the heat required for the endothermic cracking reactions. The surplus heat released causes the reactor temperature to increase, thereby accelerating the reaction rate. Cold hydrogen is injected between the reactor beds as a quench to control the reactor temperature profile.

The severity of the hydrocracking operation is measured by the degree of conversion of the feed to the lighter products. Conversion is defined as the volume percent of the feed that disappears to form the products boiling below the desired product end point. A given percent conversion at a low product endpoint represents a more severe operation than does the same percent conversion at a higher product endpoint.

1.2. Literature Survey

To study the conversion of complex feedstocks through processes like hydrocracking and catalytic cracking, most efforts have focused on the development of lumped kinetic models in which the feedstock is divided into several lumps based on the boiling point range. A simplified reaction network between these lumps is set up and the rate coefficients for the global conversion of lumps are estimated from the experimental data. For example, the kinetic model of Weekman and Nace[4] for fluidized catalytic cracking assumes that the feedstock charge is converted into the gasoline boiling fraction and the remaining fraction by the following two equations,

$$C_1 \xrightarrow{k_1} a_1 C_2 + a_2 C_3 \tag{1.1}$$

$$C_2 \xrightarrow{k_2} C_3 \tag{1.2}$$

In the above equations, C_1 represents the gas oil charged, C_2 represents the C_5-410 ^oF gasoline fraction and, C_3 represents the butanes, dry gas and, coke. The coefficients a_1 and a_2 represent the mass of C_2 and C_3 produced per mass of C_1 converted, respectively. A more detailed lumped model for FCC comprising 10 lumps was developed by Jacob et al[5]. Stangeland[6] considered the feedstock as a series of 50 ^oF boiling range cuts assuming that each heavier cut hydrocracks via a first order reaction to form a series of lighter cuts. To achieve higher accuracy in the product yields predicted by the models, more and more lumps were introduced by various researchers. Increasing the number of lumps also leads to the introduction of more parameters in the kinetic model. The major fundamental limitation of the lumped kinetic models is that the kinetic parameters depend on the composition of the feedstock. Therefore, with every different feedstock the kinetic model needs to be refitted and new sets of parameters have to be estimated.

Another approach for modeling the kinetics of the conversion of such complex feedstocks is based on the notion of continuum lumping in which the reaction mixture is considered to be a continuous mixture with respect to the feed properties like boiling point and molecular weight. A hydrocracking model based on this approach has been developed by Laxminarasimhan et al.[7] in which the true boiling point of the mixture is

used as the characterization parameter. The rate constant of hydrocracking is assumed to be a monotonic function of the true boiling point. A yield distribution function was formulated from the hydrocracking data of model compounds. The resulting integro-differential equations were solved numerically to obtain the yields of various fractions as a function of reactor residence time. Similar to the discrete lumping, this approach is also unable to capture the fundamental chemistry of the process providing thrust to the development of mechanistic models.

Mechanistic models are based more closely on the chemistry of the process. Several approaches have been developed to build the mechanistic models for catalytic and thermal conversion of complex feedstocks. For example, Liguras et al.[8, 9] represented the feedstock using hundreds of pseudo-components whose composition was calculated from MS and C-NMR spectroscopy and developed the kinetic model for catalytic cracking based on the nature of carbon centers in the pseudo-components.

Quann et al.[10] constructed the molecules by incrementing the structural units present in the hydrocarbon molecules and expressed them using a vector notation which was used to generate the reaction network. The reaction network is based on various reaction rules selected according to the chemistry of the process. This approach is called the structural oriented lumping (SOL).

Froment and co-workers[11, 12] developed a mechanistic kinetic modeling approach starting from the elementary steps of carbenium ion chemistry. This approach was named as "single event" approach. Baltanas et al.[11] generated a network of elementary steps involving carbenium ions using a computer algorithm based on the approach devised by Clymans et al.[13] and Hillewaert et al.[14]. Vynckier et al.[12] applied the single event approach to complex feedstocks by introducing the concept of lumping coefficients. Feng et al.[15] used single event to model the catalytic cracking of paraffins on a RE-Y zeolite catalyst. Svoboda et al.[16] determined the single event rate parameters for the hydrocracking of n-octane. Martens et al.[17] applied single event kinetics for the hydrocracking of C_8-C_{12} paraffins on Pt/USY zeolites. Park and Froment[18] applied the single event kinetics along with Evans-Polanyi relationship for modeling the methanol to

olefin process over HZSM-5 catalyst, and Martinis and Froment[19] to the alkylation of isobutane with butenes.

CHAPTER II

HYDROCRACKING CHEMISTRY AND REACTION NETWORK GENERATION

2.1. Hydrocracking Catalyst

Hydrocracking is carried out on dual-function catalysts having a cracking function and a hydrogenation-dehydrogenation function. The cracking function is provided by an acidic support, whereas the hydrogenation-dehydrogenation function is provided by metals. The different kinds of acidic support can be (i) amorphous oxides e.g., silica-alumina, (ii) crystalline zeolites, mostly ultra stable Y-zeolites and a binder e.g., alumina, or (iii) hybrid supports having a mixture of zeolite and amorphous oxides. Cracking and isomerization steps take place on the acidic support. The metal can be noble metals (palladium, platinum) or nonnoble metal sulfides from group VIA (molybdenum, tungsten) and group VIIIA (cobalt, nickel). These metals produce the reactive olefins for the cracking and isomerization steps and catalyze the hydrogenation of the aromatics in the feedstock as well as heteroatom removal. The ratio between the catalyst's acidic and metal activities is adjusted in order to optimize the activity and selectivity.[3]

2.2. Reaction Mechanism

The well known bifunctional mechanism of hydrocracking reactions proceeding through olefinic intermediates is widely accepted for describing the product distribution. The model developed in this work is primarily applicable to the hydrocracking of VGO on zeolite catalysts ignoring the activity of the binder. The feed molecules are sorbed into the pores of zeolites from the surrounding fluid phase, which can be gas or liquid depending upon the reactor operating conditions. Different reaction pathways are available for the paraffinic, naphthenic and aromatic species. The sorbed paraffinic and naphthenic species are chemisorbed on the metal sites and are dehydrogenated into the corresponding olefinic species which migrate from the metal sites to the nearby Brønsted acidic sites and are protonated into paraffinic and naphthenic carbenium ions. The

naphthenic species can dehydrogenate either in the side chain or inside the ring to produce the corresponding olefins. The olefinic species sorbed in the zeolite pores are assumed to be in pseudo-equilibrium with the chemisorbed olefins on the metal sites as well as with the surface carbenium ions on the acid sites. The pseudo-equilibrium of sorbed olefins between the metal sites as well as with the carbenium ions is modeled using the Langmuir adsorption isotherm.

The paraffinic carbenium ions thus produced are isomerized by hydride shift (HS), methyl shift (MS) and protonatedcyclopropane (PCP) steps. It can be noticed from Figure 2-1 that the HS and MS steps do not change the degree of branching in the carbenium ions whereas the PCP steps do. The isomerized carbenium ions with a higher degree of branching crack at the carbon-carbon bond in β-position with respect to the carbon atom carrying the positive charge, yielding a smaller carbenium ion and an olefin. The resulting carbenium ion can further crack or deprotonate on the acid sites to produce an olefin. Similarly, the olefin can be protonated to yield another carbenium ion, or alternatively can be hydrogenated on the metal sites to produce a paraffin. The probability of undergoing either protonation or hydrogenation depends on the relative strength of the acid/metal functions of the catalyst. Cyclization of paraffinic species into ring species is also encountered. The important elementary steps that occur in the paraffinic species are shown in Figure 2-1.

The naphthenic carbenium ions can undergo all the elementary steps mentioned above in their alkyl side chain. Apart from that, the hydride shift and methyl shift steps can also occur in the naphthenic rings. The PCP steps involving the ring carbon atoms result in the expansion or contraction of the ring size. It has been shown that the hydrocracking of cyclohexane proceeds through ring contraction forming methylcyclopentane which undergoes the ring opening reaction. Depending on the location of the positive charge, the naphthenic carbenium ions can undergo exocyclic β-scission producing a naphthenic olefin and severing the long alkyl chain as a paraffinic carbenium ion, or can transform through endocyclic β-scission scission producing an unsaturated carbenium ion by ring opening. One of the main differences between the β-scission in the paraffinic chain and

β-scission in the ring is that the latter is considerably more difficult than the former. Several explanations have been presented for this behavior. According to Eagan and Langlois[20], carbenium ions formed by endocyclic β-scission of a naphthenic carbenium ions have a high tendency to return to the cyclic form because the closeness of the double bond and positively charged carbon atom provides a favorable configuration for this cyclization. Studies on the hydrocracking of multi-ring naphthenes are mostly limited up to two rings and have shown that the naphthenic rings open in a sequential manner. The important steps in the hydrocracking of mononaphthenes are shown in Figure 2-2.

Figure 2-3 shows the different possibilities that can occur in the hydrocracking of a tetra-naphthene during hydrocracking. For simplicity, the positive charge has been omitted from the reaction network.

Hydroconversion of alkyl aromatics proceeds either through the typical acid-site elementary steps in their side chain or through the saturation of the aromatic ring and subsequent isomerization and cracking in the resulting naphthenic ring. Dealkylation of the benzyl carbenium ion formed by the direct protonation of the aromatic ring on the acid sites is an important step in the hydrocracking of aromatics. Figure 2-4 shows the important steps in the hydroconversion of mono-ring aromatics. Hydrocracking of polynuclear aromatics is quite complex and involves sequential hydrogenation of the aromatic rings along with parallel or subsequent isomerization, cracking and ring opening reactions as shown in Figure 2-5.

To summarize, the following types of elementary steps and reactions are considered in the current VGO hydrocracking model:

1. Dehydrogenation into olefinic species (preceding the protonation step)
2. Protonation/deprotonation
3. Hydride shift (HS) in the side chain and in the rings
4. Methyl shift (MS) in the side chain and in the rings

5. Protonated cyclopropane (PCP) in the side chain
6. Ring contraction/expansion through PCP in the ring
7. Acyclic β-scission (scission in the side chain)
8. Exocyclic β-scission (scission between ring and side chain)
9. Endocyclic β-scission or ring opening (scission in the ring)
10. Cyclization (reverse of endocyclic β-scission)
11. Dealkylation of aromatics
12. Hydrogenation of aromatics to naphthenes (and the reverse dehydrogenation)

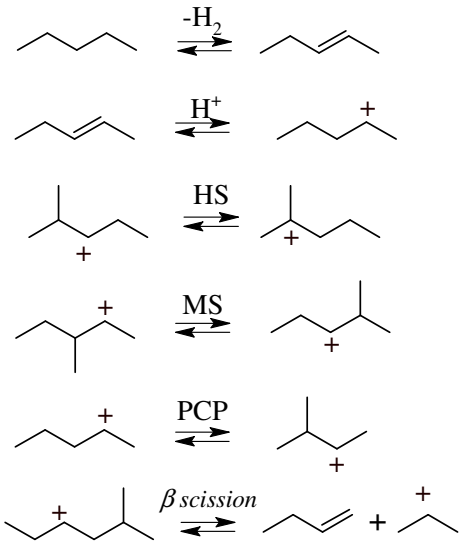

Figure 2-1. Steps involved in the hydrocracking of paraffins.

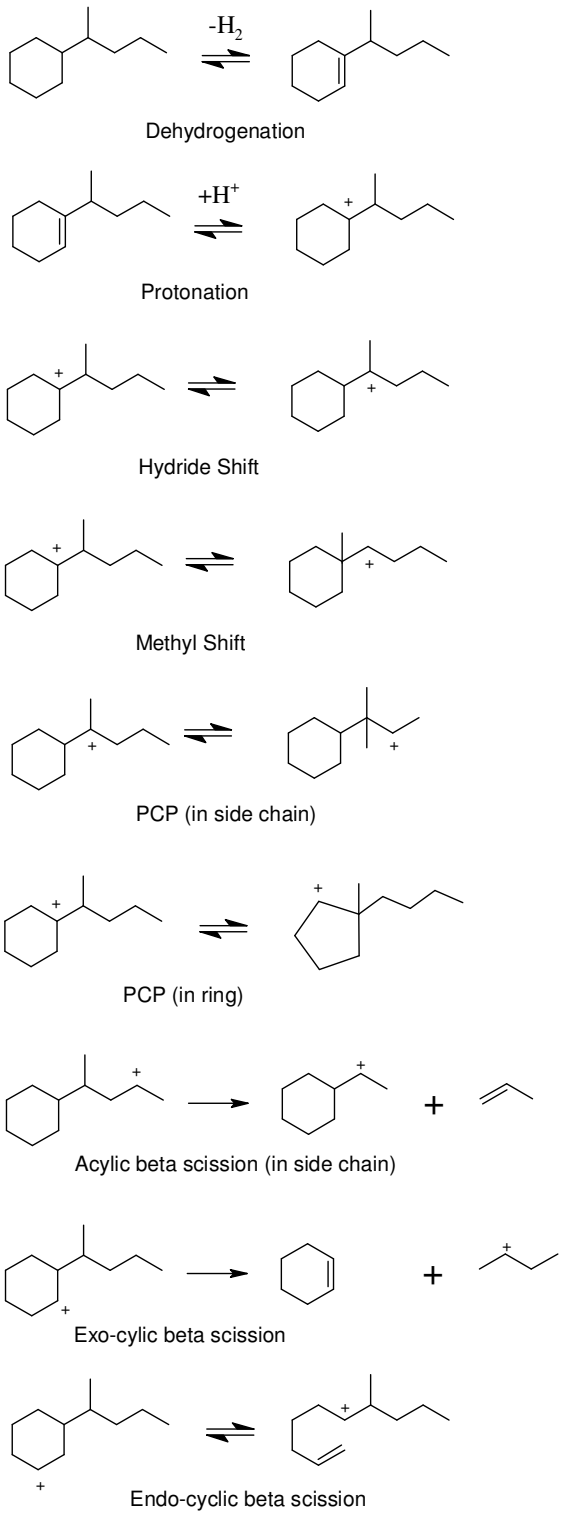

Figure 2-2. Elementary steps of mono-ring naphthenes.

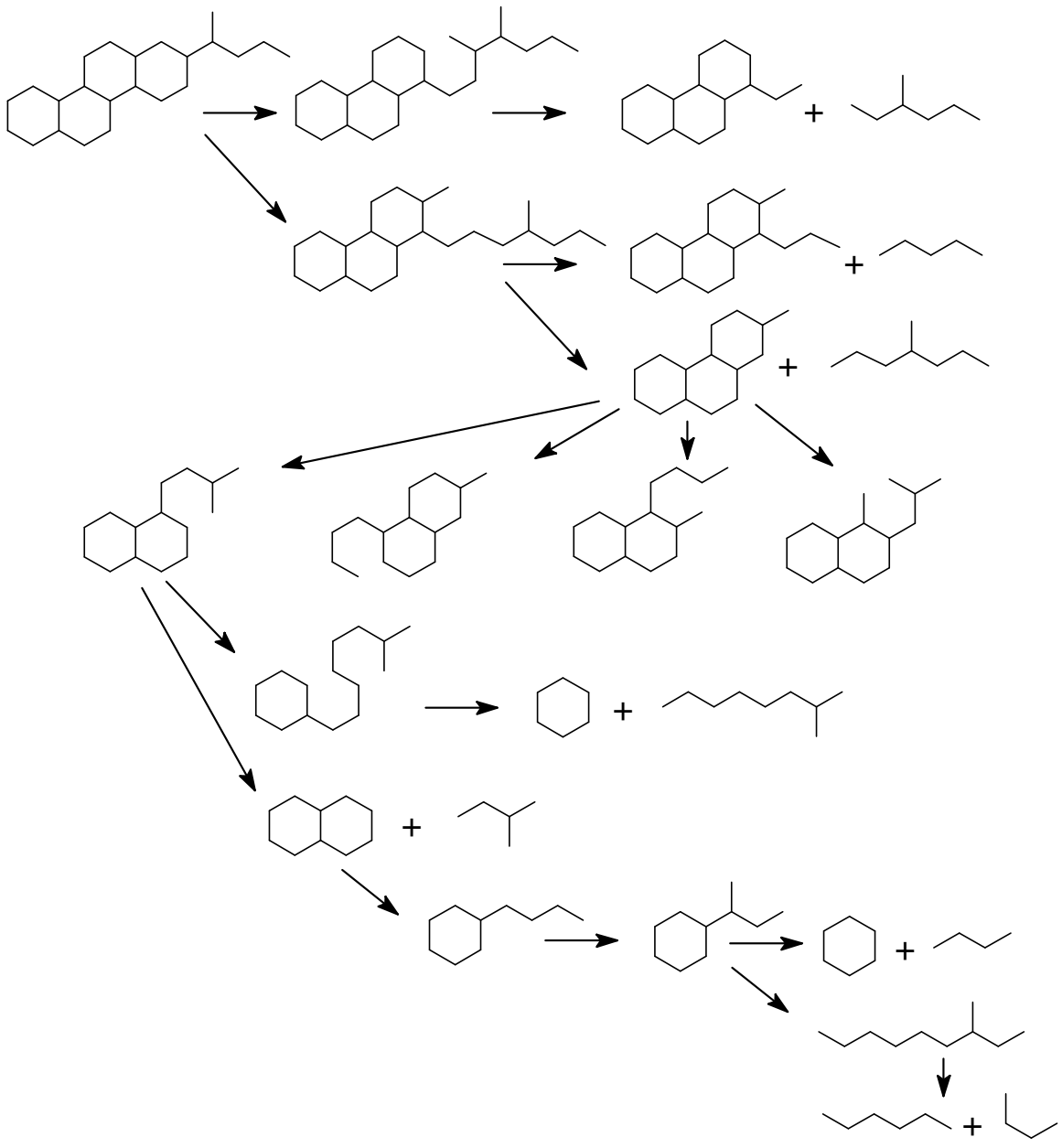

Figure 2-3. Reaction network of multi-ring naphthenes. (Shown in the form of molecular reactions instead of elementary steps for simplification).

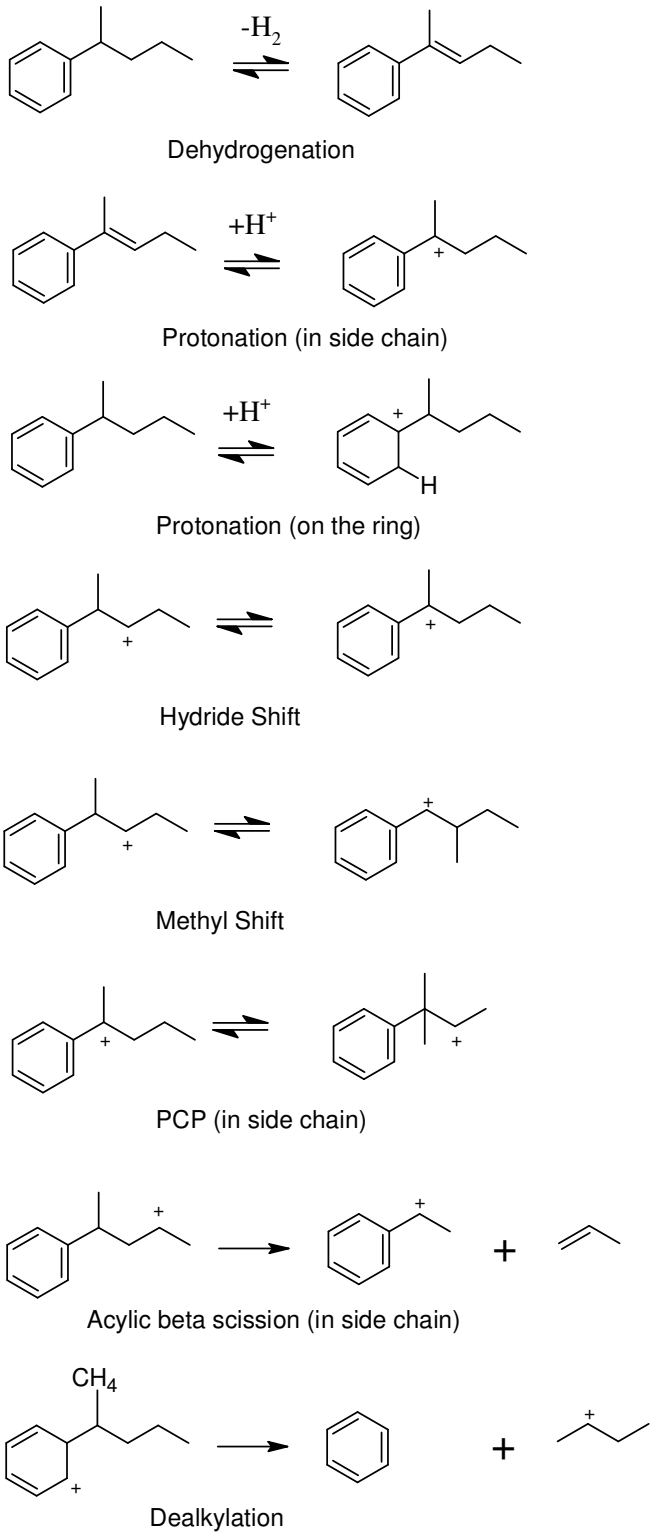

Figure 2-4. Elementary steps and reactions of monoring aromatics.

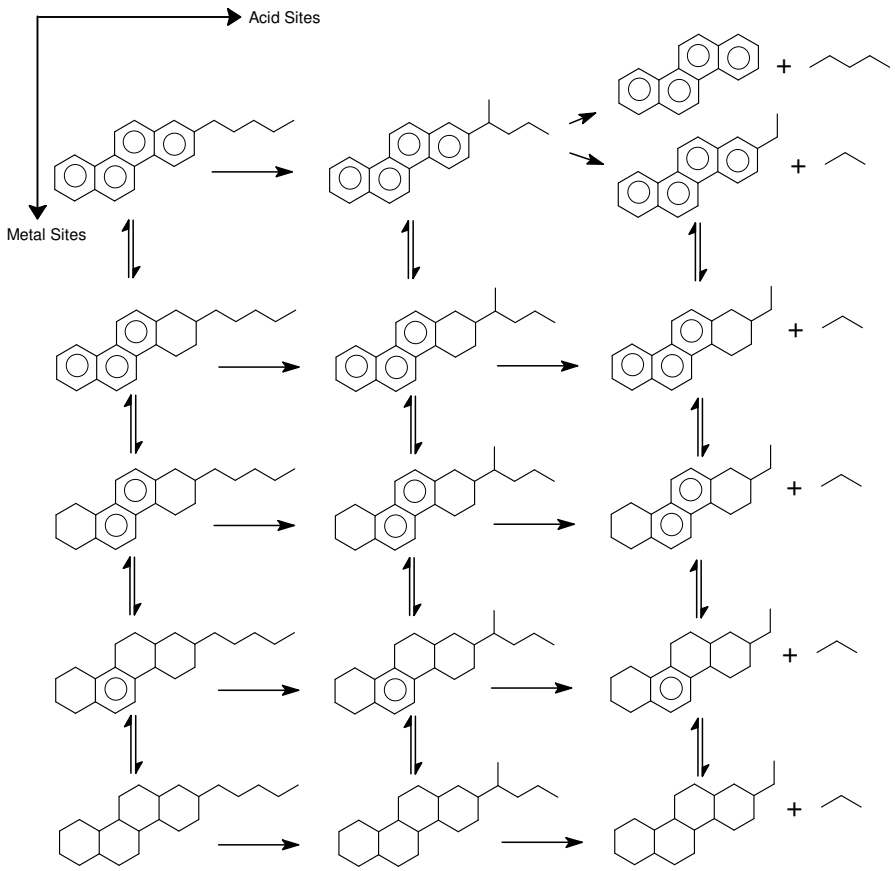

Figure 2-5. Reaction network of multi-ring aromatics. (Shown in the form of molecular reactions instead of elementary steps for simplification).

2.3. Reaction Network Generation

Considering the large number of reaction pathways in the hydrocracking of heavy feedstocks when expressed in terms of elementary steps, a reaction network for the paraffins, naphthenes and aromatics has been generated up to carbon number 40 using Boolean relation matrices and characterization vectors. The methodology and procedure for generating the reaction network has been described in the literature[13, 21, 22]. Several improvements have been made in the existing reaction network generation algorithm to

speed up the program execution. The use of dynamic memory allocation via linked lists for storing and searching the intermediate olefinic and ionic species significantly reduced the run time as compared to searching the species stored on the hard disk. The rules for deriving the number of single-events of the PCP and cracking steps have also been improved.

The total number of carbenium ions involved in VGO hydrocracking up to C_{40} is of the order of 18 million. The total number of steps and the number of rate determining steps are of the order of 126 and 15 million respectively. For illustrative purpose, some of the information extracted from the computer generated reaction network has been presented in Figure 2-6 to Figure 2-8 showing the increase in the number of species and the number of steps with carbon number.

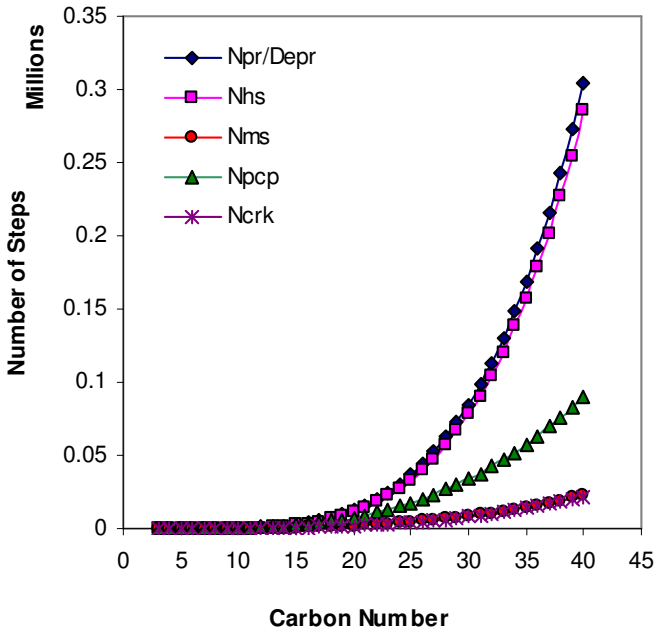

Figure 2-6. The number of different types of elementary steps in the hydrocracking of paraffins.

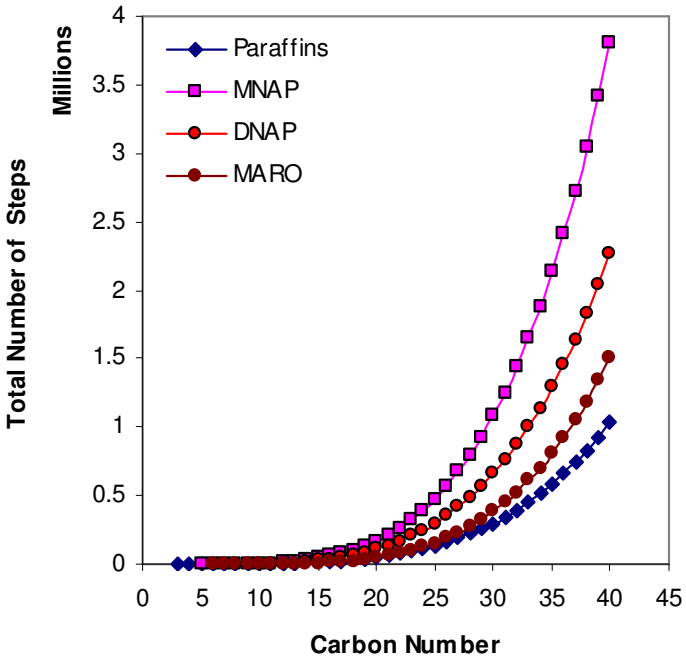

Figure 2-7. The total number of elementary steps in the network generated for paraffins, mono-naphthenes, di-naphthenes and mono-aromatics.

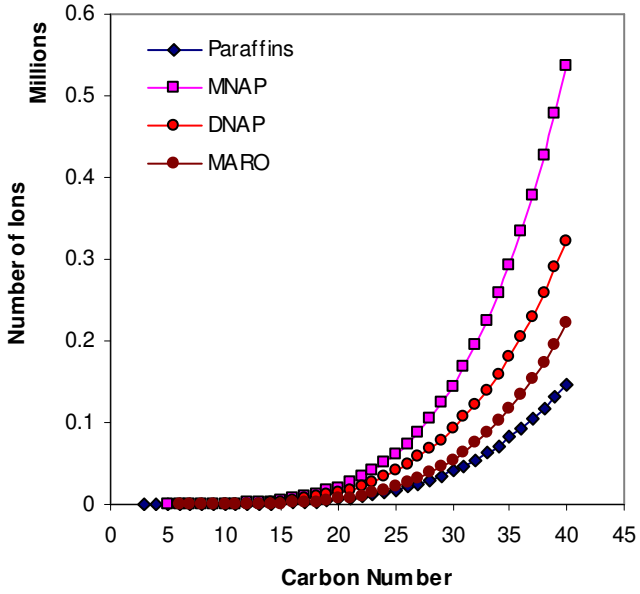

Figure 2-8. The number of carbenium ions in the network generated for paraffins, mono-naphthenes, di-naphthenes and mono-aromatics.

2.4. Composition of VGO

To develop a mechanistic kinetic model requires the knowledge of the composition of the feedstock at the molecular level. Just for the paraffins in the C_5-C_{12} range (a typical carbon number range for naphthas) the number of possible isomers amounts to more than 600. The number of isomers which have actually been experimentally observed (though not all identified) in this range is of the order of 200-400[23-26]. This kind of detailed molecular analysis of light petroleum fractions like gasoline and light naphtha can be carried out using coupled gas chromatography/mass spectroscopy. For any higher boiling range cuts, this number becomes quickly unmanageable. For higher boiling fractions, adding the isomers of paraffins, naphthenes, and aromatics as well as the heteroatom compounds, the number becomes larger by several orders of magnitudes making the complete compositional analysis of heavy fractions utterly impossible[1] even by the latest analytical techniques. However, significant developments have been made in recent years for a quite detailed analysis of these heavy mixtures with the application of modern analytical techniques including gas chromatography (GC), supercritical fluid chromatography (SFC), high performance liquid chromatography (HPLC), field ionization mass spectroscopy (FIMS), low voltage high resolution mass spectroscopy (LV-HRMS), nuclear magnetic resonance spectroscopy (NMR) etc. Boduszynski[27, 28], for example, has coupled high performance liquid chromatography (HPLC) for separations and FIMS in the analysis of several petroleum crude oils. Similarly, Allen[29] has coupled HPLC/GC compound class separations along with mass spectral, ^{13}C, ^{1}H, nuclear magnetic resonance analysis in detailed description of gas oil feedstocks. In the work of Boduszynski, the petroleum feed was fractionated into ten boiling point cuts, each of which was subjected to three HPLC extractive separations to determine nine sub-fractions: the saturates, monoaromatics, diaromatics, triaromatics, tetraaromatics, pentaaromatics, and the polar compounds (the basic, pyrolic nitrogen and acid components). Each of these sub-fractions was analyzed in detail by FIMS which gave the molecular weight distribution or carbon number distribution of different homologous series. The results available using this technique are valuable quantitative information

about the distribution of various components in the complex feedstocks. This kind of analysis allows to represent the composition of a heavy petroleum fraction in a matrix form in which the rows represent different molecular classes and the columns contain the carbon number distribution for each class. Compounds in each class have a distinct hydrogen deficiency number Z (as in C_nH_{2n+Z}), where $Z = -2(R + DB - 1)$, R is the number of rings and DB is the number of double bonds in the given class. One such *(Z-CN)* representation to characterize a VGO feedstock is presented in Table 2-1. The entire VGO is divided into 16 molecular classes and in each class the carbon number distribution is given up to C_{40} resulting in 462 pure components/lumps in total. In this representation, all the isomers belonging to a particular class with a given carbon number are placed in one lump with no distinction based on the degree of branching or ring substitution in the isomeric species.

Because of the difficulties associated with this type of detailed characterization of heavier petroleum feedstocks and at the same time its increasing importance in the development of fundamental kinetic models, a large amount of research is directed towards the determination of detailed composition from the bulk analysis of heavy hydrocarbons such as ASTM distillation curves, API gravity, Reid vapor pressure (RVP), paraffin, naphthene and aromatic (PNA) content, Conradson carbon residue (CCR) etc. using different approaches.

Neurock et al.[30, 31] devised a stochastic method to transform efficient sets of analytical characterizations into molecular representations of complex feedstocks. They assembled the important structural attributes of petroleum molecules like the number of aromatic rings, number of naphthenic rings, number and length of paraffinic side chain etc. into molecules according to quantitative probability density functions for each attribute resulting in a large ensemble of representative key components from which both molecular and global product properties were deduced. These density functions were derived from a general Monte Carlo algorithm. In a similar work Hudebine et al.[32] created the molecular composition from partial analytical data using a two-step reconstruction method. The first step called the stochastic reconstruction assumes that oil mixtures can be described by distributions of structural blocks. The choice of blocks and distributions is based on expert knowledge. The transformation from a set of distributions into a mixture of molecules is obtained by Monte-Carlo sampling while a simulated annealing procedure adjusts the parametric distributions. The second step termed as reconstruction by entropy maximization improves the representativeness of the set of constructed molecules by adjusting their molar fractions. The estimation of these mole fractions is carried out by maximizing an information entropy criterion under linear constraints. Aye et al.[33] developed a methodology for the generation of detailed composition for the gasoline range fractions from bulk properties. They used a database of the properties and molecular information in the form of Z-CN matrices of several refining streams and through the linear combination of these matrices predicted the composition of new feedstocks.

Table 2-1. (Z-CN) matrix representation of VGO in terms of 462 components/lumps.

	CN	NPAR	IPAR	MNA	DNA	TNA	QNA	MAR	DAR	TAR	QAR	NMA	NDA	NTA	DNMA	DNDA	TNMA	CN	
LPG	3	1																3	LPG
	4	2	39															4	
LNAP	5	3	40	76														5	LNAP
	6	4	41	77				193										6	
	7	5	42	78				194										7	
HNAP	8	6	43	79				195										8	HNAP
	9	7	44	80				196										9	
	10	8	45	81	112			197	228			309						10	
	11	9	46	82	113			198	229			310						11	
	12	10	47	83	114			199	230			311						12	
KERO	13	11	48	84	115			200	231			312						13	KERO
	14	12	49	85	116	143		201	232	259		313	340		390			14	
	15	13	50	86	117	144		202	233	260		314	341		391			15	
DIESEL	16	14	51	87	118	145		203	234	261		315	342		392			16	DIESEL
	17	15	52	88	119	146		204	235	262		316	343		393			17	
	18	16	53	89	120	147	170	205	236	263	286	317	344	367	394	417	440	18	
	19	17	54	90	121	148	171	206	237	264	287	318	345	368	395	418	441	19	
	20	18	55	91	122	149	172	207	238	265	288	319	346	369	396	419	442	20	
UNCONVERTED	21	19	56	92	123	150	173	208	239	266	289	320	347	370	397	420	443	21	UNCONVERTED
	22	20	57	93	124	151	174	209	240	267	290	321	348	371	398	421	444	22	
	23	21	58	94	125	152	175	210	241	268	291	322	349	372	399	422	445	23	
	24	22	59	95	126	153	176	211	242	269	292	323	350	373	400	423	446	24	
	25	23	60	96	127	154	177	212	243	270	293	324	351	374	401	424	447	25	
	26	24	61	97	128	155	178	213	244	271	294	325	352	375	402	425	448	26	
	27	25	62	98	129	156	179	214	245	272	295	326	353	376	403	426	449	27	
	28	26	63	99	130	157	180	215	246	273	296	327	354	377	404	427	450	28	
	29	27	64	100	131	158	181	216	247	274	297	328	355	378	405	428	451	29	
	30	28	65	101	132	159	182	217	248	275	298	329	356	379	406	429	452	30	
	31	29	66	102	133	160	183	218	249	276	299	330	357	380	407	430	453	31	
	32	30	67	103	134	161	184	219	250	277	300	331	358	381	408	431	454	32	
	33	31	68	104	135	162	185	220	251	278	301	332	359	382	409	432	455	33	
	34	32	69	105	136	163	186	221	252	279	302	333	360	383	410	433	456	34	
	35	33	70	106	137	164	187	222	253	280	303	334	361	384	411	434	457	35	
	36	34	71	107	138	165	188	223	254	281	304	335	362	385	412	435	458	36	
	37	35	72	108	139	166	189	224	255	282	305	336	363	386	413	436	459	37	
	38	36	73	109	140	167	190	225	256	283	306	337	364	387	414	437	460	38	
	39	37	74	110	141	168	191	226	257	284	307	338	365	388	415	438	461	39	
	40	38	75	111	142	169	192	227	258	285	308	339	366	389	416	439	462	40	
	CN	NPAR	IPAR	MNA	DNA	TNA	QNA	MAR	DAR	TAR	QAR	NMA	NDA	NTA	DNMA	DNDA	TNMA	CN	
	No of Lumps	38	37	36	31	27	23	35	31	27	23	31	27	23	27	23	23	462	

Abbreviations of different classes: nPar: Normal Paraffins, **iPar:** Iso Paraffins, **MNA:** Mono-Naphthenes, **DNA:** Di-Naphthenes, **TNA:** Tri-Naphthenes, **TETNA:** Tetra-Naphthenes, **MAR:** Mono Aromatics, **DAR:** Di-Aromatics, **TAR:** Tri-Aromatics, **TETAR:** Tetra-Aromatics, **NMA:** Naphtheno Mono Aromatics, **NMA:** Naphtheno Di-Aromatics, **NTA:** Naphtheno Tri-Aromatics, **DNMA:** Di Naphtheno Mono Aromatics, **DNDA:** Di Naphtheno Di Aromatics, **TNMA:** Tri Naphtheno Mono Aromatics

Unfortunately, the analysis of VGO even at such a detailed level (Z-CN matrix form) does not allow development of a mechanistic kinetic model in which the model parameters could be claimed to be independent of the feedstock composition. To explain the reason, refer to the strict thermodynamic lumping scheme developed in the Chapter III. This lumping scheme is based on the assumption that the isomers of a particular carbon number belonging to a class and with a given number of methyl branches reach thermodynamic equilibrium due to fast hydride shift and methyl shift elementary steps on the acid sites of the catalyst. Therefore, the model requires three lumps per carbon number for isoparaffins, i.e., monobranched, dibranched and tribranched lumps. In the VGO composition shown in Table 2-1, however, all the isomers of a given class are placed in one lump. Therefore, such a characterization of VGO would not allow the calculation of the rate of conversion of less branched isomers to more branched isomers (and vice versa) occurring through protonatedcyclopropane (PCP) mechanism, which is an important rate determining step in the hydrocracking process. In other words, according to the lumping scheme given in Table 2-1, all the isomers in a lump with different number of methyl branches would have to be assumed at pseudo-equilibrium along the entire length of the reactor which is far from reality. Vansina et al.[34] compared the experimental product distribution with the thermodynamically calculated values in the hydrocracking of n-octane and showed that the fraction of multi-branched isomers is always smaller than the thermodynamic equilibrium. Especially, the fraction of tri-branched isomers was much smaller than their thermodynamic equilibrium values. Similarly, Schulz et al.[35] reported that in the hydrocracking of n-dodecane on different catalysts, the ratios of the monomethyl isomers to the corresponding n-paraffins are greater than those of thermodynamic equilibrium, whereas the amount of dimethyl isomers are much smaller. This idea has been extended to the ring containing structures also given the presence of long paraffinic side chains in these species and the same reaction mechanism (i.e., PCP) for the change in the number of branches. Since the global rate of cracking of a lump through β-scission increases with the degree of branching, placing all the isomers per carbon number of a given class in one lump would

not give the accurate values of the global rate of conversion through β-scission steps, which are the main elementary steps responsible for the transformation of heavy hydrocarbons into the lighter ones. Consequently, in the current model to represent the carbenium ion chemistry at the fundamental level, all the classes except normal paraffins and those with four rings (naphthenic or aromatic) structures, have been further divided into subclasses based on the number of methyl branches. Normal paraffins are obviously pure components and the four ring structures are not divided because of their relatively low concentrations. According to the rules set for the reaction network generation[22], paraffinic species can have a maximum of three methyl branches; ethyl and longer branches are not allowed in the reaction network owing to relatively smaller concentrations of this kind of isomers. Therefore, the isoparaffin class has been divided into three subclasses, i.e., monobranched, dibranched and tribranched. The species containing naphthenic or aromatic rings are allowed to have only one long side chain at a given substitution, and up to three methyl branches anywhere on the ring structure or the long side chain. Therefore, for a given carbon number of any ring containing class, the first subclass contains the species having just the bare ring structure (i.e., the first member of the class, e.g. benzene in monoaromatic class), or the species having only the long side chain without any methyl branch. This subclass is referred to as unbranched in the rest of this dissertation. The other three subclasses contain species with one, two, and three methyl branches denoted by monobranched, dibranched and tribranched subclasses, respectively. According to this scheme, the 16 molecular classes are divided into 45 subclasses leading to characterization of VGO in terms of 1266 pure components/lumps. This scheme for VGO characterization is shown in Table 2-2. The summary of Table 2-2 has been presented in Table 2-3 showing the number of lumps for each subclass. Naturally, it is very difficult to characterize a heavy feedstock like VGO at such a detailed level. Mass spectrometers/high resolution mass spectrometers would not be able to distinguish among the isomers with the same chemical formula. But techniques like ^{1}H and ^{13}C NMR can give important information about the average population of carbon and hydrogen atoms of different nature, i.e., primary, secondary,

tertiary, aromatic, α-position to aromatic ring etc. of a fraction separated from VGO by GC/HPLC/SGC. This information can be utilized to get a good estimate of the distribution of isomers with different degrees of branching to convert the VGO composition from 16 classes to 45 subclasses. Development of more advanced analytical methods would certainly be useful for obtaining this kind of information.

As the information on the distribution of isomers with different degrees of branching in a class for heavy petroleum mixtures is not available, some insight has been taken from the detailed molecular level analysis of lighter petroleum fractions. It has been generally observed that in the straight run petroleum cuts, the isoparaffins contain primarily the monobranched isomers with relatively smaller amounts of multibranched paraffins. Accordingly, in the current model the distribution of monobranched, dibranched and tribranched isomers is assumed to be 65%, 25% and 10%, respectively. In the classes with aromatic and naphthenic rings, a distribution of 20%, 50%, 20% and 10% has been assumed for the unbranched, monobranched, dibranched and tribranched isomers. The distribution of the degree of branching can be significantly different in the VGOs obtained from other processing units as compared to the straight run VGOs and need to be accounted for accordingly. A sensitivity analysis has been performed to show the effect of the distribution of isomers in the feed on the hydrocracking products. It will be discussed in Chapter V.

Table 2-2. (Z-CN) matrix representation of VGO in terms of 1266 components/lumps. (Numbers 0 to 3 in the second row represent the number of methyl branches in that subclass)

Subclass	1	2	3	4	5	6	7	8	9	10	11	12	13	14	15	16	17	18	19	20	21	22	23	24	25	26	27	28	29	30	31	32	33	34	35	36	37	38	39	40	41	42	43	44	45		
	CN	NPAR	MBP	DBP	TBP	MNA0	MNA1	MNA2	MNA3	DNA0	DNA1	DNA2	DNA3	TNA0	TNA1	TNA2	TNA3	TETNA	MAR0	MAR1	MAR2	MAR3	DAR0	DAR1	DAR2	DAR3	TAR0	TAR1	TAR2	TAR3	TETAR	NMA0	NMA1	NMA2	NMA3	NDA0	NDA1	NDA2	NDA3	NTA	DNMA0	DNMA1	DNMA2	DNMA3	DNDA	TNMA	CN	
LPG	3	1																																												3	LPG
	4	2	39																																											4	
LNAP	5	3	40			145																																								5	LNAP
	6	4	41	76		146												517																											6	
	7	5	42	77	111	147	181											518																											7	
	8	6	43	78	112	148	182	215										519	552																									8	
HNAP	9	7	44	79	113	149	183	216	248									520	553	585																									9	HNAP
	10	8	45	80	114	150	184	217	249	280								521	554	586	617	648										885														10	
	11	9	46	81	115	151	185	218	250	281								522	555	587	618	649										886														11	
	12	10	47	82	116	152	186	219	251	282	311							523	556	588	619	650	679									887	916													12	
KERO	13	11	48	83	117	153	187	220	252	283	312	340						524	557	589	620	651	680	708								888	917	945												13	KERO
	14	12	49	84	118	154	188	221	253	284	313	341	368	395				525	558	590	621	652	681	709	736	763						889	918	946	973	1000					1122					14	
	15	13	50	85	119	155	189	222	254	285	314	342	369	396				526	559	591	622	653	682	710	737	764						890	919	947	974	1001					1123					15	
	16	14	51	86	120	156	190	223	255	286	315	343	370	397	422			527	560	592	623	654	683	711	738	765	790					891	920	948	975	1002	1027				1124	1149				16	
	17	15	52	87	121	157	191	224	256	287	316	344	371	398	423	447		528	561	593	624	655	684	712	739	766	791	815				892	921	949	976	1003	1028	1052			1125	1150	1174			17	
DIESEL	18	16	53	88	122	158	192	225	257	288	317	345	372	399	424	448	471	494	529	562	594	625	656	685	713	740	767	792	816	839	862	893	922	950	977	1004	1029	1053	1076	1099	1126	1151	1175	1198	1221	1244	18	DIESEL
	19	17	54	89	123	159	193	226	258	289	318	346	373	400	425	449	472	495	530	563	595	626	657	686	714	741	768	793	817	840	863	894	923	951	978	1005	1030	1054	1077	1100	1127	1152	1176	1199	1222	1245	19	
	20	18	55	90	124	160	194	227	259	290	319	347	374	401	426	450	473	496	531	564	596	627	658	687	715	742	769	794	818	841	864	895	924	952	979	1006	1031	1055	1078	1101	1128	1153	1177	1200	1223	1246	20	
UNCONVERTED	21	19	56	91	125	161	195	228	260	291	320	348	375	402	427	451	474	497	532	565	597	628	659	688	716	743	770	795	819	842	865	896	925	953	980	1007	1032	1056	1079	1102	1129	1154	1178	1201	1224	1247	21	UNCONVERTED
	22	20	57	92	126	162	196	229	261	292	321	349	376	403	428	452	475	498	533	566	598	629	660	689	717	744	771	796	820	843	866	897	926	954	981	1008	1033	1057	1080	1103	1130	1155	1179	1202	1225	1248	22	
	23	21	58	93	127	163	197	230	262	293	322	350	377	404	429	453	476	499	534	567	599	630	661	690	718	745	772	797	821	844	867	898	927	955	982	1009	1034	1058	1081	1104	1131	1156	1180	1203	1226	1249	23	
	24	22	59	94	128	164	198	231	263	294	323	351	378	405	430	454	477	500	535	568	600	631	662	691	719	746	773	798	822	845	868	899	928	956	983	1010	1035	1059	1082	1105	1132	1157	1181	1204	1227	1250	24	
	25	23	60	95	129	165	199	232	264	295	324	352	379	406	431	455	478	501	536	569	601	632	663	692	720	747	774	799	823	846	869	900	929	957	984	1011	1036	1060	1083	1106	1133	1158	1182	1205	1228	1251	25	
	26	24	61	96	130	166	200	233	265	296	325	353	380	407	432	456	479	502	537	570	602	633	664	693	721	748	775	800	824	847	870	901	930	958	985	1012	1037	1061	1084	1107	1134	1159	1183	1206	1229	1252	26	
	27	25	62	97	131	167	201	234	266	297	326	354	381	408	433	457	480	503	538	571	603	634	665	694	722	749	776	801	825	848	871	902	931	959	986	1013	1038	1062	1085	1108	1135	1160	1184	1207	1230	1253	27	
	28	26	63	98	132	168	202	235	267	298	327	355	382	409	434	458	481	504	539	572	604	635	666	695	723	750	777	802	826	849	872	903	932	960	987	1014	1039	1063	1086	1109	1136	1161	1185	1208	1231	1254	28	
	29	27	64	99	133	169	203	236	268	299	328	356	383	410	435	459	482	505	540	573	605	636	667	696	724	751	778	803	827	850	873	904	933	961	988	1015	1040	1064	1087	1110	1137	1162	1186	1209	1232	1255	29	
	30	28	65	100	134	170	204	237	269	300	329	357	384	411	436	460	483	506	541	574	606	637	668	697	725	752	779	804	828	851	874	905	934	962	989	1016	1041	1065	1088	1111	1138	1163	1187	1210	1233	1256	30	
	31	29	66	101	135	171	205	238	270	301	330	358	385	412	437	461	484	507	542	575	607	638	669	698	726	753	780	805	829	852	875	906	935	963	990	1017	1042	1066	1089	1112	1139	1164	1188	1211	1234	1257	31	
	32	30	67	102	136	172	206	239	271	302	331	359	386	413	438	462	485	508	543	576	608	639	670	699	727	754	781	806	830	853	876	907	936	964	991	1018	1043	1067	1090	1113	1140	1165	1189	1212	1235	1258	32	
	33	31	68	103	137	173	207	240	272	303	332	360	387	414	439	463	486	509	544	577	609	640	671	700	728	755	782	807	831	854	877	908	937	965	992	1019	1044	1068	1091	1114	1141	1166	1190	1213	1236	1259	33	
	34	32	69	104	138	174	208	241	273	304	333	361	388	415	440	464	487	510	545	578	610	641	672	701	729	756	783	808	832	855	878	909	938	966	993	1020	1045	1069	1092	1115	1142	1167	1191	1214	1237	1260	34	
	35	33	70	105	139	175	209	242	274	305	334	362	389	416	441	465	488	511	546	579	611	642	673	702	730	757	784	809	833	856	879	910	939	967	994	1021	1046	1070	1093	1116	1143	1168	1192	1215	1238	1261	35	
	36	34	71	106	140	176	210	243	275	306	335	363	390	417	442	466	489	512	547	580	612	643	674	703	731	758	785	810	834	857	880	911	940	968	995	1022	1047	1071	1094	1117	1144	1169	1193	1216	1239	1262	36	
	37	35	72	107	141	177	211	244	276	307	336	364	391	418	443	467	490	513	548	581	613	644	675	704	732	759	786	811	835	858	881	912	941	969	996	1023	1048	1072	1095	1118	1145	1170	1194	1217	1240	1263	37	
	38	36	73	108	142	178	212	245	277	308	337	365	392	419	444	468	491	514	549	582	614	645	676	705	733	760	787	812	836	859	882	913	942	970	997	1024	1049	1073	1096	1119	1146	1171	1195	1218	1241	1264	38	
	39	37	74	109	143	179	213	246	278	309	338	366	393	420	445	469	492	515	550	583	615	646	677	706	734	761	788	813	837	860	883	914	943	971	998	1025	1050	1074	1097	1120	1147	1172	1196	1219	1242	1265	39	
	40	38	75	110	144	180	214	247	279	310	339	367	394	421	446	470	493	516	551	584	616	647	678	707	735	762	789	814	838	861	884	915	944	972	999	1026	1051	1075	1098	1121	1148	1173	1197	1220	1243	1266	40	
	CN	NPAR	MBP	DBP	TBP	MNA0	MNA1	MNA2	MNA3	DNA0	DNA1	DNA2	DNA3	TNA0	TNA1	TNA2	TNA3	TETNA	MAR0	MAR1	MAR2	MAR3	DAR0	DAR1	DAR2	DAR3	TAR0	TAR1	TAR2	TAR3	TETAR	NMA0	NMA1	NMA2	NMA3	NDA0	NDA1	NDA2	NDA3	NTA	DNMA0	DNMA1	DNMA2	DNMA3	DNDA	TNMA	CN	
Lumps	38	37	35	34	36	34	33	32	31	29	28	27	27	25	24	23	23	35	33	32	31	31	29	28	27	27	25	24	23	23	31	29	28	27	27	25	24	23	23	27	25	24	23	23	23	1266	
Cumulative	38	75	110	144	180	214	247	279	310	339	367	394	421	446	470	493	516	551	584	616	647	678	707	735	762	789	814	838	861	884	915	944	972	999	1026	1051	1075	1098	1121	1148	1173	1197	1220	1243	1266		

Table 2-3. The number of lumps/pure components in different subclasses.

S. No.	Subclass	No. of lumps up to C_{40}
1	NPAR	38*
2	MBP	37
3	DBP	35
4	TBP	34
5	MNA0	36*
6	MNA1	34
7	MNA2	33
8	MNA3	32
9	DNA0	31*
10	DNA1	29
11	DNA2	28
12	DNA3	27
13	TNA0	27*
14	TNA1	25
15	TNA2	24
16	TNA3	23
17	TETNA	23
18	MAR0	35*
19	MAR1	33
20	MAR2	32
21	MAR3	31
22	DAR0	31*
23	DAR1	29
24	DAR2	28
25	DAR3	27
26	TAR0	27*
27	TAR1	25
28	TAR2	24
29	TAR3	23
30	TETAR	23

Table 2-3. Continued.

S. No.	Subclass	No. of lumps up to C_{40}
31	NMA0	31*
32	NMA1	29
33	NMA2	28
34	NMA3	27
35	NDA0	27*
36	NDA1	25
37	NDA2	24
38	NDA3	23
39	NTA	23
40	DNMA0	27*
41	DNMA1	25
42	DNMA2	24
43	DNMA3	23
44	DNDA	23
45	TNMA	23
	Total	**1266**

(*) 310 pure components.

CHAPTER III

KINETIC MODEL DEVELOPMENT FOR THE HYDROCRACKING OF VGO

As shown in Chapter II, in the hydrocracking of a complex feedstock like VGO, the number of elementary steps and reactions occurring on the acidic sites and metal sites of the catalyst is extremely large. Yet every elementary step and reaction has a finite contribution towards the final distribution of products. For such complex processes, conventional kinetic modeling approaches would result in such a large number of reaction rate coefficients that it would be truly impractical to estimate their values from the experimental data. The solution of this problem lies in modeling the rate parameters of these steps in addition to modeling the rate equations. The first step in developing a methodology for modeling the rate parameters is the exploitation of the fact that in spite of the excessive number of elementary steps occurring on the acid sites, the 'types' of elementary steps to which they belong is much smaller. Assigning a unique rate coefficient to all the elementary steps of one type would be too much of a simplification, indeed. The differences in the structures and the energy levels of the reactants and the corresponding activated complexes of the elementary steps of a given type contribute differently towards their frequency factors and activation energies. To account for the effect of the structures on the frequency factors, Froment and coworkers[11, 12, 36] introduced the concept of single event kinetics. In the hydrocracking of VGO, the activation energies of the elementary steps are modeled based on the nature (secondary or tertiary) of the reactant and product carbenium ions. A more rigorous treatment for the modeling of the activation energies is presented in Chapter VI, dealing with the hydrocracking of pure paraffinic feedstocks. This approach is based on the application of the Evans-Polanyi relationship which explicitly accounts for the differences in the energy levels of the reactants and the products starting from their heats of formation.

The present Chapter discusses the methodology for the modeling of the frequency factors and the activation energies for acid site steps, the development of the rate

expressions for the individual elementary steps and the reaction mechanism and rate expressions for the saturation of the aromatic species. Based on thermodynamic principles, a strict lumping scheme is devised (as discussed partly in Chapter II) and the resulting rate expressions for the global rate of conversion between the lumps are developed.

3.1. Modeling of the Frequency Factors

Single-event kinetics has been applied to model the frequency factors of the elementary steps taking place on acidic sites of the catalyst. In the single event kinetics, the effect of molecular structure on the frequency factor of an elementary step is described with the help of transition state theory and statistical thermodynamics. The rate coefficient of an elementary step is given by transition state theory[37] as,

$$k = \left(\frac{k_B T}{h}\right)\exp\left(\frac{\Delta S^{o\dagger}}{R}\right)\exp\left(\frac{-\Delta H^{o\dagger}}{RT}\right) \tag{3.1}$$

According to statistical thermodynamics, the entropy of a species is the sum of transnational, rotational, vibrational and electronic contributions,

$$S^o = S^o_{Trans} + S^o_{Vib} + S^o_{Rot} + S^o_{Elec} \tag{3.2}$$

$$\text{where } S^o_{Rot} = S^o_{ExtRot} + S^o_{IntRot} \tag{3.3}$$

The rotational part of the entropy is composed of an intrinsic term, $\hat{S}^o$ and a contribution from the symmetry of the molecule, $R\ln\sigma$, i.e.,

$$S^o_{ExtRot} = \hat{S}^o_{ExtRot} - R\ln\left(\sigma_{Ext}\right) \tag{3.4}$$

$$S^o_{IntRot} = \hat{S}^o_{IntRot} - R\ln\left(\sigma_{Int}\right) \tag{3.5}$$

For racemic mixtures of optically active species, an additional entropy contribution of $-R\ln(2^n)$ due to the mixing of different enantiomers has to be considered, where n is the number of chiral centers in the molecule.

$$S^{o}_{Rot} = \hat{S}^{o}_{Rot} - R\ln\left(\frac{\sigma_{Ext}\sigma_{Int}}{2^{n}}\right) \tag{3.6}$$

where $\hat{S}^{o}_{Rot} = \hat{S}^{o}_{ExtRot} + \hat{S}^{o}_{IntRot}$ (3.7)

and $\left(\frac{\sigma_{Ext}\sigma_{Int}}{2^{n}}\right) =$ Global Symmetry Number, σ_{gl} (3.8)

The global symmetry number σ_{gl} quantifies all the symmetry contributions of a species. Using the above equations, the standard entropy of activation for an elementary step can be written as

$$\Delta S^{o\ddagger} = \Delta S^{o\ddagger}_{Trans} + \Delta S^{o\ddagger}_{Vib} + \Delta S^{o\ddagger}_{Elec} + \Delta \hat{S}^{o\ddagger}_{Rot} + R\ln\left(\frac{\sigma^{R}_{gl}}{\sigma^{\ddagger}_{gl}}\right) \tag{3.9}$$

The last term of equation (3.9) gives the difference in standard entropy due to the symmetry changes in going from reactant to activated complex. Equation (3.9) can also be written as,

$$\Delta S^{o\ddagger} = \Delta \hat{S}^{o\ddagger} + R\ln\left(\frac{\sigma^{R}_{gl}}{\sigma^{\ddagger}_{gl}}\right) \tag{3.10}$$

where $\Delta \hat{S}^{o\ddagger} = \Delta S^{o\ddagger}_{Trans} + \Delta S^{o\ddagger}_{Vib} + \Delta S^{o\ddagger}_{Elec} + \Delta \hat{S}^{o\ddagger}_{Rot}$ (3.11)

Using eqns (3.1) and (3.10), the effect of changes in symmetry in going from reactant to activated complex on the rate coefficient of an elementary step can be factored out. i.e.,

$$k = \left(\frac{\sigma^{R}_{gl}}{\sigma^{\dagger}_{gl}}\right)\left(\frac{k_B T}{h}\right)\exp\left(\frac{\Delta \hat{S}^{o\dagger}}{R}\right)\exp\left(\frac{-\Delta H^{o\dagger}}{RT}\right) \tag{3.12}$$

Hence, the frequency factor for this elementary step can be given by,

$$A = \left(\frac{\sigma^{R}_{gl}}{\sigma^{\dagger}_{gl}}\right)\left(\frac{k_B T}{h}\right)\exp\left(\frac{\Delta \hat{S}^{o\dagger}}{R}\right) \tag{3.13}$$

Defining the ratio of the global symmetry numbers shown in the first bracket as the number of single-events, $n_{e,,}$ i.e., $n_e = \left(\frac{\sigma_{gl}^{R}}{\sigma_{gl}^{\ddagger}} \right)$, the frequency factor for a given elementary step is expressed as

$$A = n_e \tilde{A} \tag{3.14}$$

where the single event frequency factor $\tilde{A}$ is given by

$$\tilde{A} = \left(\frac{k_B T}{h} \right) \exp\left(\frac{\Delta \hat{S}^{o\dagger}}{R} \right) \tag{3.15}$$

For all the unimolecular elementary steps, the contribution of the translational motion to entropy of activation would be zero as the masses of the reactant and the activated complex in any unimolecular elementary step would be identical. It can be seen from eqn (3.14) that the difference in symmetry between the reactant and the activated complex has been factored out by introducing the number of single events, n_e. Once the effect of the symmetry has been factored out from the rotational entropy of activation, the remaining *intrinsic* contribution arising due to the difference in the moments of inertia of the reactant and the activated complex can be assumed to be the same for all the elementary steps of one *type* considering the similarity in the structural transformations occurring in the elementary steps of a given *type*. The same argument can be given for the vibrational contribution of the entropy of activation, i.e., similar changes in the frequencies of vibrational modes of the reactant and the activated complex in the vicinity of the reaction center (i.e., the positively charged carbon atom for the transformations on acidic sites), for all the elementary steps belonging to one *type*. Similarly, the electronic contribution to the entropy of activation, which depends on the number of unpaired electrons in the reactant and the activated complex would be the same for all the elementary steps of one type. Therefore, the single event frequency factor $\tilde{A}$ becomes independent of the structures of the reactant and activated complex for all the different elementary steps of a given type. As a result, the application of the

single event concept requires only 1 independent parameter, namely the single event frequency factor $\tilde{A}$, to model the frequency factors of all the elementary steps of one type. Consequently, for the six types of elementary steps occurring on the acidic sites, i.e., PCP, acyclic β-scission, endocyclic β-scission, exocyclic β-scission, dealkylation, and cyclization, 6 single event frequency factor are used as the model parameters. The values of the number of single events are estimated for all the elementary steps during the reaction network generation and stored with the respective elementary steps.

3.2. Modeling of the Activation Energies

The activation energies for the acid site elementary steps are modeled based on the nature of the reactant and the product carbenium ions. It is considered that the difference in the energy levels of the reactant and product carbenium ion depends only on their nature, i.e., secondary or tertiary. In other words, energy levels are assumed to depend only on the number of α-carbon atoms relative to the positively charged carbon atom, as the secondary and tertiary carbenium ions have two and three α-carbon atoms respectively. Therefore, the effect of the charge delocalization on the energy levels of carbenium ions because of the differences in the number of β-carbon atoms has been ignored in the hydrocracking model for VGO. With this assumption, four distinct activation energies, namely, $E_{(s;s)}$, $E_{(s;t)}$, $E_{(t;s)}$ and $E_{(t;t)}$ are required for the four subtypes of a given type of elementary steps, leading to 24 parameters for 6 different types of steps.

A reduction in the total number of parameters required for modeling of the activation energies is carried out by observing the similarity in structural transformation in different types of elementary steps, viz., acyclic β-scission, exocyclic β-scission and endocyclic β-scission. It can be seen from Figure 2-2 that in all the acyclic β-scission steps, i.e., when β-scission takes place in the paraffin or in the side chain of the ring species, the double bond would be formed in the paraffinic fragment or in the side chain of the naphthenic fragment. However, in all the exocyclic β-scission steps, the double bond would be formed in the naphthenic ring. The presence of the double bond in the

naphthenic ring causes an additional ring strain leading to average heat of reaction for exocyclic steps of any given subtype, say *(s;s),* to be higher than the average heat of reaction of the corresponding subtype of acyclic β-scission steps, provided that other differences are small. Considering the application of the Evans-Polanyi relationship [eqn (6.15)], the activation energies for the exocyclic steps would be higher than those of acyclic steps by an amount of $\alpha\left|\Delta H_{exo-\beta} - \Delta H_{acyc-\beta}\right|$ assuming the intrinsic activation energy E_o for these two types of steps is same. Therefore, the activation energies for the four subtypes of exocyclic steps have been obtained from activation energies of corresponding acyclic steps by introducing only one additional parameter, $\Delta E_{exo-\beta(m;n)}$ which accounts for the increase in the activation energies, i.e., $E_{exo-\beta(m;n)} - E_{acyc-\beta(m;n)}$; m and n represent secondary or tertiary.

It has been observed that the rate of the naphthenic ring opening via endocyclic β-scission is quite low compared to the rate of β-scission in the paraffinic species. One explanation for this behavior, provided by Eagan et al.[20], claims that the noncyclic carbenium ion formed by β-scission of a naphthenic ion has a high tendency to return to the cyclic form because of the favorable configuration of the olefinic carbenium ions, as shown in Figure 3-1.

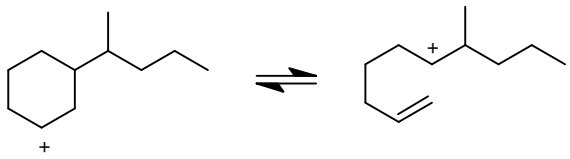

Figure 3-1. Favorable configuration of the cyclization of olefinic carbenium ion formed by endocyclic β-scission.

An approach similar to exocyclic β-scission has been followed for modeling the activation energies of the endocyclic β-scission steps. Only one parameter $\Delta E_{endo-\beta(m;n)}$ has been introduced to account for the difference in the activation energies of a given subtype of endocyclic steps from the corresponding subtype of acyclic steps, i.e., $E_{endo-\beta(m;n)} - E_{acyc-\beta(m;n)}$.

Cyclization steps are the reverse of endocyclic β-scission. However, in the absence of the equilibrium coefficients of the endocyclic steps at the surface of the catalyst, four different activation energies $E_{cyc(s;s)}$, $E_{cyc(s;t)}$, $E_{cyc(t;s)}$ and $E_{cyc(t;t)}$ are used for the four subtypes of cyclization steps.

The reacting carbenium ions (or the benzenium ions) for the dealkylation of aromatics are the ring protonated aromatic species. Because of the much larger delocalization of positive charge on the aromatic ring, the energy levels of the ring protonated aromatic species can not be distinguished based on their secondary or tertiary nature. Therefore, depending on the nature of the paraffinic carbenium ions formed in the dealkylation steps, only two activation energies $E_{dealk(s)}$ and $E_{dealk(t)}$ are used for all the dealkylation steps.

3.3. Development of Rate Equations

Figure 3-2 depicts physical and chemical phenomena occurring inside the catalyst pellet during the hydrocracking of VGO. Paraffins, naphthenes and aromatic species (PNA) are sorbed from the liquid phase to the zeolite pores. Depending upon the difference in the reactive intermediate involved, all the elementary steps occurring on the acid sites of the catalyst are classified into three groups:

(a) PCP, acyclic β-scission, exocyclic β-scission, endocyclic β-scission: these steps proceed through *olefinic intermediates* which are protonated into the carbenium ions for the elementary step to occur.

(b) Cyclization: proceeds through *diolefinic intermediates*, which are protonated into olefinic carbenium ions before the cyclization step.

(c) Dealkylation: for these elementary steps to occur, the aromatic species sorbed inside the zeolite pores are directly protonated on the ring.

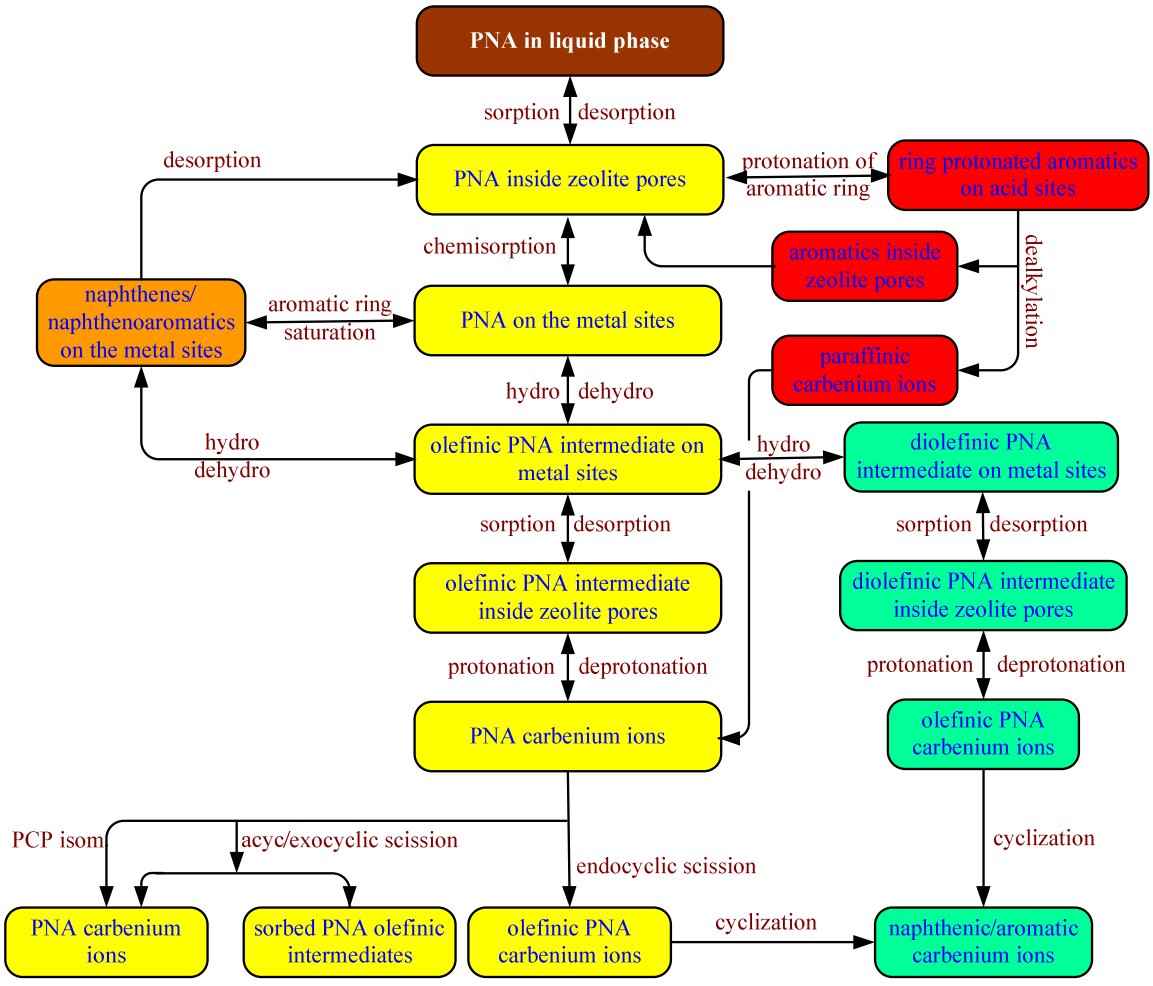

Figure 3-2. Physical and chemical phenomena inside the catalyst pellet.

Different rate expressions are developed for the three groups of acid site steps as explained below. Modeling of the rate coefficients, reaction mechanism and the rate expressions for the aromatic ring saturation on the metal sites will be dealt in the next section.

3.3.1. Group (a)- PCP, Acyclic/Exo/Endo β-Scission

A paraffinic, naphthenic or aromatic (and naphtheno aromatic) species S_i is sorbed from the liquid phase into the zeolite pores.

$$S_i^{liq} \rightleftarrows S_i^{sorbed} \tag{3.16}$$

The concentration of species S_i inside the pore is obtained using Langmuir type sorption isotherm

$$[S_i] = \frac{H_{Si} C_{Si}^{liq}}{D_L} \tag{3.17}$$

in which Henry's coefficient for the sorption of species S_i is given by

$$H_{Si} = K_{L,Si} c_{sat,Si} \text{ and } D_L = \left[1 + \sum_i K_{L,Si} C_{Si}^{liq} \right] \tag{3.18}$$

For group (a) elementary steps, the species S_i^{sorbed} is chemisorbed on the metal sites of the catalyst as S_i^m and dehydrogenated into the corresponding olefinic species, S_{Oij}^m. Naphthenic species can dehydrogenate either in the side chain or in the ring. Aromatic species can dehydrogenate in the side chain only.

$$S_i \rightleftarrows S_{Oij}^m + H_2^{liq} \tag{3.19}$$

It is assumed that the catalyst has sufficient metal/acid activity to bring these hydrogenation/dehydrogenation steps to quasi-equilibrium. The resulting olefinic species are desorbed from the metal sites into the zeolite pores. Assuming that the Henry's

coefficients for the species S_i and the corresponding olefinic species S_{Oij} are the same, the concentration of the olefinic species in the zeolite pores is given by

$$\left[S_{Oij}\right] = \frac{H_{Si} C_{Si}^{liq} K_{DH,ij}^{liq}}{D_L C_{H_2}^{liq}} \tag{3.20}$$

these species are protonated on the acidic sites into carbenium ions, i.e.,

$$S_{Oij}^{sorbed} + H^+ \rightleftarrows S_{Rik}^+ \tag{3.21}$$

Protonation/deprotonation steps have been shown to be potentially much faster than the other steps on the acidic sites and therefore are assumed to be in quasi-equilibrium. The concentration of the surface carbenium ions $\left[S_{Rik}^+\right]$ is therefore obtained as,

$$\left[S_{Rik}^+\right] = K_{pr(S_{Oij} \rightleftarrows S_{Rik}^+)} \left[S_{Oij}\right]\left[H^+\right] \tag{3.22}$$

It should be noted that one particular olefin can produce a maximum of two carbenium ions depending upon the location of the double bond. If the double bond is in the terminal position, one of the produced carbenium ion will be primary and will not be considered in the reaction network. The index *k* in equation (3.21) is used to describe all the possible carbenium ions that can be produced by protonation of all the olefins obtained from S_i on dehydrogenation. The concentration of the vacant acidic sites $\left[H^+\right]$ in eqn (3.22) can be eliminated by the acid site balance as,

$$\left[H^+\right] + \sum_{ik} \left[S_{Rik}^+\right] = C_t \tag{3.23}$$

Using eqn. (3.22), the concentration of the vacant acid site is expressed as,

$$\left[H^+\right] = \frac{C_t}{1 + \sum_{ij} K_{pr(S_{Oij} \rightleftarrows S_{Rik}^+)} \left[S_{Oij}\right]} \tag{3.24}$$

In the hydrocracking of pure paraffins, it has been observed that the surface concentration of the carbenium ions is negligible as compared to the total acid site

concentration, so that $\left[H^+\right] \approx C_t$, because the concentrations of the olefinic intermediates is several orders of magnitude smaller then the paraffinic species. In the case of VGO hydrocracking this would not be true. The presence of significant amount of aromatics in typical VGO feedstocks and their preferential protonation on the acid sites would require the use of equation (3.24) without neglecting the second term in the denominator. In previous work[22] on the modeling of VGO hydrocracking, the influence of the competitive chemisorption of aromatics on the acid sites was not considered.

In the current work, the values of the protonation equilibrium coefficients have been estimated from the gas phase proton affinities of different species and statistical thermodynamics to estimate the value of the denominator in eqn (3.24). This has been described in section 3.7

Combining eqns. (3.22) and (3.24),

$$\left[S^+_{Rik}\right] = \frac{K_{pr(S_{Oij} \rightleftarrows S^+_{Rik})} \left[S_{Oij}\right] C_t}{1 + \sum_{ij} K_{pr(S_{Oij} \rightleftarrows S^+_{Rik})} \left[S_{Oij}\right]} \tag{3.25}$$

As can be seen from eqn (3.21), the carbenium ion S^+_{Rik} can be formed from more than one olefins. Therefore, in the kinetic model, the concentration of the carbenium ion has been calculated from an average over all the possible olefins [not shown in eqn (3.25)].

Based on the concentration of the carbenium ion S^+_{Rik}, the rate of an elementary step $S^+_{Rik} \rightarrow S^+_{Ruv}$ of group (a) is given by,

$$r_{\omega(m;n)} = n_{e,ikuv} \tilde{k}_{\omega(m;n)} \frac{K_{pr(S_{Oij} \rightleftarrows S^+_{Rik})} \left[S_{Oij}\right] C_t}{D_A} \tag{3.26}$$

In which $D_A = 1 + \sum_{ij} K_{pr(S_{Oij} \rightleftarrows S^+_{Rik})} \left[S_{Oij}\right]$ and ω represents the type of the elementary step belonging to group (a). *m* and *n* represent the nature of the reactant and product

carbenium ions. The concentration of olefin in eqn (3.26) is eliminated in terms of the observable concentration of species S_i by using eqn (3.20),

$$r_{\omega(m;n)} = n_{e,ikuv}\tilde{k}_{\omega(m;n)}K^{liq}_{DH,ij}K_{pr(S_{Oij}\rightleftarrows S^{+}_{Rik})}C_t\frac{H_{Si}C^{liq}_{Si}}{D_L D_A C^{liq}_{H_2}} \tag{3.27}$$

3.3.2. Group (b)-Cyclization

As mentioned earlier, cyclization steps are the reverse of the endocyclic β-scission. To model the rate of cyclization steps, a reaction mechanism is proposed which proceeds through the sequential formation of monoolefin and diolefin species followed by the protonation on the acidic sites to produce olefinic carbenium ions. Cyclization of these carbenium ions result in the formation of an extra naphthenic ring as shown in Figure 3-3.

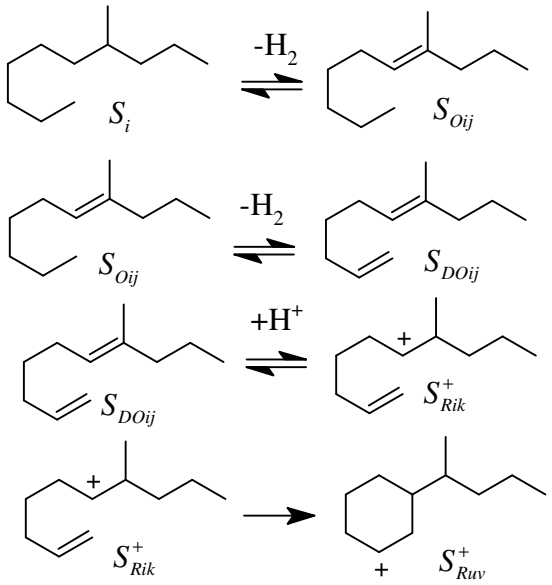

Figure 3-3. Mechanism for the cyclization steps.

Sorbed concentrations of olefin S_{Oij} and di-olefin S_{DOij} can be obtained as

$$\left[S_{Oij}\right] = \frac{K^{liq}_{DH(Si \rightleftarrows S_{Oij})} H_{Si} C^{liq}_{Si}}{D_L C^{liq}_{H_2}} \tag{3.28}$$

$$\left[S_{DOij}\right] = \frac{K^{liq}_{DH(Si \rightleftarrows S_{Oij})} K^{liq}_{DH(S_{Oij} \rightleftarrows S_{DOij})} H_{Si} C^{liq}_{Si}}{D_L C^{liq\,2}_{H_2}} \tag{3.29}$$

With the protonation/deprotonation equilibrium coefficient of S_{DOij}, the concentration of surface carbenium ion S^{+}_{Rik} is given by,

$$\left[S^{+}_{Rik}\right] = K^{liq}_{DH(Si \rightleftarrows S_{Oij})} K^{liq}_{DH(S_{Oij} \rightleftarrows S_{DOij})} K_{pr(S_{DOij} \rightleftarrows S^{+}_{Rik})} C_t \frac{H_{Si} C^{liq}_{Si}}{D_L D_A C^{liq\,2}_{H_2}} \tag{3.30}$$

The rate of cyclization of carbenium ion S^{+}_{Rik} is now given by

$$r_{cyc(m;n)} = n_{e,ikuv} \tilde{k}_{cyc(m;n)} K^{liq}_{DH(Si \rightleftarrows S_{Oij})} K^{liq}_{DH(S_{Oij} \rightleftarrows S_{DOij})} K_{pr(S_{DOij} \rightleftarrows S^{+}_{Rik})} C_t \frac{H_{Si} C^{liq}_{Si}}{D_L D_A C^{liq\,2}_{H_2}} \tag{3.31}$$

3.3.3. Group (c)- Dealkylation of Aromatics

For the dealkylation of aromatics the reactive intermediate is formed by the protonation of the aromatic ring itself, and therefore the dehydrogenation step to yield the olefinic species, as is the case in paraffins and naphthenes, is not involved. The surface concentration of the ring protonated ions is given in terms of the liquid phase concentration of the aromatic specie S_{Ai} as,

$$\left[S^{+}_{Aik}\right] = K_{pr(S_{Ai} \rightleftarrows S^{+}_{Aik})} C_t \frac{H_{S_{Ai}} C^{liq}_{S_{Ai}}}{D_L D_A} \tag{3.32}$$

Similar to the rate expressions of the other groups, the rate of dealkylation steps is given by,

$$r_{dealk(m)} = n_{e,ikuv} \tilde{k}_{dealk(m)} K_{pr(S_{Ai} \rightleftarrows S^{+}_{Aik})} C_t \frac{H_{S_{Ai}} C^{liq}_{S_{Ai}}}{D_L D_A} \tag{3.33}$$

where *m* is the nature of the product paraffinic carbenium ion.

3.3.4. Saturation of Aromatics

Several experimental studies and review articles have been published on the hydrogenation of aromatics involving model compounds like benzene, toluene, alkyl benzenes, tetraline, naphthalene, biphenyl, phenanthrene, pyrene, chrysene, flourene and fluoranthene etc.[38-58]. In most of the studies, especially those involving polyaromatic hydrocarbons, large reaction networks have been proposed to represent the ring saturation kinetics. In the current work, aromatic species from one to four rings are considered in the feedstock. The following sections discuss the reaction mechanism considered for the saturation of mono and multi-ring aromatic hydrocarbons.

3.3.4.1. Saturation of Monoaromatics

Kinetics of the hydrogenation of benzene and substituted benzene has been studied extensively both on supported group noble metals (Pt, Pd) and on metal sulfides (MoS_2, WS_2, $CoMoS/Al_2O_3$, $NiMoS/Al_2O_3$, and $NiWS/Al_2O_3$) catalysts[59]. Modeling for the hydrogenation of benzene has been studied considering stepwise addition of hydrogen, either molecularly or atomically. Aben et al.[60] proposed the Langmuir type rate expression for the hydrogenation of benzene on supported Pt, Pd, and Ni catalysts in a flow system as,

$$\gamma = k_o \frac{bP_{H_2}}{1 + bP_{H_2}} \tag{3.34}$$

where b is the adsorption coefficient for molecular hydrogen and k_o is the rate coefficient. The form of the rate expression implies that hydrogen is molecularly adsorbed and the reaction order in benzene is zero. An activation energy of approximately 14 kcal/mol was found for all the three catalysts. In other studies[61], in gas phase hydrogenation of benzene on Ni/SiO_2 catalyst the reaction order for benzene has been shown to vary from 0.5 at 25 ^oC to 2-3 at 200 ^oC. The reaction order of hydrogen on supported Pd catalyst has been shown to increase from 0.5 to about 4 as the

temperature is increased from 80 ^{o}C to 300 ^{o}C, whereas the reaction order for benzene increased from 0 to 0.8 in the same temperature range.[62, 63] Lin and Vannice[39, 40, 42] proposed a mechanism in which hydrogen is added atomically and the addition of the first hydrogen is considered as rate determining because this step breaks the resonance structure of the benzene molecule. They also assumed that hydrogen and benzene are adsorbed on different catalytic sites and used this mechanism to fit the benzene hydrogenation data taken on a supported Pt catalyst. Subsequent use of this mechanism for the liquid phase hydrogenation of benzene by Singh and Vannice[57, 58, 64] also led to a good fit to the experimental data. As the hydrocracking reactors operate in the three-phase regime, the mechanism proposed by Lin et al. was first attempted in the current model with minor simplifications by ignoring the presence of dehydrogenated benzene species[64]. This mechanism considers the following sequence of steps,

$$
\begin{aligned}
&H_2 + 2* \rightleftharpoons 2H* \\
&S_{Ai} + m \rightleftharpoons S_{Ai}m \\
&S_{Ai}m + H* \rightarrow \ \ S_{A1i}m + * \ \ (RDS) \\
&S_{A1i}m + H* \rightleftharpoons S_{A2i}m + * \\
&S_{A2i}m + H* \rightleftharpoons S_{A3i}m + * \\
&S_{A3i}m + H* \rightleftharpoons S_{A4i}m + * \\
&S_{A4i}m + H* \rightleftharpoons S_{A5i}m + * \\
&S_{A5i}m + H* \rightleftharpoons S_{Ni}m + * \\
&S_{Ni}m \rightleftharpoons S_{Ni} + m
\end{aligned}
\tag{3.35}
$$

where S_{Ai} and S_{Ni} represent the aromatic and naphthenic species and S_{A1i} to S_{A5i} are the reaction intermediates. Hydrogen is dissociatively chemisorbed at the * sites and the aromatic molecule is chemisorbed at the m sites. The net rate of hydrogenation of aromatics using this mechanism is given by

$$
r_{hyd} = \frac{k_{hyd} K_{C,S_{Ai}} c_m c_* \sqrt{K_{C,H_2}} \left(C^{liq}_{S_{Ai}} C^{liq^3}_{H_2} - \dfrac{C^{liq}_{S_{Ni}}}{K^{liq}_{eqm}} \right)}{C^{liq^{5/2}}_{H_2} \left[1 + \sum_i K_{C,S_{Ai}} C^{liq}_{S_{Ai}} + K_{C,S_{Ni}} C^{liq}_{S_{Ni}} + K_{C,S_{Pi}} C^{liq}_{S_{Pi}} \right]}
\tag{3.36}
$$

In the above equation, adsorption terms in the denominator corresponding to H_2 and intermediate species S_{A1i} through S_{A5i} have been neglected. The last term in the denominator accounts for the occupancy of the m sites by the paraffinic species present in the reaction mixture. The values of the gas phase hydrogenation equilibrium coefficient K_{eqm}^{gas} have been estimated using the Benson's group contribution method[65] to get the liquid phase hydrogenation equilibrium coefficient K_{eqm}^{liq} by using the molar concentration of the liquid phase and the vapor-liquid equilibrium partition coefficients K^{VLE} of hydrogen, aromatic and the naphthenic species as,

$$K_{eqm}^{liq} = K_{eqm}^{gas}\left(\frac{C_{total}^{liq}}{K_{H_2}^{VLE}}\right)^3\left(\frac{K_{S_{Ni}}^{VLE}}{K_{S_{Ai}}^{VLE}}\right) \tag{3.37}$$

The VLE partition coefficients have been estimated using the Peng-Robinson equation of state[66].

Reactor simulations for a given VGO feedstock were performed at different reactor pressures using eqn (3.36) and the effect of pressure on the aromatics content in the product was compared with the experimental data of Dufresne et al.[67] These authors studied the effect of hydrogen pressure on the aromatics content in the hydrotreatment of Arabian Light VGO containing 47 wt % aromatics. When the hydrogen pressure is increased from 70 bar to 140 bar, the total aromatics in the products decreased from 31 wt% to 9.6 wt% at a given space time. Table 3-1 shows the effect of pressure on the amount of individual aromatic classes.

Table 3-1. Effect of hydrogen pressure on the aromatics content in the hydrotreatment of Arabian Light VGO[67].

	Feed VGO	Products at 70 Bar	Products at 140 Bar
Total aromatics (wt%)	47	31	9.6
Monoaromatics (wt%)	24	21	8.2
Diaromatics (wt%)	11	6.1	1.0
Triaromatics (wt%)	12	4.4	0.4

It was found from the reactor simulations that the decrease in the yield of aromatics with the increase in reactor pressure was much smaller compared to the above experimental data when using eqn (3.36) for modeling the hydrogenation of aromatics. This was attributed to a low 'effective' order of hydrogen of 0.5 based on this rate expression. A different rate expression was tried based on the more recent work of Melis et al.[68] They proposed a model for the interpretation of hydrogenation of aromatic compounds during hydroprocessing of gas oil considering the adsorption of hydrogen and aromatic species on different sites,

$$r_j = \frac{k_j x_j P_{H_2}^n - k_j^{-1} x_k}{\left(1+\sum K_j x_j\right)\left(1+K_{H_2} P_{H_2}\right)^n} \tag{3.38}$$

where x_j is the weight fraction of the i^{th} lump, k_j and k_j^{-1} are the forward and reverse rate coefficients constrained by the equilibrium coefficient, K_j is the adsorption coefficient and n is the number of moles of H_2 molecules involved in the reaction. This model was fitted with experimental data at various pressures using a commercial $NiMo/Al_2O_3$ catalyst. The model was also tested for different feedstocks, temperature and LHSV and showed good agreement. However, in the absence of the kinetic parameters in their published work, the importance of the different terms in the denominator could not be established. A similar rate expression has been used by Korre

et al.[48, 50] for the hydrogenation of polyaromatic hydrocarbons except that the chemisorption of hydrogen is not considered in the rate expression,

$$r_j = \frac{k_j K_j (C_j P_{H_2}^n - C_k / K_{jk}^{eqm})}{\left(1 + \sum K_j C_j\right)} \tag{3.39}$$

in which C_j and C_k are the molar concentrations of the aromatic and naphthenic species respectively. They established a relationship between molecular structures and hydrogenation reactivities in heavy oil hydroprocessing via elucidation of the controlling reaction pathways and kinetics of one-, two- three- and four fused ring aromatics. They studied the hydrogenation reaction of o-xylene, tetralin, naphthalene, phenanthrene, anthracene, pyrene, and chrysene and their multicomponent mixtures in a cyclohexane solvent using presulfided $CoMo/Al_2O_3$ catalyst and found good agreement with the experimental data. The same rate expression has been used in the current model with the hydrogen partial pressure replaced by the liquid phase molar concentration of hydrogen and liquid phase concentration of hydrocarbons by their sorbed concentrations to account for the sorption of hydrocarbons in the zeolite pores. The sorbed concentrations are then eliminated in terms for the observable liquid phase concentrations using eqn (3.17) so that,

$$r_{hyd} = \frac{k_{hyd,3H_2}^{comp} K_{C,S_{Ai}} H_{S_{Ai}} \left(C_{S_{Ai}}^{liq} C_{H_2}^{liq^3} - \frac{C_{S_{Ni}}^{liq}}{K_{eqm}^{liq}} \right)}{\left[D_L + \sum_i K_{C,S_{Ai}} H_{S_{Ai}} C_{S_{Ai}}^{liq} + K_{C,S_{Ni}} H_{S_{Ni}} C_{S_{Ni}}^{liq} + K_{C,S_{Pi}} H_{S_{Pi}} C_{S_{Pi}}^{liq} \right]} \tag{3.40}$$

In the above equation $k_{hyd,3H_2}^{comp}$ is the composite rate coefficient for the hydrogenation of monoaromatics given by the product of the rate coefficient of the surface controlling reaction and the total concentration of the active metal sites, i.e., $k_{hyd,3H_2} c_m$. The subscript $3H_2$ signifies the consumption of three moles of hydrogen consumed per mole of aromatics.

3.3.4.2. Saturation of Polyaromatics

Korre et al.[48, 50] estimated 45 hydrogenation rate parameters and the same number of equilibrium ratios for 36 aromatic compounds from experimental data using the rate expression in eqn (3.39). These values were used in the evaluation of five adsorption parameters for ring species as a function of the number of aromatic rings and naphthenic rings. Based on close scrutiny of the parameters and experimental observations, they found the following trends in the hydrogenation of polyaromatics:

a) Hydrogenation of polynuclear aromatics proceeds sequentially in a ring by ring manner. No partially hydrogenated compounds such as di- or hexahydro naphthalenes were detected.

b) Hydrogenation reactivity increased with the number of aromatic rings. The hydrogenation of single-aromatic ring moieties was the slowest, that of isolated two-ring aromatics intermediate, and the hydrogenation of the middle of the three fused aromatic ring was fastest.

c) In groups with the same number of fused aromatic rings, hydrogenation reactivity increased with the presence of alkyl substituents and/or naphthenic rings.

Based on the observations of Korre et al. and the structures of the polyaromatic species considered during the reaction network generation in the current work, only two hydrogenation rate coefficients have been used for all the possible aromatic hydrogenation reactions. One rate coefficient is used for all the reactions in which three moles of hydrogen are consumed and another rate coefficient is used for all the reactions in which two moles of hydrogen are consumed.

Table 3-2 shows all the possible hydrogenation modes for one to four ring aromatic species that are considered in the reaction network of aromatics. The 'H' in the ring represents the ring to be hydrogenated. All the molecular classes of subgroup 1 have been assumed to have the same hydrogenation rate coefficient irrespective of the length and number of alkyl substituents on these species. The same is true for the classes of subgroup 2. For the non-isothermal reactor model, two activation energies and two pre-exponential factors are required in the kinetic model. The difference in the reactivities of the molecules of each subgroup is accounted for by the differences in their sorption equilibrium coefficients in the zeolite pores and their chemisorption equilibrium coefficients on the metal sites. As all the classes of subgroup 1 require 3 moles of hydrogen per mole of hydrocarbon, the rate expression for the hydrogenation of all these aromatics is given by eqn (3.40). For the molecular classes of subgroup 2 where only two moles of hydrogen are consumed in hydrogenation, the rate equation has been modified as,

$$r_{hyd} = \frac{k_{hyd,2H_2}^{comp} K_{C,S_{Ai}} H_{S_{Ai}} \left(C_{S_{Ai}}^{liq} C_{H_2}^{liq^2} - \frac{C_{S_{Ni}}^{liq}}{K_{eqm}^{liq}} \right)}{\left[D_L + \sum_i K_{C,S_{Ai}} H_{S_{Ai}} C_{S_{Ai}}^{liq} + K_{C,S_{Ni}} H_{S_{Ni}} C_{S_{Ni}}^{liq} + K_{C,S_{Pi}} H_{S_{Pi}} C_{S_{Pi}}^{liq} \right]} \tag{3.41}$$

The composite frequency factors $A_{hyd,3H_2}^{comp}$ and $A_{hyd,2H_2}^{comp}$ and the activation energies $E_{hyd,3H_2}$ and $E_{hyd,2H_2}$ for the two subgroups have been estimated from the experimental data.

Table 3-2. Classification of aromatics based on the number of moles of hydrogen required for hydrogenation. (The symbol 'H' in a ring represents the ring to be hydrogenated).

Subgroup-1: Each molecule requires three moles of hydrogen
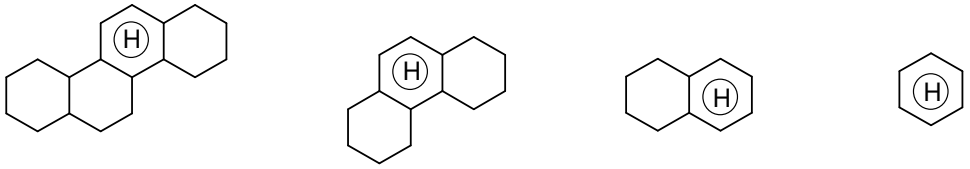
Subgroup-2: Each molecule requires two moles of hydrogen
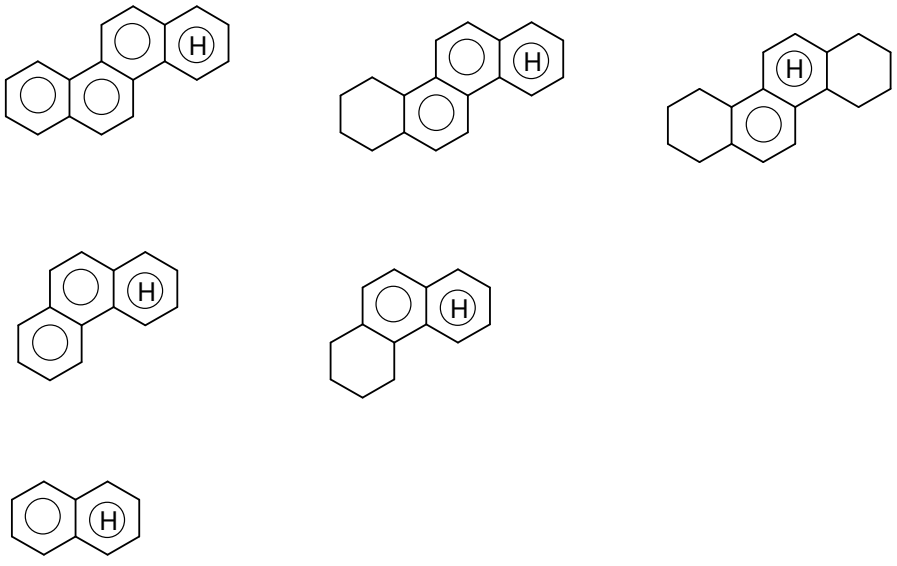

3.4. Competitive Chemisorption on the Metal Sites

It is well established that the chemisorption coefficient for aromatics increases with the increase in the number of aromatic rings. This could be attributed to the increased acid-base interaction of the catalyst and aromatics. It has also been observed that the chemisorption coefficient increases with the increase in the number of hydrogenated rings as well, but to a lesser extent as compared to aromatic rings[69]. Korre et al.[46, 50] regressed the chemisorption coefficients from their extensive experimental data and established temperature independent correlations for chemisorption coefficients on a CoMo/Alumina catalyst as a function of the number of aromatic rings and the number of saturated rings in the ring hydrocarbons. They found the following correlation in which the number of aromatic rings and number of saturated rings are used as the indices,

$$\ln K_C = p_{const}^{chem} + \left(\frac{p_{aro\_rings}^{chem} N_{AR} + p_{sat\_rings}^{chem} N_{SR}}{RT} \right) \tag{3.42}$$

The values of p_{const}^{chem}, $p_{aro\_rings}^{chem}$ and $p_{sat\_rings}^{chem}$ obtained by them were 1.324, 0.887 and 0.123 respectively for their operating conditions and catalyst. The same correlation has been used in the current model considering p_{const}^{chem}, $p_{aro\_rings}^{chem}$ and $p_{sat\_rings}^{chem}$ to be adjustable parameters because of the differences in the catalyst and operating conditions. As seen from the above correlation, the effect of the length and number of side chains has not been considered, as the aromatics studied in this group were mostly bare rings, except for the xylenes. In a typical VGO feedstock, however, the ring species contain long alkyl side chains. No information is currently available on the effect of long side chains on the chemisorption coefficient of ring species. It has been considered negligible in the current model. The chemisorption equilibrium coefficient for paraffins is given using a single parameter by the following equation

$$\ln K_C = p_{paraf}^{chem} \tag{3.43}$$

The dimensionless parameters p_{const}^{chem}, $p_{aro\_rings}^{chem}$, $p_{sat\_rings}^{chem}$ and p_{paraf}^{chem} would give the chemisorption equilibrium coefficient in kg_{cat}/kmol when calculated using eqns (3.42) and (3.43).

3.5. Development of Global Rate Expressions for Acid Site Steps

The rate expression for the conversion of a particular carbenium ion on the acidic sites has been developed in Sections 3.3.1 to 3.3.3 and for the hydrogenation of a given aromatic molecule, the form of the rate expression employed in the kinetic model has been discussed in Section 3.3.4. These rate expressions involve the concentration of a single molecular species present in the VGO feedstock. Since the molecular level composition of complex feedstocks like VGO is not currently accessible using the present day analytical techniques, a certain amount of relumping of individual components is required in the model. Unlike the conventional lumping approaches, this lumping strategy is based on strict thermodynamic principles, grouping only the isomeric species of a homologous series which attain a thermodynamic equilibrium through fast interconversion[*]. A short review on the state-of-the-art characterization techniques for complex petroleum mixtures, a detailed explanation of the lumping strategy employed, and the analysis/composition of the VGO feedstock required as input in the current model has been presented in Section 2.4. It was shown that a total of 1266 pure components/lumps were required for a VGO containing the species up to carbon number 40. All the isomers in a particular lump belong to one molecular class and have the same number of methyl branches. Grouping of the components based on this approach allows the determination of the rates of individual elementary steps using the rate expressions developed in Section 3.3. By using the exhaustive computer generated reaction network of elementary steps, the contribution of each individual elementary step is summed up to estimate the global rate of conversion of a lump '*g*' into another lump

[*] To avoid the confusion in the definition of lump with the less rigorous models, the word 'lump' will be replaced by 'group of isomers' or 'GOI' in the future work and publications based on this dissertation.

'*h*' which are required in the development of continuity equations. This is shown schematically in Figure 3-4 for the case of paraffinic components.

Therefore, the global rate of conversion of a lump '*g*' into another lump '*h*' through $\omega(m;n)$ type of elementary steps of group (a) on the acidic sites is given as follows by using eqn (3.27),

$$R_{\omega(m;n)}^{(g;h)} = \sum n_{e,ikuv} \tilde{k}_{\omega(m;n)} K_{DH,ij}^{liq} K_{pr(S_{Oij} \rightleftarrows S_{Rik}^{+})} C_t \frac{H_{Si} C_{Si}^{liq}}{D_L D_A C_{H_2}^{liq}} \tag{3.44}$$

where the summation is carried out over all the $\omega(m;n)$ type of elementary steps in which carbenium ions of nature *m* belonging to lump *g* are converted to carbenium ions of nature *n* belonging to lump *h*. In eqn (3.44), the concentration of species S_i is obtained from its equilibrium distribution in lump *g* as,

$$C_{Si}^{liq} = y_{Si}^{eqm} C_{Sg}^{liq} \tag{3.45}$$

The same value of Henry's coefficient is used for all the isomers of a lump, so that the denominator term for sorption in the zeolite pores is given by

$$D_L = \left[1 + \sum_{g=1}^{N_{lumps}} K_{L,g} C_{Sg}^{liq} \right] \tag{3.46}$$

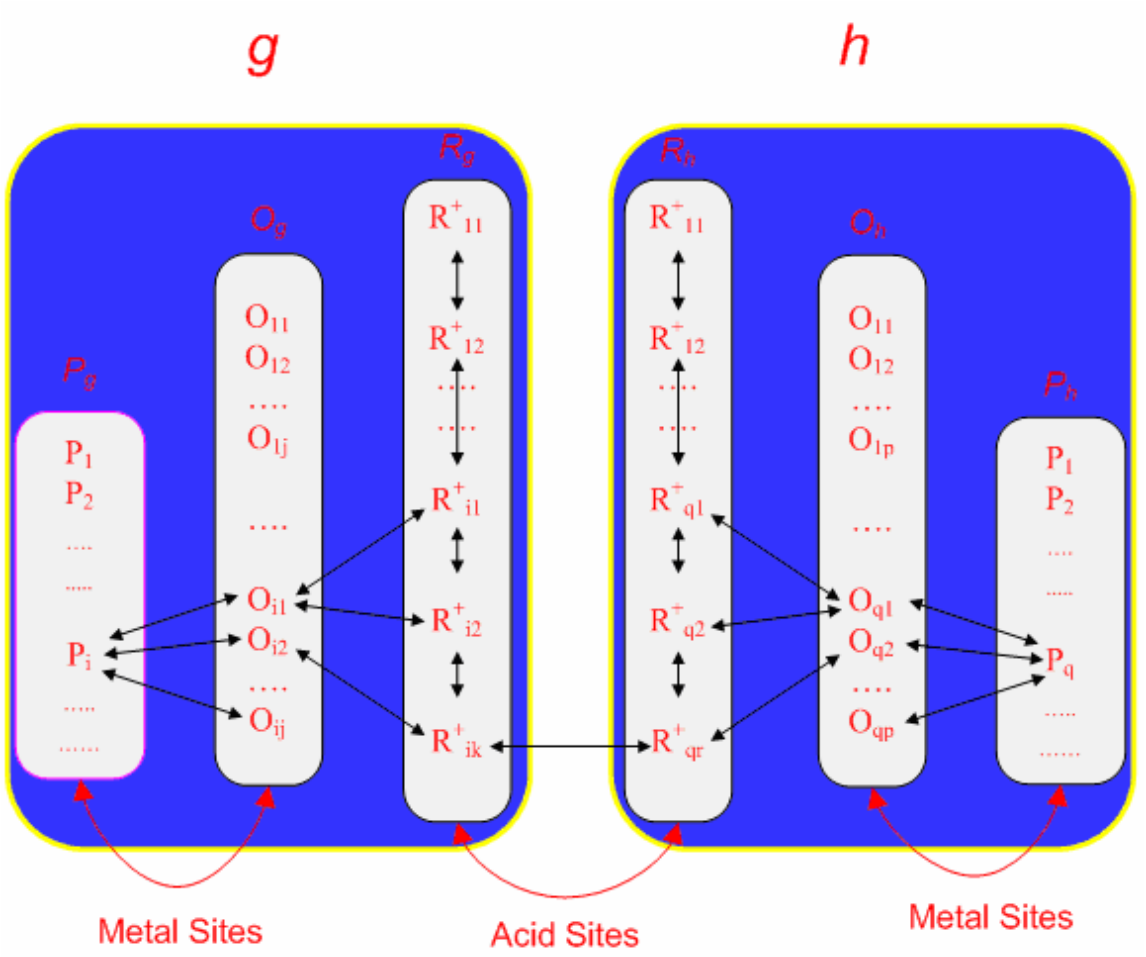

Figure 3-4. Illustration of the lumping of components for the estimation of the global rate of conversion between lumps.

Similarly, for the purpose of estimating the value of D_A, the same value of equilibrium coefficient is considered for the protonation of all olefinic species originating from the isomers of a lump. For the aromatic lumps, the protonation is assumed to occur directly on the aromatic ring,

$$D_A = 1 + \sum_{g=1}^{N_{sat\_lumps}} K_{pr,Og}\left[S_{Og}\right] + \sum_{g=N_{sat\_lumps}+1}^{N_{sat\_lumps}+N_{aro\_lumps}} K_{pr,Ag}\left[S_{Ag}\right] \qquad (3.47)$$

where $\left[S_{Og} \right]$ is the sorbed concentration of the olefins formed from the isomers of lump g in the case of paraffinic and naphthenic lumps and $\left[S_{Ag} \right]$ is the sorbed concentration of aromatic lump g.

The liquid phase dehydrogenation equilibrium coefficients $K_{DH,ij}^{liq}$ are obtained from the gas phase dehydrogenation equilibrium coefficients $K_{DH,ij}^{gas}$ by,

$$K_{DH,ij}^{liq} = K_{DH,ij}^{gas} \left(\frac{C_{total}^{liq}}{K_{H_2}^{VLE}} \right) \tag{3.48}$$

which in turn are estimated using the Benson's group contribution method. The protonation equilibrium coefficient $K_{pr(S_{Oij} \rightleftarrows S_{Rik}^{+})}$ can be expressed in terms of the single event protonation equilibrium coefficient by taking out the symmetry contributions as,

$$K_{pr(S_{Oij} \rightleftarrows S_{Rik}^{+})} = \left(\frac{\sigma_{gl}^{S_{Oij}}}{\sigma_{gl}^{S_{Rik}^{+}}} \right) \tilde{K}_{pr(S_{Oij} \rightleftarrows S_{Rik}^{+})} \tag{3.49}$$

In previous work[11, 22, 70] on single event kinetic modeling of hydrocracking, the protonation equilibrium coefficient was estimated by involving a reference olefin S_{Or} so that the protonation step $S_{Oij} \rightleftarrows S_{Rik}^{+}$ was written as,

$$S_{Oij} \rightleftarrows S_{Or} \rightleftarrows S_{Rik}^{+} \tag{3.50}$$

The reference olefin was chosen from the same class as the parent species S_i in such a way so that the double bond is located between a secondary and tertiary carbon atom. It was further assumed that the protonation equilibrium coefficient of the reference olefin can have only two values depending on the nature of the protonated carbenium ion. Therefore, from eqn (3.50)

$$\tilde{K}_{pr(S_{Oij} \rightleftarrows S_{Rik}^{+})} = \tilde{K}_{isom(S_{Oij} \rightleftarrows S_{Or})} \tilde{K}_{pr(S_{Or} \rightleftarrows m)} \tag{3.51}$$

where *m* can be *s* or *t*. The isomerization equilibrium coefficient was calculated from the Benson's group contribution method. It has been shown in the current work that the involvement of the reference olefin is not necessary for obtaining the protonation equilibrium coefficients. Therefore, irrespective of the olefinic species S_{Oij}, only two single event protonation equilibrium coefficients, $\tilde{K}_{pr(S_{Oij} \rightleftarrows s)}$ and $\tilde{K}_{pr(S_{Oij} \rightleftarrows t)}$ are required in the model. This will be discussed in more details in section 3.6.

The final rate equation is obtained by combining eqns (3.44), (3.45), (3.48) and (3.49):

$$R_{\omega(m;n)}^{(g;h)} = \sum n_{e,ikuv} \left(\frac{\sigma_{gl}^{S_{Oij}}}{\sigma_{gl}^{S_{Rik}^+}} \right) K_{DH,ij}^{gas} y_{Si}^{eqm} \tilde{k}_{\omega(m;n)} \tilde{K}_{pr(S_{Oij} \rightleftarrows m)} C_t \frac{H_g C_{Sg}^{liq}}{D_L D_A C_{H_2}^{liq}} \left(\frac{C_{total}^{liq}}{K_{H_2}^{VLE}} \right) \quad (3.52)$$

The above equation can be expressed as,

$$R_{\omega(m;n)}^{(g;h)} = LC_{\omega(m;n)}^{(g;h)} \tilde{k}_{\omega(m;n)}^{comp} \frac{H_g C_{Sg}^{liq}}{D_L D_A C_{H_2}^{liq}} \left(\frac{C_{total}^{liq}}{K_{H_2}^{VLE}} \right) \quad (3.53)$$

where $LC_{\omega(m;n)}^{(g;h)}$ is called the lumping coefficient of formation *(LCF)* of lump *h* from lump *g* and is given by,

$$LC_{\omega(m;n)}^{(g;h)} = \sum n_{e,ikuv} \left(\frac{\sigma_{gl}^{S_{Oij}}}{\sigma_{gl}^{S_{Rik}^+}} \right) K_{DH,ij}^{gas} y_{Si}^{eqm} \quad (3.54)$$

The lumping coefficients are functions of temperature only and do not depend on the feedstock composition. The values of lumping coefficients are calculated at a temperature interval of 5 ^{o}C and are utilized during the integration of the ODEs in the non-isothermal reactor simulations. Using the central difference approach, the lumping coefficients evaluated at temperature t are used for reactor temperature from $t - \frac{\Delta t}{2}$ to $t + \frac{\Delta t}{2}$, where Δt is 5 ^{o}C. As the total number of pure components/lumps is quite large, viz. 1266, and each one can be consumed through a maximum of 26 subtypes of

elementary steps/reactions (obtained by summing over $\omega(m;n)$, cyclization, dealkylation and ring hydrogenation/dehydrogenation), the *LCF* is a three dimensional matrix of size 1266 x 1266 x 26, and therefore requires a large amount of hard disk space at each temperature. To save hard disk space and the CPU time in reading the large files during the non-isothermal reactor simulations, only the non-zero elements of *LCF* are stored along with their indices resulting in more than 99% saving in disk space. To find the cumulative lumping coefficient for the consumption of a lump *g* to all possible lumps through a given type of elementary step, the elements of the *LCF* matrix are summed up as follows to generate a two dimensional matrix called the lumping coefficient of consumption *(LCC)* of size 1266 x 26,

$$LCC^{g}_{\omega(m;n)} = \sum_{h} LC^{(g;h)}_{\omega(m;n)} \tag{3.55}$$

This matrix is stored along with *LCF* for each temperature interval to avoid the repetitive summation during the integration of ODEs for computational efficiency. The lumping coefficient for the consumption of different classes through *pcp(s;s)* elementary steps at 350 ^{o}C are plotted in Figure 3-5, showing the increase in the lumping coefficients with the carbon number in a homologous series. As mentioned earlier (Section 2.4), the four ring species are not divided based on the number of branches and thus have only one curve, shown in blue.

$\tilde{k}^{comp}_{\omega(m;n)}$ in eqn (3.54) is the composite single event rate coefficient given by,

$$\tilde{k}^{comp}_{\omega(m;n)} = \tilde{k}_{\omega(m;n)} \tilde{K}_{pr(S_{Oij} \rightleftarrows m)} C_t \tag{3.56}$$

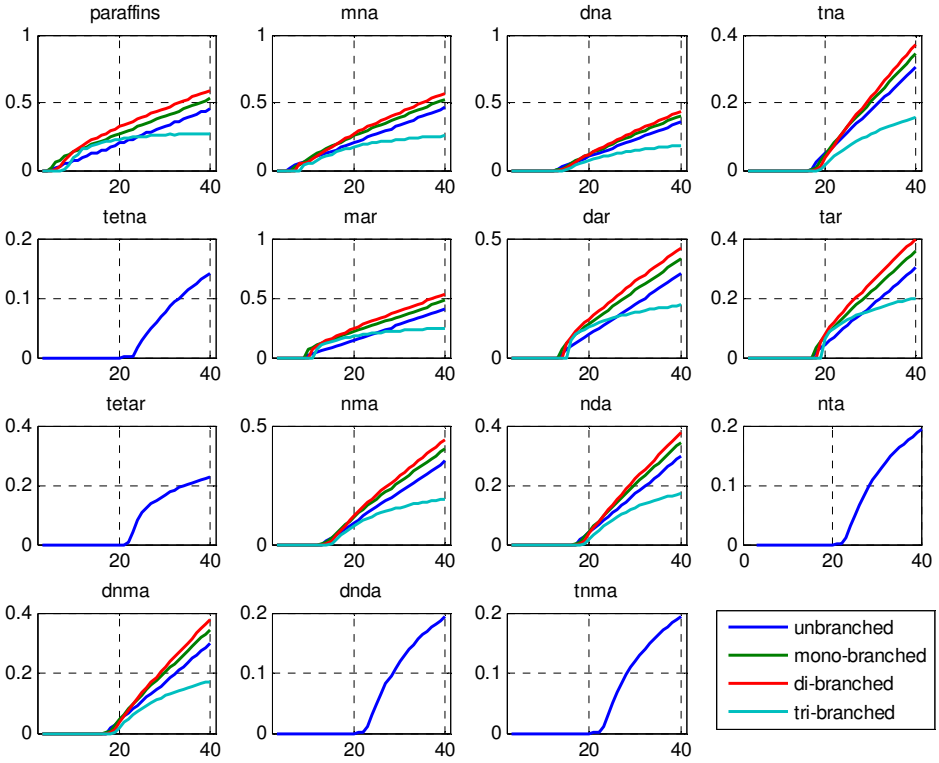

Figure 3-5. Lumping coefficients for the consumption of different classes through *pcp(s;s)* steps. (The x-axis is the carbon number).

Using the thermodynamic constraints on the rate coefficients of the forward and reverse steps[11], it can be shown that the composite rate coefficients for the *(s;t)* and *(t;s)* isomerization steps are identical, i.e., $\tilde{k}^{comp}_{isom(s;t)} = \tilde{k}^{comp}_{isom(t;s)}$.

From eqn (3.56), assuming that the *intrinsic* entropy of protonation does not depend on the nature of the product carbenium ion, the composite single event frequency factor and the composite activation energy are expressed as

$$\tilde{A}^{comp}_{\omega} = \tilde{A}_{\omega} C_t \exp\left(\frac{\Delta \hat{S}_{pr}}{R}\right) \tag{3.57}$$

$$E^{comp}_{\omega(m;n)} = E_{\omega(m;n)} + \Delta H_{pr(S_{Oij} \rightleftarrows m)} \tag{3.58}$$

These parameters are estimated from the experimental data. Rate expressions similar to eqn (3.53) are derived for the elementary steps of group (b) and (c) also.

3.6. Elimination of the Need of Reference Olefins

The concept of reference olefins was introduced by Baltanas et al.[11] to model the rate coefficients for the deprotonation steps as the protonation/deprotonation steps were not considered to be at pseudo-equilibrium. Svoboda et al.[16] later showed that the protonation/deprotonation steps are potentially much faster than other acid sites elementary steps and reach a pseudo-equilibrium. Based on the assumed structure of the activated complex of the protonation step, it was hypothesized that the single event protonation equilibrium coefficient $\tilde{K}_{pr(S_{Oij} \rightleftarrows S^{+}_{Rik})}$ depends on the structure of the olefin and the nature of the product carbenium ion but not on its structure. The dependency of the structure of the reacting olefin was factored out using a reference olefin so that the single event protonation equilibrium coefficient for $S_{Oij} \rightleftarrows S^{+}_{Rik}$ was given by eqn (3.51) repeated here for reference,

$$\tilde{K}_{pr(S_{Oij} \rightleftarrows S^{+}_{Rik})} = \tilde{K}_{isom(S_{Oij} \rightleftarrows S_{Or})} \tilde{K}_{pr(S_{Or} \rightleftarrows m)} \tag{3.51}$$

In the proposed approach it is hypothesized based on to the similarities in the structures that the differences in the energies and intrinsic entropies of the reacting olefins and corresponding carbenium ions in different protonation steps are constant, and therefore, the single event protonation equilibrium coefficient depends only on the nature of the product carbenium ion, leading to only two values. In other words, this hypothesis accounts for the dependence of the energies of carbenium ions on their nature as well as their structures, however, the latter effect is cancelled out because of the similar olefin structure. In this work a group contribution method has been developed to estimate the heats of formation of the paraffinic carbenium ions in gas phase. By calculating the heats of formation of the reacting olefins using the Benson's group contribution method, the

lumping coefficients are calculated using the true values of the protonation equilibrium coefficients and compared with the lumping coefficients calculated based on the old and new hypothesis, proving the superiority of the latter.

To make this comparison, the effect of the structure of the carbenium ion on the protonation equilibrium coefficient is factored out by introducing a reference carbenium ion S_{Rr}^{+} corresponding to the given reference olefin S_{Or} so that,

$$\tilde{K}_{pr(S_{Oij} \rightleftarrows S_{Rik}^{+})} = \tilde{K}_{isom(S_{Oij} \rightleftarrows S_{Or})} \tilde{K}_{pr(S_{Or} \rightleftarrows S_{Rr}^{+})} \tilde{K}_{isom(S_{Rr}^{+} \rightleftarrows S_{Rik}^{+})} \tag{3.59}$$

The reference carbenium ion can be secondary or tertiary, depending on the nature of the original carbenium ion R_{ik}^{+}. By comparing eqns (3.51) and (3.59) it can be observed that in the previous approach, the isomerization equilibrium coefficients from the reference carbenium ion to the actual product carbenium ion, $\tilde{K}_{isom(S_{Rr}^{+} \rightleftarrows S_{Rik}^{+})}$ was assumed to be unity. On the other hand, in the proposed approach the product $\tilde{K}_{isom(S_{Oij} \rightleftarrows S_{Or})} \tilde{K}_{isom(S_{Rr}^{+} \rightleftarrows S_{Rik}^{+})}$ is assumed to be unity, as only two single event protonation equilibrium coefficients are required. It can be inferred from the comparisons shown in Figure 3-6 that these two equilibrium coefficients are correlated inversely so that their product has less deviation from unity compared to the deviation from unity of $\tilde{K}_{isom(S_{Rr} \rightleftarrows S_{Rik}^{+})}$ alone.

Figure 3-6 shows the lumping coefficients for the consumption of paraffins through β-scission steps for three different cases:

3.6.1. Lumping Coefficients with Reference Olefins (Case 1)

In this case, it is assumed that $\tilde{K}_{isom(S_{Rr}^{+} \rightleftarrows S_{Rik}^{+})}$ is unity. Therefore, these are the LCs based on the old hypothesis. These plots are named as ‘wro’ i.e., ‘with reference olefins’.

3.6.2. Lumping Coefficients without Reference Olefins (Case 2)

In this case, it is assumed that the product $\tilde{K}_{isom(S_{Oij} \rightleftarrows S_{Or})} \tilde{K}_{isom(S^+_{Rr} \rightleftarrows S^+_{Rik})}$ is unity. These plots are names as 'nro' i.e., 'no reference olefin' as they have been estimated without using the reference olefin as per the new hypothesis.

3.6.3. True Lumping Coefficients (Case 3)

These lumping coefficients are calculated using the true gas phase protonation equilibrium coefficient $\tilde{K}_{pr(S_{Oij} \rightleftarrows S^+_{Rik})}$ which is estimated from on the precise values of the heats of formation of the olefin and the protonated carbenium ion. Obviously, this case does not need any reference olefin or reference carbenium ion and the lumping coefficients are obtained from the complete eqn (3.59). This approach has been used in the hydrocracking of pure paraffins [Chapter VI] as the method to estimate the heats for formation of paraffinic carbenium ions is available. It should be noticed that this approach can not be used currently for naphthenic and aromatic species due to the unavailability of a group contribution type of estimation method for the heats of formation of ring containing ions. Therefore, the lumping coefficients based on old and new approaches are compared with the true LCs for the paraffinic species and the new approach, which is found to be superior, has been followed for the naphthenic and aromatic species in the VGO hydrocracking model.

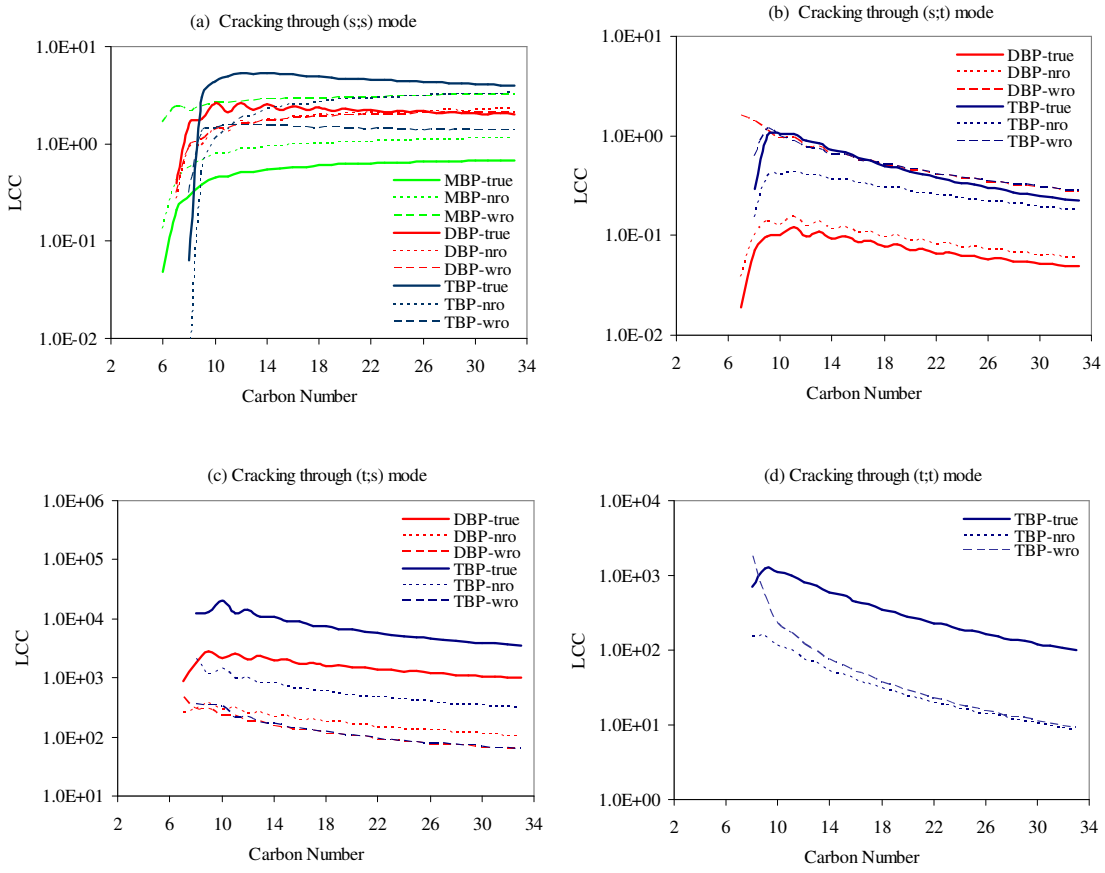

Figure 3-6. Comparison of the *true* lumping coefficients with the lumping coefficients calculated with and without reference olefins.

It can be seen from Figure 3-6 that, except for the cracking of tribranched paraffins through *(s,t)* and *(t,t)* modes [plots (b) and (d)], the proposed method (Case 2) gives lumping coefficients much closer to the true values (Case 3), as compared to the old approach (Case 1). Even in these two exceptions, the lumping coefficients in Case 1 are only slightly better than Case 2. Based on the plots it can also be inferred that $\tilde{K}_{isom(S_{Oij} \rightleftarrows S_{Or})}$ and $\tilde{K}_{isom(S^{+}_{Rr} \rightleftarrows S^{+}_{Rik})}$ are correlated inversely, as speculated. This phenomenon can be explained based on the similarities of the skeleton structures of a

given olefin O_{ij} with the corresponding carbenium ion R_{ik}^{+} and the differences in their structures from their respective reference species. An example can be given based on the differences in the degree of branching. For a dibranched olefin O_{ij}, the carbenium ion R_{ik}^{+} would be dibranched, whereas both the reference olefin and the reference carbenium ion would be monobranched. Therefore, $\tilde{K}_{isom(S_{Oij} \rightleftarrows S_{Or})}$ corresponds to a decrease in the degree of branching, whereas $\tilde{K}_{isom(S_{Rr}^{+} \rightleftarrows S_{Rik}^{+})}$ corresponds to an analogous increase in the degree of branching, tending to offset their deviations from unity in a way so that their product is more close to unity than either one separately.

3.7. Competitive Chemisorption on the Acidic Sites

To account for the strong competitive chemisorption of aromatics on the acidic sites eqn (3.53) (as well as the rate expressions for group (b) and (c)) contains the denominator term D_A, which is given by eqn (3.47). The evaluation of D_A requires the values of the protonation equilibrium coefficients. In all the rate expressions for acid site transformations except those for the group (c), i.e., dealkylation of aromatics, the numerator contains the equilibrium coefficients for the protonation of the reactive olefinic species. The concentration of these reactive olefinic species is very low because of the small values of the dehydrogenation equilibrium coefficients and high hydrogen pressure. Therefore, the contribution towards the total coverage of acidic sites due to the protonation of these species would be relatively small. Because of this, the estimate of the equilibrium coefficient for the protonation of the olefinic species to be used in the denominator has been obtained from the literature (as discussed below) and is considered constant for a given catalyst during the parameter estimation. On the other hand, the (single event) protonation equilibrium coefficient in the numerator is coupled with the single event rate coefficients of the elementary steps as seen from eqn (3.56) and this composite rate coefficient is estimated from the experimental data on VGO hydrocracking. Similarly for the dealkylation of the aromatics, the rate coefficient coupled with the corresponding ring protonation equilibrium coefficients is estimated

from the experimental data and the ring protonation equilibrium coefficients for different aromatic classes to be used in the denominator have been estimated from the literature information. The approach for the estimation of various terms required to calculate the acid site denominator is discussed below.

3.7.1. Dehydrogenation Equilibrium Coefficient

A single average value has been used for the dehydrogenation equilibrium coefficient of paraffins to estimate the concentration of corresponding olefins. This is justified given the small contribution of olefins towards the acid site coverage when large amount of aromatics are present in the feed. The value of the dehydrogenation equilibrium coefficient depends primarily on the nature of the carbon atoms where the double bond is formed if the effect of the olefin structure in the vicinity of the double bond is ignored. Therefore, five different dehydrogenation equilibrium coefficients can be considered for the *(p-s)*, *(p-t), (s-s)*, *(s-t)* and *(t-t)* modes. The heats of dehydrogenation for these 5 modes range from approximately 105 to 126 kJ/mol. A value of 109 kJ/mol has been retained. It corresponds to the *(s-t)* mode which is most important for the production of tertiary carbenium ions having the highest occupancy on the acid sites. The olefins produced through *(p-s)* and *(s-s)* modes can only produce secondary ions and *(p-t)* and *(t-t)* modes have a much smaller contribution towards the formation of total olefins than the *(s-t)* mode. Similarly, the entropy of dehydrogenation has been taken to be 120 J/mol/K for the *(s-t)* mode. For naphthenes with 1-ring to 4-rings, it has been assumed that dehydrogenation is taking place primarily in the ring because of the higher affinity of the ring towards the chemisorption on the metal sites. The heat of dehydrogenation and entropy of dehydrogenation of 112 kJ/mol and 136 J/mol/K respectively for the *(s-t)* mode in the molecule shown in Figure 3-7 are taken as the representative values for all the naphthenic components/lumps. These values are used to estimate the concentration of the olefinic species in eqn (3.47).

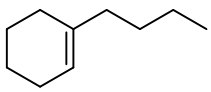

Figure 3-7. The representative molecule considered for the dehydrogenation equilibrium coefficients of naphthenes.

3.7.2. Heats of Protonation

The values of the gas phase standard state heats of protonation are obtained from the corresponding proton affinities (PA) compiled by Hunter and Lias[71]. The available values of proton affinities of some species relevant to this work are given in Table 3-3.

A single value of PA has been considered for all the lumps of a particular class assuming that it does not change with the carbon number. Since the proton affinities of all the classes considered in the model are not available, certain simplifying assumptions were made based on the trends of the above data.

For linear olefins formed from normal paraffins, PA corresponds to the formation of secondary carbenium ions. Because of much higher stability of tertiary carbenium ions compared to secondary ions, it has been assumed that all the isoparaffins and naphthenes form the tertiary ions. Consequently, for the branched olefins formed from isoparaffins, a PA of 821.4 kJ/mol is used. In the absence of any published information for multiring naphthenic olefins, the PA of 1-methylcyclohexene has been used as the representative value for all the naphthenes. It can be seen from the above data that increasing the substitution on the benzene ring increases the PA, but the increase in the side chain length does not affect it very much. An Increase in the number of aromatic rings also increases PA.

Table 3-3. Gas phase proton affinities for the formation of most stable carbenium ion. (taken from Hunter and Lias[71]).

Species	Gas phase proton affinity (kJ/mol)
Linear Olefins (protonated to -sec ions, an average value)	773.3
Branched Olefins (protonated to -ter ions, an average value)	821.4
Cyclopentene	766.3
1-methylcyclopentene	816.5
Cyclohexene	784.5
1-methylcyclohexene	825.1
Benzene	750.4
Toluene	784.0
Ethylbenzene	788.0
Propylbenzene	790.1
Isopropyl benzene	791.6
n-butyl benzene	791.9
p-xylene	794.4
o-xylene	796.0
m-xylene	812.1
1,3,5 trimethylbenzene	836.2
Tetraline	809.7
Naphthalene	802.9
2-methylnaphthalene	831.9
Phenanthrene	825.7
Chrysene	840.9
1,2,3,4,5,6,7,8 octahydrophenthranene	846.2

The possible effect of the degree of substitution has been applied for different aromatic classes based on the data of the above table. On an average, the PA of the mono substituted aromatic species are taken in the model and an average of 10 kJ/mol have been added to the values of PA to account for the effect of substitution on bare ring aromatics. When the PA for naphtheno-aromatics are not available, their values are obtained from the corresponding aromatics with the same number of aromatic rings. i.e., the value of PA for dinaphtheno-diaromatics (DNDA) is considered identical to that of diaromatics (DAR). Based on these assumptions, the values shown in Table 3-4 are used for the gas phase proton affinities of different classes in the model. The gas phase heats of protonation are obtained as the negative of the corresponding proton affinities.

Table 3-4. Proton affinities for different classes used in the model.

Sr. No.	CLASS	PA (kJ/mol)	Reasoning
1.	NPA	773.3	For secondary carbenium ions
2.	IPA	821.4	For tertiary carbenium ions
3.	Naphthenes	825.1	Value of 1-methylcyclohexene
4.	MAR	791.9	The value of butyl benzene
5.	DAR, NDA, DNDA	831.9	The value of 2-methyl-naphthalene
6.	TAR, NTA	835.7	The value of phenanthrene + 10.0 kJ/mol for 1 substitution
7.	QAR	850.9	The value of chrysene + 10.0 kJ/mol for 1 substitution
8.	NMA	819.7	The value of tetraline + 10.0 kJ/mol for 1 substitution
9.	DNMA, TNMA	846.2	The value of octahydrophenanthrene

3.7.3. Heats of Stabilization

To get the heats of protonation at the surface of the catalyst, the heats of stabilization of carbenium ions from gas phase to the catalyst surface are required. Refer Chapter VI for derivation of the equation to relate the gas phase heats of protonation to the surface heats of protonation as,

$$\Delta H_{pr}^{sur} = \Delta H_{pr}^{gas} + \Delta q(z,m) \tag{3.60}$$

where Δq is the negative of the relative heat of stabilization of the carbenium ions defined as the difference in the heat of stabilization of proton and carbenium ion. Considering that the extent of stabilization of a carbenium ion would depend primarily on the local structure in the vicinity of the positive charge, it is assumed that Δq does not depend on the carbon number and depends only on its nature and the molecular class to which it belongs. The estimates of the values of Δq for paraffins have been reported by several authors[72-75]. As the heats of stabilization depend on the acidity of the catalyst, the values reported by different authors vary significantly. The difference in the heats of stabilization of the secondary and tertiary paraffinic carbenium ions has been determined from the experimental data on the hydrocracking of pure n-hexadecane in the current work (Chapter VI) and is used in the VGO hydrocracking model. In the absence of any published information, the heats of stabilization of naphthenic carbenium ions have been given the same values as those for the tertiary paraffinic carbenium ions. The relatively lower importance of this parameter due to the low contribution of paraffinic and naphthenic species on the total acid site coverage justifies this assumption. For aromatics and naphtheno-aromatics, Δq has been assumed to be independent of the nature of the carbenium ions due the charge delocalization at the aromatic rings. In the absence of information on the heats of stabilization of different aromatic ring containing classes, a single value, $\Delta q(S_A^+)$, has been considered as a parameter in the model for all these classes. This parameter was then adjusted from the experimental data on the hydrocracking of VGO available to us.

3.7.4. Entropy of Protonation

The entropy of protonation has been estimated using statistical thermodynamics based on the loss of various degrees of freedom (DOF) in the protonation step. As the protonation takes place, the olefinic and aromatic species from the sorbed phase are attached to the acidic sites and thus the change in the entropy from the sorbed state to the protonated state is of interest. As a molecule loses some of its rotational or translational degrees of freedom, it gains some extra vibrational degree of freedom. It has been assumed that the difference in the sum of the rotational and vibrational degrees of freedom of the molecule from sorbed state and protonated state is negligible. Further assuming that the sorption step results in the loss of one translation degree of freedom and the protonated species has no translational motion, two translational DOF are taken as the entropy of the protonation step in the model. The entropy corresponding to three translational DOF is calculated from eqn (3.61) in which the translational partition function is given by eqn (3.62).

$$S_t / R = \ln(Q_t) + 5/2 \tag{3.61}$$

$$Q_t = \left(\frac{2\pi m k_B T}{h^2} \right)^{3/2} V \tag{3.62}$$

3.8. Parameters for Sorption

To estimate the concentration of the sorbed species in the zeolite pores, the Henry coefficients for sorption is required, as shown in eqns (3.17) and (3.18). Very few experimental data is available in the literature on the sorption of complex compounds found in the heavy petroleum feedstocks. Denayer et al.[76] carried out experiments for the sorption of alkanes, aromatics and some organic molecules in the liquid phase and in the dense vapor phase on FAU zeolites, normally employed in the hydrocracking process. They reported the values of the partition coefficients for normal paraffins from C_5 to C_{16}, some light isoparaffins, benzene, toluene and mesitylene in Na-USY zeolite at room temperature with n-octane and methanol as the mobile phases. With the non polar n-octane as the mobile liquid phase, the partition coefficients of paraffins were found to be

very week functions of the carbon number of the adsorbate. On the other hand, with methanol as the mobile liquid phase, the partition coefficients of paraffins increased with the carbon number because of the polarity of the mobile phase. No data is available for the effect of carbon number on the partition coefficients of naphthenes and aromatics. In the hydrocracking of pure paraffins (Chapter VI), the Henry coefficients are assumed to be constant with respect to the carbon number of adsorbent, considering the absence of any polar compounds. In the hydrocracking of VGO on the other hand, considering the presence of some polar compounds, it is assumed that the partition coefficients increase with the carbon number. Three different base values of partition coefficients are selected: one for paraffins, naphthenes and aromatics each, i.e., $K_{paraf,base}$, $K_{Nap,base}$ and $K_{Aro,base}$. An increase in the partition coefficient by 8% per carbon number has been considered to account for the effect of chain length. The increase in the value of the partition coefficients in the ring compounds from its base value is related to the number of saturated acyclic carbon atoms in the molecule. For example, a diaromatic C_{15} molecule contains 5 saturated acyclic carbon atoms, so that its partition coefficient is calculated from the base value as,

$$K_{DAR,C15} = K_{Aro,base} \mathrm{x} \left(1.08\right)^5 \tag{3.63}$$

Initial estimates of the base values of partition coefficients were taken from the literature[76]. The percent increase per carbon number and the base values were later adjusted during the parameter estimation by using the VGO hydrocracking experimental data. The Henry coefficients were calculated from the partition coefficients by dividing them by the catalyst bulk density. The Langmuir adsorption coefficient $K_{L,Si}$ for lump S_i is finally obtained from (3.18) by using the saturated density $c_{sat,Si}$ of lump S_i.

CHAPTER IV

REACTOR MODEL AND PARAMETER ESTIMATION

4.1. Reactor Model

The global rate expressions developed in Chapter III are plugged into a three-phase multibed tubular reactor model operated adiabatically with inter-stage hydrogen quenching. Under typical industrial operating conditions, hydrocracking reactors operate in trickle flow regime with a fixed bed of porous catalyst particles and a vapor phase and a liquid phase flowing co-currently. It is assumed in what follows that the particles are completely wetted and the gas and liquid phases are in plug flow. As the aromatic hydrogenation and hydrocracking reactions proceed, H_2 is transferred from gas to the liquid phase and the lighter products formed by cracking steps are transferred from the liquid phase into the gas phase. This inter-phase mass transfer flux is described using the two film theory.[77] For a particular lump S_g, the molar flux from gas to liquid phase is given by the following equation

$$N_{Sg} = k_{O,Sg}\left(\frac{C_{Sg}^{gas}}{K_{Sg}^{C,VLE}} - C_{Sg}^{liq}\right) \tag{4.1}$$

In the above equation, the overall mass transfer coefficient is given by

$$\frac{1}{k_{O,Sg}} = \frac{1}{k_G K_{Sg}^{C,VLE}} + \frac{1}{k_L} \tag{4.2}$$

For the trickle flow regime, the value of the liquid phase mass transfer coefficient $k_L a_v$ has been calculated from a correlation given by Sato[78] and the gas side mass transfer coefficient $k_G a_v$ is calculated from Reiss'[79] correlation. The gas-liquid interfacial area a_v is calculated by the correlation given by Charpentier.[80] $K_{Sg}^{C,VLE}$ is the *concentration* equilibrium partition coefficient relating the equilibrium concentrations of lump S_g in the gas and liquid phases as

$$K_{Sg}^{C,VLE} = \frac{C_{Sg}^{gas}}{C_{Sg}^{liq}} \tag{4.3}$$

$K_{Sg}^{C,VLE}$ is expressed in terms of the *true* equilibrium partition coefficient K_{Sg}^{VLE} as $K_{Sg}^{C,VLE} = \left(\frac{y_{Sg}}{x_{Sg}}\right)\left(\frac{C_{total}^{gas}}{C_{total}^{liq}}\right) = K_{Sg}^{VLE}\left(\frac{C_{total}^{gas}}{C_{total}^{liq}}\right)$. The values of the equilibrium partition coefficient K_{Sg}^{VLE} are calculated using the Peng-Robinson equation of state. The continuity equations for the gas phase components/lumps and hydrogen are written as

$$\frac{1}{\Omega}\frac{dF_{Sg}^{gas}}{dz} = -k_{O,Sg}a_v\left(\frac{C_{Sg}^{gas}}{K_{Sg}^{C,VLE}} - C_{Sg}^{liq}\right) \quad g = 1,2,.....N_{lumps} \tag{4.4}$$

The continuity equations for components/lumps in the liquid phase also take into account the net rate of formation of component/lump *g* along with the gas-liquid mass transfer flux term,

$$\frac{1}{\Omega}\frac{dF_{Sg}^{liq}}{dz} = k_{O,Sg}a_v\left(\frac{C_{Sg}^{gas}}{K_{Sg}^{C,VLE}} - C_{Sg}^{liq}\right) + R_{Sg,net}^{Form} \quad g = 1,2,.....N_{lumps} \tag{4.5}$$

The mass transfer resistance between the liquid and solid phases and the intra-particle diffusional resistance has been considered to be negligible. As discussed earlier, the composition of VGO in this model is defined in terms of 1266 lumps/pure components. Therefore in the three-phase hydrocracking of VGO, 1267 (viz., 1266 + 1 for hydrogen) continuity equations for the liquid phase and the same number of continuity equations for the gas-phase components/lumps are required.

A significant amount of heat is released during the hydrogenation of aromatics/naphtheno-aromatics and the hydrocracking reactions. The liquid phase temperature profile along the reactor bed is obtained from eqn (4.6)

$$\frac{dT^{liq}}{dz} = \frac{\left(\sum_{g=1}^{N_{lumps}} \left(-\Delta H_{f,g}^{liq}\right) R_{Sg,net}^{Form} - \sum_{g=1}^{N_{lumps}} \frac{dF_{Sg}^{gas}}{dz} \lambda_{Sg} \right)}{\sum_{g=1}^{N_{lumps}} \left(F_{Sg}^{gas} C_{P,Sg}^{gas} + F_{Lg}^{liq} C_{P,Sg}^{liq} \right)} \tag{4.6}$$

In the numerator of eqn (4.6), the first term represents the total heat of reaction and is calculated using the heats of formation of individual lumps/pure components obtained from the Benson's group contribution method. The second term accounts for the heat consumed during the vaporization of lighter components from the liquid to the gas phase. The heat transfer resistance between the gas and liquid phase has been assumed to be negligible. The temperature of the solid phase is obtained from eqn (4.7)

$$T^{solid} = T^{liq} + \frac{\sum_{g=1}^{N_{lumps}} \left(-\Delta H_{f,g}^{liq}\right) R_{Sg,net}^{Form}}{a_{LS}\, h_{LS}} \tag{4.7}$$

in which the solid-liquid heat transfer coefficient h_{LS} has been estimated using the correlation of Whitaker[81].

The set of equations given by (4.4), (4.5) and (4.6) consists of 2,535 (= 1267 x 2 +1) *stiff* ODEs which is solved using the backward differentiation method (BDF). The subroutine DLSODA of the FORTRAN library ODEPACK has been used for the integration of ODEs. The integration of this set of ODE was found to be extremely slow with numerically calculated Jacobian matrices because of the large number of function evaluations for each Jacobian. A subroutine has been written to get an approximate analytical Jacobian for this system reducing the total integration time by 2-3 orders of magnitude.

The initial conditions for the gas and liquid molar flow rates are obtained by a VLE flash calculation at the reactor inlet temperature and pressure. A maximum allowable temperature rise ΔT_{max} is specified for each reactor bed. The integration is carried out till the reactor temperature reaches $T_{in} + \Delta T_{max}$ after which a cold stream of hydrogen at

temperature T_{H_2} is injected to quench the reaction mixture. The amount of hydrogen required to bring the temperature of the reaction mixture back to the temperature of the inlet to the previous bed, T_{in} is calculated from:

$$F_{H_2,quench} = \frac{\sum_{g=1}^{N_{lumps}} \left(F_{Sg}^{gas} C_{P,Sg}^{gas} + F_{Lg}^{liq} C_{P,Sg}^{liq} \right) \left(T_{out} - T_{in} \right)}{C_{P,H_2}^{gas} \left(T_{H_2} - T_{in} \right)} \tag{4.8}$$

4.2. Estimation of Properties

The various physical and chemical properties of the lumps/pure components involved in the model are estimated using the following methods:

Critical temperature and critical pressure are calculated using Jobak's group contribution method[82] and API recommended methods.

Saturated and compressed liquid phase densities are estimated using Hankinson and Thomson (HBT) method[82].

The viscosities of gas and liquid phases are calculated by the method of Twu et al.[83]

Vapor pressures and latent heat of vaporization are calculated using the method of Prausnitz et al.[84]

Heats of formation, entropies, equilibrium coefficients, and gas phase heat capacities are calculated using Benson's group contribution method[65].

Liquid phase heat capacities are estimated from Garvin et al.[85]

4.3. Parameter Estimation

The parameters involved in the VGO hydrocracking model are summarized in Table 4-1 with their definition and units. These parameters have been estimated from a relatively small amount of experimental data on the three phase hydrocracking of a VGO feedstock obtained from a lab scale tubular reactor. The product composition was available in terms of the weight percent of normal and isoparaffins, one to four ring naphthenes, and

one to four ring aromatics classes. The composition of naphtheno-aromatic classes was not available separately and was combined with the corresponding aromatics classes, e.g., one ring aromatics include the monoaromatics, naphtheno-monoaromatics, dinaphtheno-monoaromatics and trinaphtheno-monoaromatics. An estimate of the carbon number distribution was available for normal paraffins, isoparaffins, mononaphthenes, dinaphthenes and trinaphthenes classes. The initial guess of the parameters were obtained from the literature[46, 70, 72, 73, 76, 86] when available or have been selected judiciously otherwise. This information was utilized to estimate the model parameters first by manual tuning followed by the application of Levenberg-Marquardt's optimization algorithm to minimize the sum of square of the residuals between the experimental and model predicted responses. The final values of the parameters have not been reported in the dissertation because of proprietary reasons as the model has been licensed to an industrial organization. The optimized parameters related to steps on the acid sites have been found to satisfy the rules of carbenium ion chemistry. The activation energies corresponding to the saturation of aromatics are in the range of 25 to 50 kJ/mol as reported in the literature[46, 59]. The relative magnitude of the parameters related to the sorption in the zeolite pores and the chemisorption on the metal sites are in accordance with their physico-chemical nature. The fit of the model to the experimental data has been shown as normalized parity plots in Figure 4-1 and Figure 4-2. It can be seen from Figure 4-2 (a) and (b) that the normal paraffins are relatively overpredicted whereas the isoparaffins are slightly under predicted. The carbon number distribution of the total paraffins [Figure 4-1 (b)] shows a very good fit to the experimental data, however. The agreement of the carbon number distribution of the entire reactor effluents [Figure 4-1 (a)], mononaphthenes [Figure 4-2 (c)], dinaphthenes [Figure 4-2 (d)], the composition of different classes [Figure 4-1 (c)] and of different commercial fractions [Figure 4-1 (d)] is quite good, considering the complexity of the reaction network and the relatively small number of temperature and feedstock independent parameters employed in the model.

Table 4-1. Model parameters employed in the VGO hydrocracking model.

S. No.	Parameter	Definition	Units
1.	$\tilde{A}^{comp}_{pcp}$	$\tilde{A}_{pcp} C_t \exp\left(\frac{\Delta\hat{S}_{pr}}{R}\right)$	[kmol/kg$_{cat}$/hr]
2.	$E^{comp}_{pcp(s;s)}$	$E_{pcp(s;s)} + \Delta H_{pr(S_{Oij} \rightleftarrows s)}$	[kJ/mol]
3.	$E^{comp}_{pcp(s;t)}$	$E_{pcp(s;t)} + \Delta H_{pr(S_{Oij} \rightleftarrows s)}$	[kJ/mol]
4.	$E^{comp}_{pcp(t;t)}$	$E_{pcp(t;t)} + \Delta H_{pr(S_{Oij} \rightleftarrows t)}$	[kJ/mol]
5.	$\tilde{A}^{comp}_{acyc-\beta}$	$\tilde{A}_{acyc-\beta} C_t \exp\left(\frac{\Delta\hat{S}_{pr}}{R}\right)$	[kmol/kg$_{cat}$/hr]
6.	$E^{comp}_{acyc-\beta(s;s)}$	$E_{acyc-\beta(s;s)} + \Delta H_{pr(S_{Oij} \rightleftarrows s)}$	[kJ/mol]
7.	$E^{comp}_{acyc-\beta(s;t)}$	$E_{acyc-\beta(s;t)} + \Delta H_{pr(S_{Oij} \rightleftarrows s)}$	[kJ/mol]
8.	$E^{comp}_{acyc-\beta(t;s)}$	$E_{acyc-\beta(t;s)} + \Delta H_{pr(S_{Oij} \rightleftarrows t)}$	[kJ/mol]
9.	$E^{comp}_{acyc-\beta(t;t)}$	$E_{acyc-\beta(t;t)} + \Delta H_{pr(S_{Oij} \rightleftarrows t)}$	[kJ/mol]
10.	$\tilde{A}^{comp}_{exo-\beta}$	$\tilde{A}_{exo-\beta} C_t \exp\left(\frac{\Delta\hat{S}_{pr}}{R}\right)$	[kmol/kg$_{cat}$/hr]
11.	$\Delta E_{exo-\beta(m;n)}$	$E_{exo-\beta(m,n)} - E_{acyc-\beta(m,n)}$	[kJ/mol]
12.	$\tilde{A}^{comp}_{endo-\beta}$	$\tilde{A}_{endo-\beta} C_t \exp\left(\frac{\Delta\hat{S}_{pr}}{R}\right)$	[kmol/kg$_{cat}$/hr]
13.	$\Delta E_{endo-\beta(m;n)}$	$E_{endo-\beta(m,n)} - E_{acyc-\beta(m,n)}$	[kJ/mol]
14.	$\tilde{A}^{comp}_{dealk}$	$\tilde{A}_{dealk} C_t \exp\left(\frac{\Delta\hat{S}_{pr-ring}}{R}\right)$	[kmol/kg$_{cat}$/hr]
15.	$E^{comp}_{dealk(s)}$	$E^{comp}_{dealk(s)} + \Delta H_{pr-ring}$	[kJ/mol]

Table 4-1. Continued.

S. No.	Parameter	Definition	Units
16.	$E^{comp}_{dealk(t)}$	$E^{comp}_{dealk(t)} + \Delta H_{pr-ring}$	[kJ/mol]
17.	$\tilde{A}^{comp}_{cyc}$	$\tilde{A}_{cyc} C_t \exp\left(\frac{\Delta \hat{S}_{pr-diole}}{R}\right)$	[kmol/kg$_{cat}$/hr]
18.	$E^{comp}_{cyc(s;s)}$	$E_{cyc(s;s)} + \Delta H_{pr(S_{DOij} \rightleftarrows s)}$	[kJ/mol]
19.	$E^{comp}_{cyc(s;t)}$	$E_{cyc(s;t)} + \Delta H_{pr(S_{DOij} \rightleftarrows s)}$	[kJ/mol]
20.	$E^{comp}_{cyc(t;s)}$	$E_{cyc(t;s)} + \Delta H_{pr(S_{DOij} \rightleftarrows t)}$	[kJ/mol]
21.	$E^{comp}_{cyc(t;t)}$	$E_{cyc(t;t)} + \Delta H_{pr(S_{DOij} \rightleftarrows t)}$	[kJ/mol]
22.	$A^{comp}_{hyd,3H_2}$	$A_{hyd,3H_2} c_m$	[(kmol/kg$_{cat}$/hr)(m^3/kmol)^3]
23.	$A^{comp}_{hyd,2H_2}$	$A_{hyd,2H_2} c_m$	[(kmol/kg$_{cat}$/hr)(m^3/kmol)^2]
24.	$E_{hyd,3H_2}$	-	[kJ/mol]
25.	$E_{hyd,2H_2}$	-	[kJ/mol]
26.	p^{chem}_{const}	-	[Dimensionless]
27.	$p^{chem}_{sat\_rings}$	-	[Dimensionless]
28.	$p^{chem}_{aro\_rings}$	-	[Dimensionless]
29.	p^{chem}_{paraf}	-	[Dimensionless]
30.	$\Delta q(S_A^+)$	$q(H^+) - q(S_A^+)$	[kJ/mol]
31.	$K_{paraf,base}$	-	[Dimensionless]
32.	$K_{Nap,base}$	-	[Dimensionless]
33.	$K_{Aro,base}$	-	[Dimensionless]

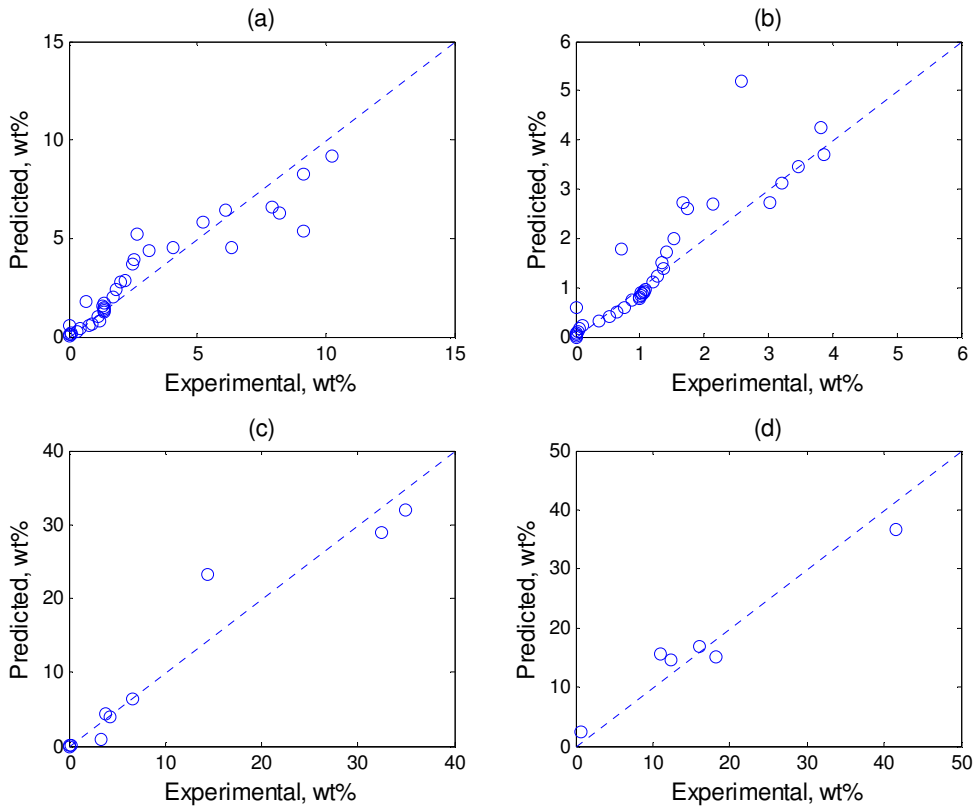

Figure 4-1. Comparison of the experimental and predicted product composition in the hydrocracking of VGO. (a) Carbon number distribution (C_3 to C_{40}) of the total reactor effluents. (b) Carbon number distribution (C_3 to C_{40}) of the total paraffins. (c) Weight percent composition of normal paraffins, isoparaffins, one to four ring naphthenes and one to four ring aromatics. (d) Weight percent of different commercial fractions, i.e., LPG, light naphtha, heavy naphtha, kerosene, diesel and the unconverted VGO.

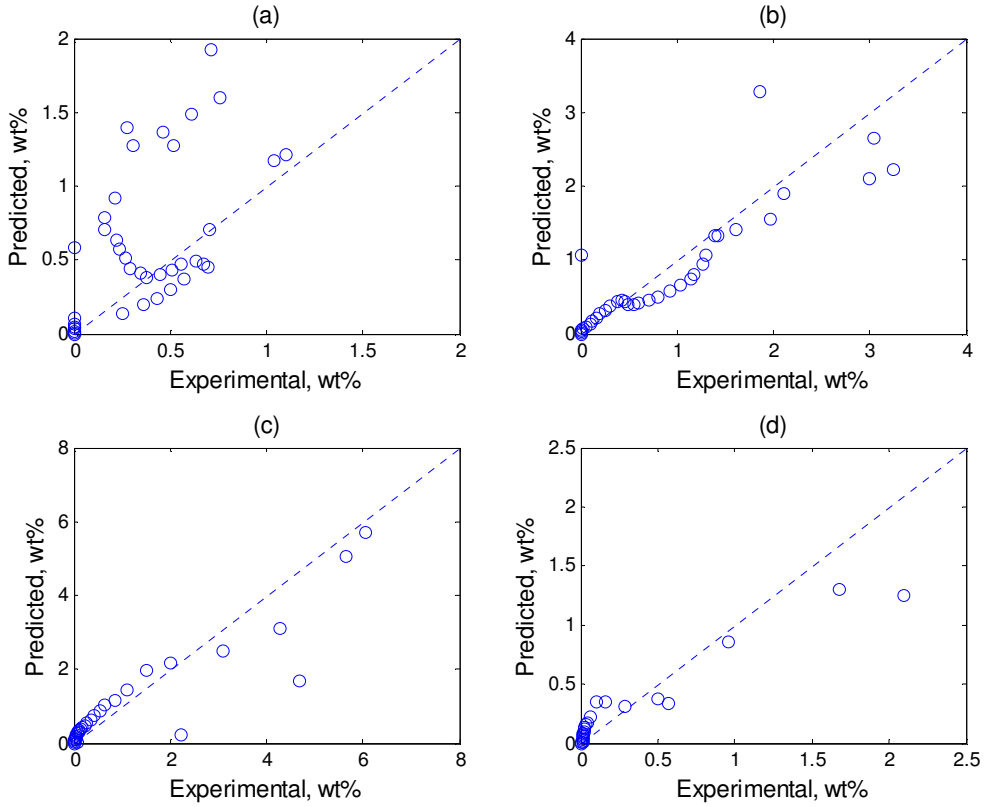

Figure 4-2. Comparison of the experimental and predicted product composition in the hydrocracking of VGO. (a) Carbon number distribution (C_3 to C_{40}) of the normal paraffins. (b) Carbon number distribution (C_4 to C_{40}) of the isoparaffins. (c) Carbon number distribution (C_5 to C_{40}) of the mononaphthenes. (d) Carbon number distribution (C_{10} to C_{40}) of the dinaphthenes.

CHAPTER V

REACTOR SIMULATIONS

The parameters estimated in Chapter IV have been used to carry out a number of non-isothermal reactor simulations in an industrial scale hydrocracking reactor for a wide range of operating conditions. The reactor geometry taken from the literature[87] and the catalyst properties selected for these simulations are shown in Table 5-1. The composition of the feedstock vacuum gas oil has been taken from Moustafa et al.[88] and is given in Table 5-2. The actual feedstock composition required as the input for the reactor simulations is derived from this information as discussed in section 5.2.3. The products obtained from the hydrocracking of this feedstock have been classified into different commercial fractions based on their carbon number range as shown in Table 5-3. The conversion of VGO is defined based on the cracking of C_{20}+ feed into C_{20} and lighter products and is calculated by

$$X = \left(\frac{W_{C20+}^{feed} - W_{C20+}^{prod}}{W_{C20+}^{feed}} \right) \times 100 \tag{5.1}$$

In the above eqn, *Ws* have the units of weight. This criterion for calculating the conversion is analogous to the one used in industry which is based on the end point of diesel.

A maximum temperature increase of 15 ^{o}C per bed has been adopted for all the simulations carried out in this study and is used as the criterion to switch to the next catalyst bed, i.e., when the temperature of the reaction mixture reaches $T_{in} + 15\,^{o}C$, quenching hydrogen stream at 40 ^{o}C is injected to reduce the temperature to T_{in}. Consequently, the number and length of different beds depends on the total amount of heat released during the hydrocracking reactions and the heat release profile corresponding to the selected operating conditions. The model can also be used to simulate an existing hydrocracking unit with a given number of beds and pre-specified

bed lengths to obtain the temperature increase and conversion in each bed and the composition of final products.

Table 5-1. Reactor geometry and catalyst properties for the reactor simulations.

Reactor Geometry	
Total Bed Length	11.6 m
Reactor Diameter	3.7 m
Catalyst Properties	
Catalyst Bulk Density	830 kg_{cat}/m^3_r
Particle Equivalent Diameter	3.0 mm
Bed Porosity	0.4
Catalyst micropore volume	$2.8x10^{-4}$ m^3/kg_{cat}

Table 5-2. Composition of the VGO. (weight percent).

CN	nPar	iPar	MNA	DNA	TNA	TETNA	MAR	DAR	TAR	NMA	NDA	NTA	Total
14	0	0	0	0	0	0	0.827	0.047	0	0.413	0	0	1.287
15	0.002	0	0	0	0	0	2.330	0.359	0	0	0.180	0	2.871
16	0.016	0.002	0.004	0	0	0	2.710	1.010	0	0	0.500	0	4.242
17	0.077	0.002	0.032	0.021	0	0	2.320	0.950	0.323	0	0.470	0	4.195
18	0.167	0.039	0.128	0.131	0.022	0	1.610	0.915	0.459	0	0	0.230	3.701
19	0.365	0.152	0.339	0.312	0.109	0.018	0.718	0.335	0.126	0	0	0.063	2.537
20	0.729	0.333	0.614	0.613	0.247	0.196	0.246	0.168	0.078	0	0	0.039	3.263
21	1.010	0.570	1.030	1.050	0.541	0.447	0.086	0.113	0.047	0	0	0.023	4.917
22	1.430	0.910	1.470	1.380	0.650	0.723	0.012	0.020	0.010	0	0	0	6.605
23	1.560	1.270	1.920	1.770	0.873	0.793	0	0	0	0	0	0	8.186
24	1.860	1.600	2.380	2.220	1.240	0.873	0	0	0	0	0	0	10.173
25	2.070	1.720	2.790	2.460	1.370	0.693	0	0	0	0	0	0	11.103
26	1.650	1.450	2.590	2.270	1.090	0.533	0	0	0	0	0	0	9.583
27	1.270	1.360	2.380	2.110	0.897	0.439	0	0	0	0	0	0	8.456
28	0.900	1.110	2.070	1.930	0.615	0.395	0	0	0	0	0	0	7.020
29	0.538	0.723	1.550	1.520	0.403	0.235	0	0	0	0	0	0	4.969
30	0.343	0.426	1.150	1.140	0.163	0.118	0	0	0	0	0	0	3.340
31	0.183	0.268	0.712	0.608	0.090	0.082	0	0	0	0	0	0	1.943
32	0.115	0.163	0.405	0.248	0.092	0.060	0	0	0	0	0	0	1.083
33	0.040	0.070	0.236	0.015	0.125	0.047	0	0	0	0	0	0	0.533
Total	14.325	12.168	21.80	19.798	8.527	5.652	10.859	3.917	1.043	0.413	1.150	0.355	100.000

Table 5-3. Definition of different commercial fractions based on carbon number range. (The last column has the atmospheric equivalent boiling points[1] of normal paraffins for this carbon number range).

Commercial Fraction	Carbon No.	Atmospheric Equivalent Boiling Points (^oC)
LPG	$C_3 - C_4$	-
Light Naphtha (LNAP)	$C_5 - C_7$	40 – 110
Heavy Naphtha (HNAP)	$C_8 - C_{12}$	110 – 220
Kerosene (KERO)	$C_{13} - C_{15}$	220 – 260
Diesel (DIES)	$C_{16} - C_{20}$	260 – 350
Unconverted (UNCONV)	$> C_{20}$	> 350

The simulations performed to study the effect of the reactor inlet temperature and total pressure on the hydrocracking products are discussed in Section 5.1 and 5.1.2 respectively. The effect of the change in the distribution of isomers of a class with different degrees of branching on the hydrocracking conversion and evolution of various subclasses is discussed in Section 5.2.3.

5.1. Effect of Inlet Temperature

To study the effect of temperature on the VGO conversion and product distribution, the simulations have been carried out at two different reactor inlet temperatures (T_{in}): 350 ^oC and 370 ^oC; both at a total pressure of 150 bar and a H_2 to Hydrocarbon molar ratio of 15.0 (~ 5000 Std. ft^3/barrel). The VGO flow rate has been taken as 620 kmol/hr. The

various simulation results are shown in Figure 5-1 to Figure 5-6 with solid lines corresponding to the simulations at 350 ^{o}C and the dotted lines at 370 ^{o}C. Figure 5-1 (a) shows the temperature profiles of the solid and liquid phases along the reactor. At T_{in} = 350 ^{o}C, the total temperature increase in the reactor is 40.8 ^{o}C in three beds. It can be seen that the length of the first bed is smaller than the second one, showing a higher rate of heat release in first bed due to higher rates of exothermic aromatics hydrogenation and cracking reactions. At T_{in} = 370 ^{o}C on the other hand, the total temperature increase in the reactor is 58.8 ^{o}C with a total of four beds. A higher inlet temperature results in higher rates of aromatics hydrogenation and hydrocracking reactions giving a higher rate of temperature increase in each bed as compared to 350 ^{o}C. The heat is generated in the solid catalytic phase from where it is transferred to the liquid phase. Because of the higher rate of heat release, the average ΔT between solid and liquid phases at T_{in} = 370 ^{o}C is slightly higher (~ 0.4 ^{o}C) as compared to T_{in} = 350 ^{o}C (~0.2 ^{o}C).

The profile of the VGO conversion along the beds can be seen from Figure 5-1 (b) indicating 88.6 % total conversion at T_{in} = 370 ^{o}C as compared to only 56.7 % conversion at T_{in} = 350 ^{o}C. A conversion increase of approximately 26 % has been reported in the literature[89] with a temperature increase of 22 ^{o}C. Although the increase in conversion with temperature depends on the composition of the feedstock as well as the catalyst, the predicted increase in the total conversion is comparable to the reported value. Figure 5-1 (c) shows the flux of hydrogen in the gas and liquid phases along the reactor. The gas phase hydrogen flux (blue lines) drops along a bed due to the transfer of hydrogen from gas to the liquid phase with a faster drop at high temperature, indicating faster consumption of hydrogen. A step increase in gas phase hydrogen flux occurs at the bed exits because of the injection of quench hydrogen. The amount of each quench hydrogen shot is approximately 10 % of the inlet hydrogen at both temperatures. The hydrogen flux in the liquid phase depends on the solubility of hydrogen in the liquid phase, the rate of hydrogen transfer from gas to liquid phase and the total amount of hydrocarbons present in the liquid phase. It can be seen from Figure 5-1 (d) that the

weight % vaporization of hydrocarbons increases very rapidly at higher temperature because of more amounts of lighter hydrocarbons formed due to faster cracking, resulting in a faster decrease in the total amount of the liquid phase hydrocarbons. This ultimately contributes to the significantly high drop in the hydrogen flux in liquid phase at 370 ^{o}C. Figure 5-1 (d) also indicates that at the inlet of the reactor, the percentage of vaporization is higher at high temperature as the initial amounts of the vapor and liquid phases are obtained by a VLE flash calculation at the reactor inlet conditions. A sudden increase in the percentage of vaporization at the bed exits is also observed because of the addition of quench hydrogen.

5.1.1. Effect of Temperature on the Yields of Various Commercial Fractions

Figure 5-2 (a) shows the effect of temperature on the evolution of various commercial fractions along the reactor. It can be seen that at T_{in} = 350 ^{o}C, the diesel fraction (DIES) initially increases in the first bed and remains almost steady in the last two beds, ultimately resulting in a maximum diesel yield among all commercial fractions. At T_{in} = 370 ^{o}C, the yield of the diesel fraction increases quite fast in the first bed, maintains almost a steady value in the second bed and then sharply decreases in the last two beds. This faster increase in the diesel yield is caused by the faster cracking of VGO at higher temperature. As approximately 64 % of VGO conversion takes place in the first two beds itself, the cracking of diesel range hydrocarbons starts dominating in the third bed, resulting in a decrease in the diesel yield accompanied with a sharp increase in the heavy naphtha (HNAP) yield. It can also be observed that unlike 350 ^{o}C, the yield of heavy naphtha is highest among all the fractions at 370 ^{o}C indicating a shift in the hydrocracking from middle distillate to the naphtha mode. The yield of kerosene (KERO) at 370 ^{o}C increases faster in the first bed as compared to 350 ^{o}C but reaches almost the same value at the exit of the reactor. Both the light naphtha (LNAP) and LPG yield increase monotonically along the reactor and show a marked increase with temperature.

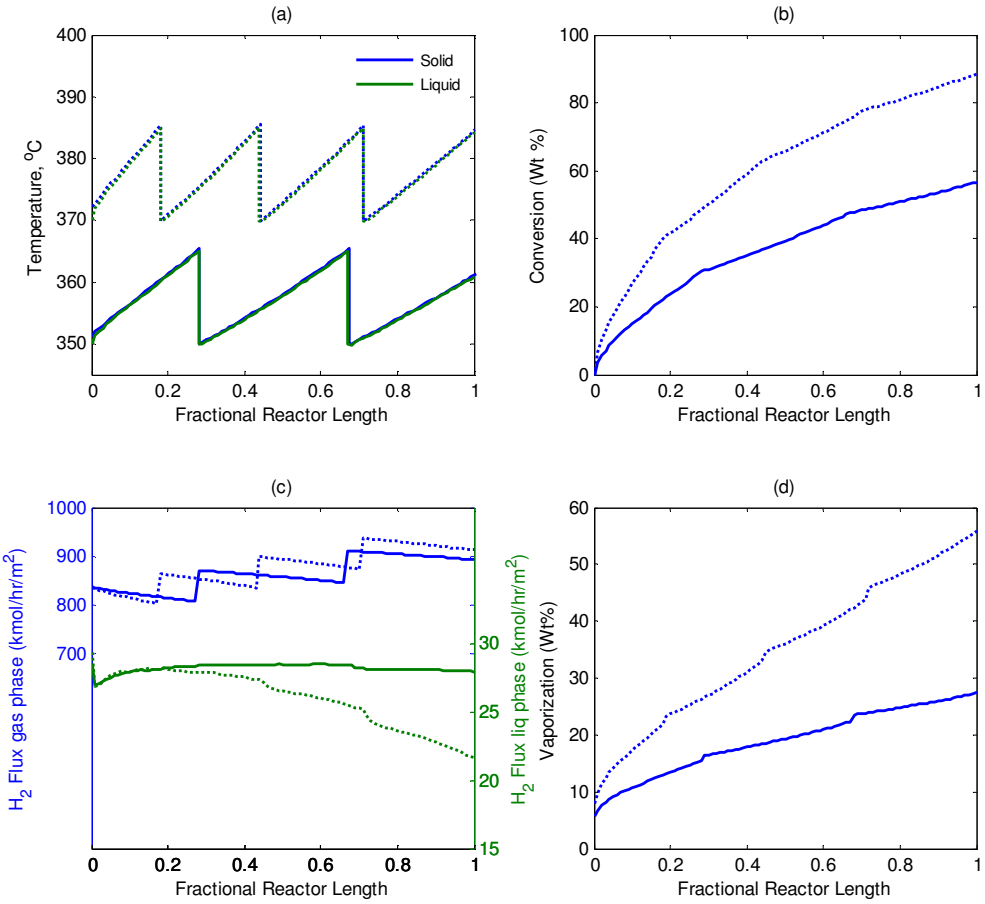

Figure 5-1. Effect of reactor inlet temperature on the (a) Temperature profile of solid and liquid phases along the reactor beds. (b) Weight percent conversion of VGO. (c) Hydrogen flux in the gas and liquid phases along the reactor beds. (d) Weight percent vaporization of hydrocarbons along the reactor beds. (solid lines: 350 ^{o}C, dotted lines: 370 ^{o}C).

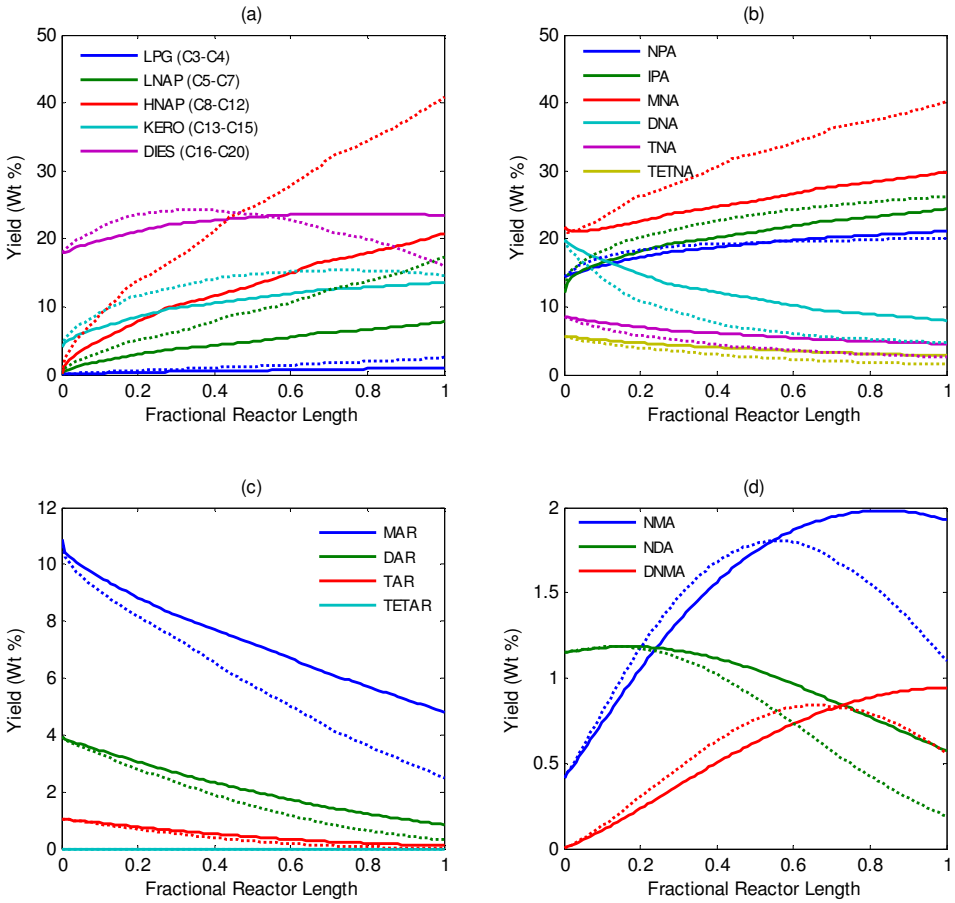

Figure 5-2. Effect of reactor inlet temperature on the (a) Evolution of various commercial fractions. (b) Evolution of paraffins and one to four ring naphthenes. (c) Evolution of one to four ring aromatics. (d) Evolution of naphtheno-aromatics. (solid lines: 350 ^{o}C, dotted lines: 370 ^{o}C).

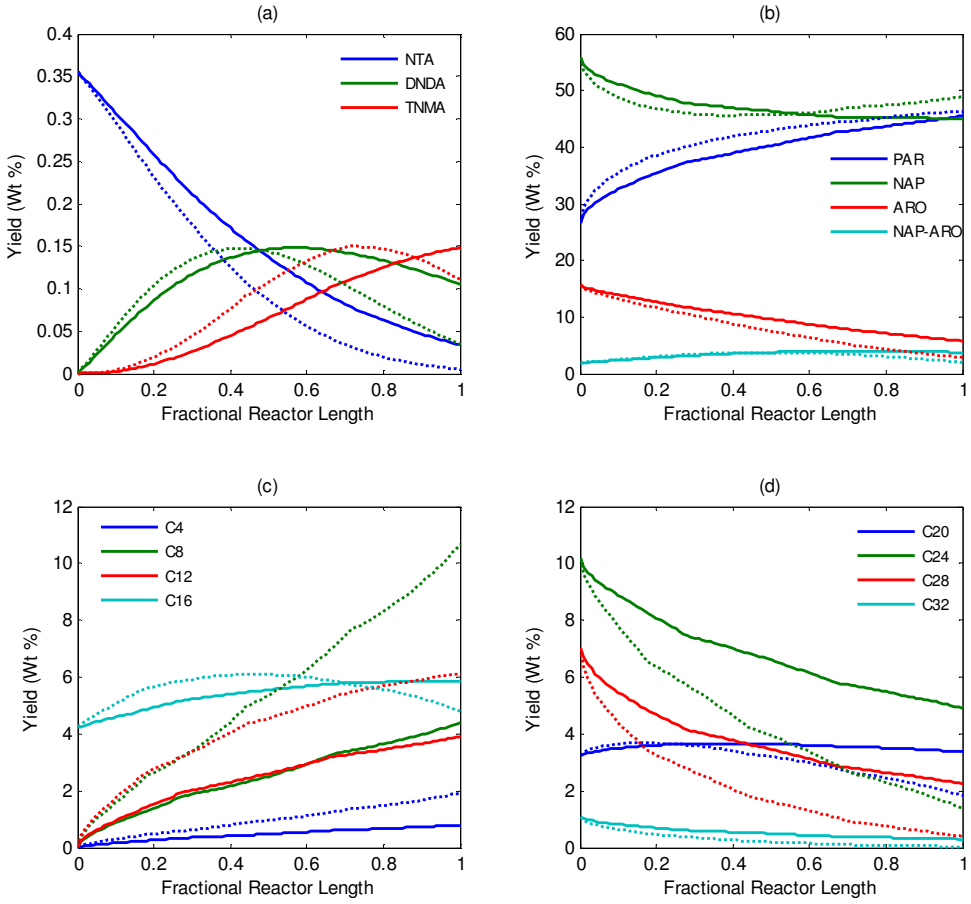

Figure 5-3. Effect of reactor inlet temperature on the (a) Evolution of naphtheno-aromatics. (b) Evolution of total paraffins, naphthenes, aromatics and naphtheno-aromatics. (c, d) Evolution of C_4 to C_{32} hydrocarbons. (solid lines: 350 ^{o}C, dotted lines: 370 ^{o}C).

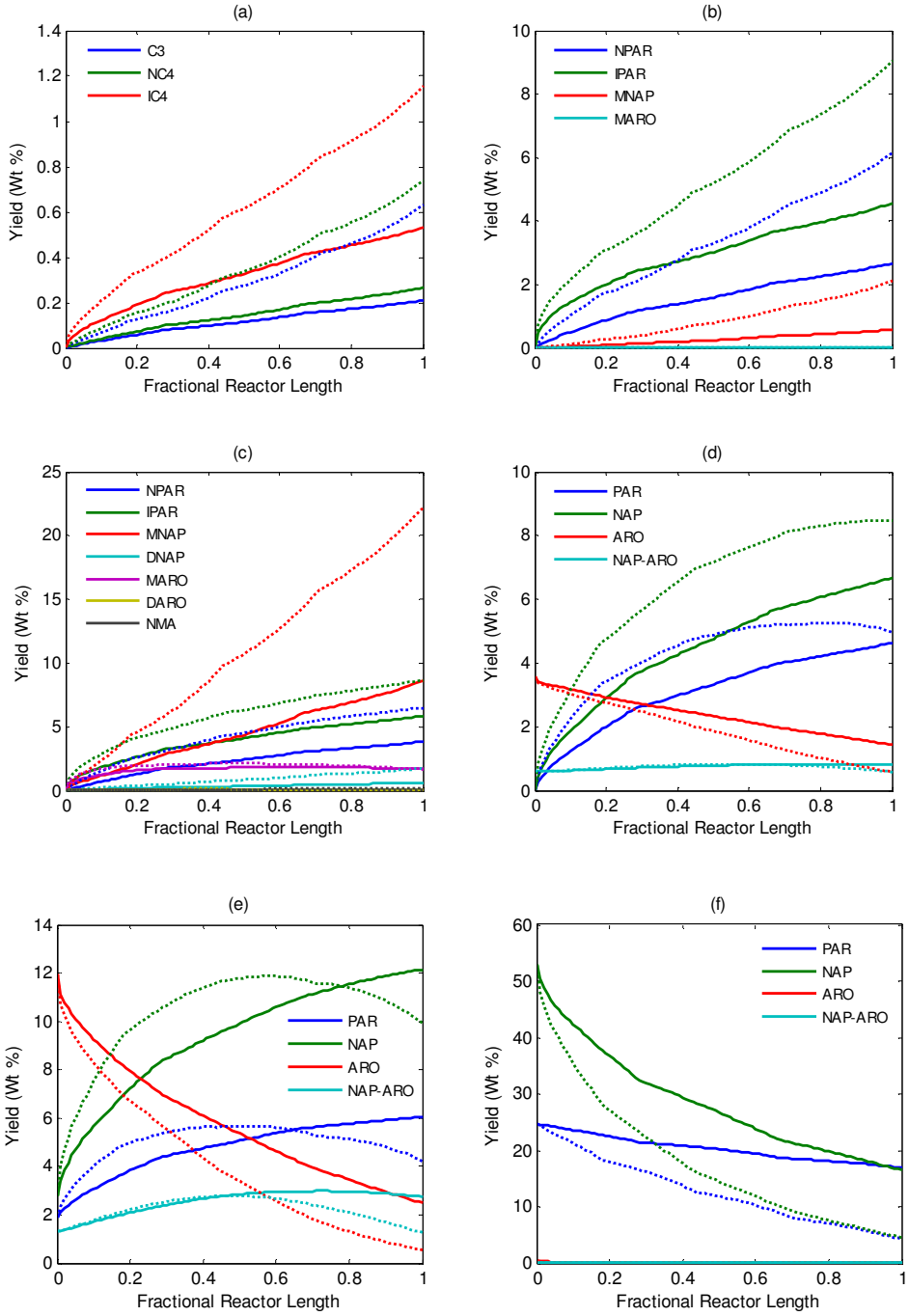

Figure 5-4. Effect of reactor inlet temperature on the (a) Evolution of different components of LPG. (b) Evolution of different classes of light naphtha. (c) Evolution of different classes of heavy naphtha. (d) Evolution of different classes of kerosene. (e) Evolution of different classes of diesel. (f) Evolution of different classes of unconverted fraction. (solid lines: 350 ^{o}C, dotted lines: 370 ^{o}C).

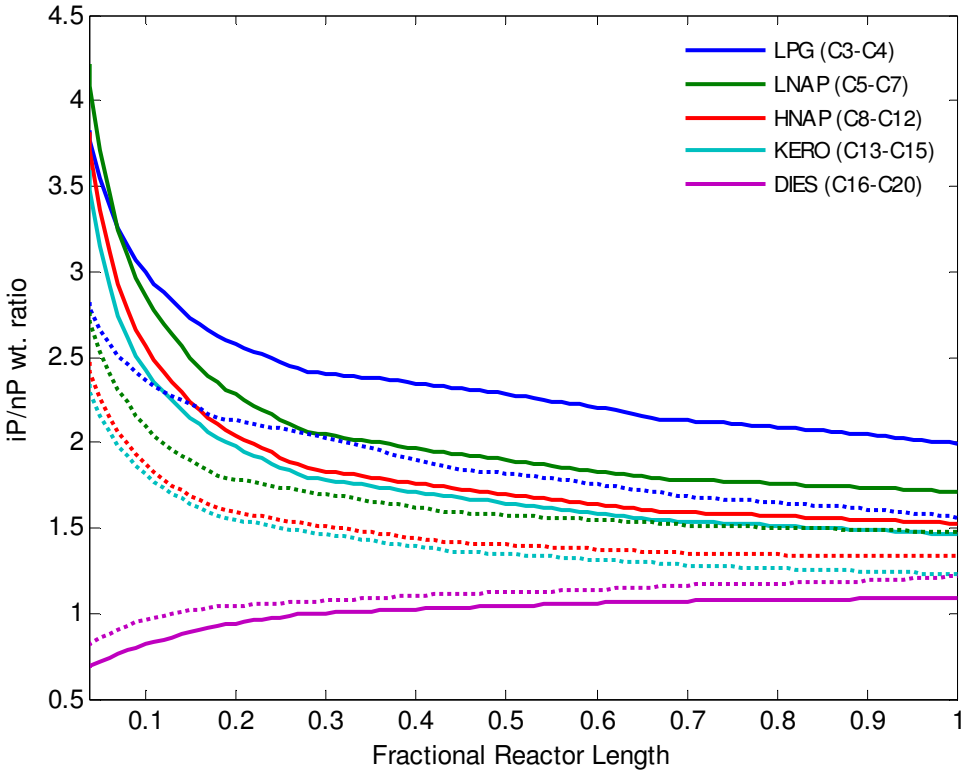

Figure 5-5. Effect of reactor inlet temperature on the iso to normal paraffins ratio of various commercial fractions. (solid lines: 350 ^{o}C, dotted lines: 370 ^{o}C).

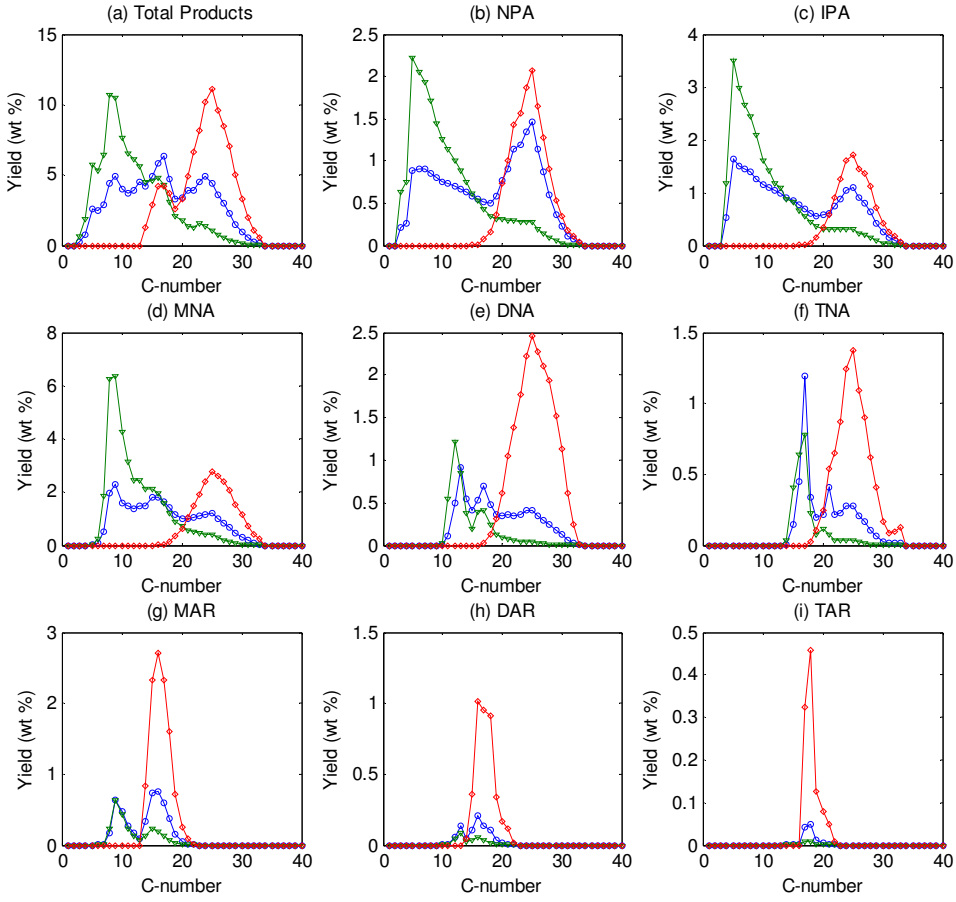

Figure 5-6. Effect of reactor inlet temperature on the carbon number distribution of hydrocarbon classes. (diamonds: feed. circles: products at 350 ^{o}C. triangles: products at 370 ^{o}C).

5.1.2. Effect of Temperature on the Yields of Various Hydrocarbon Classes

Figure 5-2 (b) shows the effect of temperature on the evolution of various paraffinic and naphthenic classes along the reactor. At 350 ^{o}C, the yields of dinaphthenes (particularly), trinaphthenes and tetranaphthenes show a sharp decrease in the first bed with a slower decrease in the last two beds. This occurs primarily because of the ring opening reactions, as can be seen from the increase in the yield of mononaphthenes, and, to a lesser extent, because of the scission in the alkyl side chains of these species. The yield of mononaphthenes at a given temperature also increases along the reactor because of the hydrogenation of monoaromatics and cyclization of paraffins. As the inlet temperature is increased to 370 ^{o}C, the rate of decrease of the dinaphthenes yield increases significantly accompanied by a marked increase in the yield of mononaphthenes. The increase in the yield of mononaphthenes at higher temperature also indicates higher rates of cyclization of paraffins. The yield of normal and isoparaffins increases along the reactor because of the cracking in the alkyl side chain of a number of ring species. The normal paraffins are converted into isoparaffins only through PCP(s;s) elementary steps. These were found to have the highest composite activation energy as compared to other acid site PCP and cracking steps. Because of this, the yield of isoparaffins slightly increases with a decrease in the yield of normal paraffins as the temperature is increased from 350 ^{o}C to 370 ^{o}C.

Figure 5-2 (c) shows the effect of temperature on the evolution of monoaromatics, diaromatics and triaromatics along the reactor. No tetraaromatics are present in the VGO feedstock. As the temperature is increased, all the aromatics are hydrogenated at a faster rate, thus decreasing their yields. Figure 5-2 (d) shows the effect of temperature on the evolution of different naphtheno-aromatics along the reactor. At 350 ^{o}C, the yield of naphtheno-monoaromatics (NMA) first increases as they are formed from the hydrogenation of diaromatics (DAR). Subsequent hydrogenation of NMA to dinaphthenes occurs after 80% reactor length causing a slight decrease in their yield. Naphtheno-diaromatics (NDA) are formed from the hydrogenation of triaromatics

(TAR) causing a slight increase in their yield in the first 20 % of the reactor. At the same time, hydrogenation of NDA produces dinaphtheno-monoaromatics (DNMA) with a decrease in their yield. When the temperature is increased to 370 ^{o}C, NMA and DNMA are produced faster in the beginning, reach a maximum and are subsequently hydrogenated to more saturated products in the later part of the reactor. Figure 5-3 (a) shows the evolution of a number of four ring naphtheno-aromatics along the reactor and the effect of temperature on their profiles. Only 0.35 wt% of naphtheno-triaromatics (NTA) are present in the feedstock. They are hydrogenated into dinaphtheno-diaromatics (DNDA). These are primary products as can be seen from their non-zero initial slope. Subsequent hydrogenation of DNDA produces trinaphtheno-monoaromatics (TNMA) with a zero slope, characterizing them as secondary products. The effect of temperature on the evolution of these classes is analogous to NMA, NDA and DNMA classes.

Figure 5-3 (b) shows the evolution of the total amount of paraffins, naphthenes, aromatics and naphtheno-aromatics and the effect of temperature on their profiles. As can be concluded from the previous discussion, the total aromatics yield decreases along the reactor and the rate of decrease increases with temperature. Because of the sequential nature of ring saturation, the hydrogenation of naphtheno-aromatics produces another naphtheno-aromatics except when the reacting species has only one aromatic ring. Therefore, at 350 ^{o}C, naphtheno-aromatics keep of increasing along the reactor, however, at 370 ^{o}C, the complete saturation of these species results in the decrease in their yield causing an increase in the yield of naphthenes in the later part of the reactor. The total paraffins yield increases along the reactor at both the temperatures as they are formed from the dealkylation of aromatics and cracking in the side chain of naphthenic and aromatic species. At higher temperature, the initial rate of increase of the paraffin's yield is increased because of the higher rate of cracking. The experimental data used in this study for the parameter estimation showed a significant amount of cyclization of paraffins to mononaphthenes. As the cyclization elementary steps proceeds through diolefinic species, the *effective* activation energy for these steps include twice the heat of dehydrogenation of paraffins and the composite activation energies of cyclization. A

value of 25-30 kcal/mol of the heat of dehydrogenation of paraffins leads to large *effective* activation energies for the cyclization steps. This can be seen from the increase in the yield of total naphthenes at high temperature at the exit of the reactor. A significant increase in the value of rate coefficient for the cyclization of paraffins to mononaphthenes has been reported by Filimonov et al.[90] as the temperature is increased. Part of this increase can be attributed to the complete saturation of naphtheno-aromatics, as mentioned above; the remaining increase is due to the cyclization of the paraffins.

5.1.3. Effect of Temperature on the Yields of Hydrocarbons of Different Chain Length

Figure 5-3 (c) and (d) show the evolution of hydrocarbons of different chain lengths from C_4 to C_{32} and the effect of temperature on their yields. The yields of C_4, C_8 and C_{12} increase along the reactor as they are always formed from the heavier hydrocarbons. The rate of increase is faster at higher temperature because of higher rates of cracking. The yield of C_{16} at 350 ^oC increases in the first 70% of the reactor and maintains almost a constant value afterwards, indicating its rate of formation from heavier hydrocarbons to be almost equal to its rate of cracking to lighter ones. At 370 ^oC, on the other hand, C_{16} is formed at a faster rate from the heavier hydrocarbons, reaches a maxima, and subsequently the rate of cracking of C_{16} becomes more than the rate at which it is formed from heavier hydrocarbons, resulting in a significant drop in its yield. C_{20} shows a similar behavior. The yields of hydrocarbons heavier than C_{20} always decrease along the reactor, the more so as the temperature is increased.

5.1.4. Effect of Temperature on the Yields of Individual Classes of Various Commercial Fractions

Figure 5-4 (a) shows the evolution of different components of LPG along the reactor. The yield of isobutane is always higher than that of n-butane, as can be seen from a typical composition of LPG obtained from the hydrocracking process. The yields of all the components increase along the reactor and the rate of increase of these yields more than doubles with a temperature increase of 20 ^oC.

The evolution of different classes of light naphtha (LNAP: C_5-C_7) is shown in Figure 5-4 (b). In light naphtha also isoparaffins have the maximum yield followed by n-paraffins and mononaphthenes. The yields of these classes increase monotonically along the reactor. The increase is faster at the elevated temperature. Only negligible amounts of monoaromatics are present in this fraction.

The evolution of different classes belonging to the heavy naphtha fraction (HNAP: C_8-C_{12}) is shown in Figure 5-4 (c). Components belonging to the mononaphthenes class constitute a significant amount in the heavy naphtha fraction. The yield of mononaphthenes increases drastically from 8% to 22% as the temperature is increased from 350 ^oC to 370 ^oC. The increase in the yield of normal and isoparaffins with temperature is much less pronounced than that of mononaphthenes. This can be attributed to the increased rate of cyclization of paraffins to form mononaphthenes as the temperature is increased, already discussed above. The yield of dinaphthenes, although low, also increases with temperature because of higher rate of cracking of the side chains of the heavier dinaphthenes as well as the increased rate of ring opening of trinaphthenes belonging to the HNAP fraction. The yield of monoaromatics is not affected very much with a temperature increase. The latter increases the rate at which monoaromatics are produced from the dealkylation and side chain scission of heavier monoaromatics, which in turn is compensated by an increase in the rate of hydrogenation of monoaromatics components in the HNAP fraction. Diaromatics and naphtheno-monoaromatics are essentially absent in heavy naphtha because of the presence of very small amounts of these species in the VGO feedstock and their faster hydrogenation.

The evolution of paraffins, naphthenes, aromatics and naphtheno-aromatics in the kerosene (KERO: C_{13}-C_{15}), diesel (DIES: C_{16}-C_{20}) and unconverted VGO (UNCOV: C_{21}-C_{33}) fraction is shown in Figure 5-4 (d), (e) and (f) respectively. At 350 ^oC, the yields of paraffins and naphthenes increase along the reactor in the kerosene and diesel fractions. On the Contrary, at 370 ^oC, their yields increases at a faster rate in early zones of the bed, reaches a maximum and then drops in the last part of the reactor. The decrease in the yield of paraffins begins faster than that of naphthenes, indicating either a

relatively higher rate of cracking of the paraffins of this fraction than naphthenes at the elevated temperature or the increase in the rate of cyclization of paraffins to naphthenes. For both the kerosene and diesel fractions, the yield of aromatics decreases along the reactor because of ring saturation. Given the larger amount of aromatics in the diesel fraction, its rate of decrease is significantly higher as compared to that of kerosene fraction. The rate of aromatics hydrogenation is accelerated as the temperature is increased. The temperature increase causes the same effect on the profiles of naphtheno-aromatics in the kerosene and diesel fractions as on the total naphtheno-aromatics, discussed above [Figure 5-3 (b)]. Paraffins and naphthenes in the unconverted VGO keep on decreasing along the reactor at a rate that increases with temperature, as expected. No aromatics and naphtheno-aromatics are present in the carbon number range of unconverted fraction as can be seen from the composition of the feedstock.

5.1.5. Effect of Temperature on the Iso/Normal Paraffin Ratio

The iso/normal paraffin ratios of various commercial fractions are shown in Figure 5-5. For LPG, light naphtha, heavy naphtha and kerosene fractions the ip/np ratio decreases along the reactor. The decrease in the ip/np ratio of all the fractions is quite high in the first 40% of the reactor with a relatively much slower decrease in the latter part. At a given temperature, the ip/np ratio is always greater than unity at the exit, is highest for the lightest fraction and decreases as the average carbon number of the fraction increases. A drop in this ratio is observed when the reaction temperature is increased. The decrease in the ip/np ratio with temperature has been reported by Sullivan et al.[91] for C_5 and C_6 fractions. Contrary to lighter fractions, the ip/np ratio of diesel increases along the reactor. Bourne et al.[92] have reported the increase in the ip/np ratio along the reactor in their gas oil fraction (437–700 F) obtained from the hydrocracking of highly aromatic Kuwait gas oil. The current simulations showed a slight increase with temperature of this ratio which can be attributed to a higher rate of isomerization of the long chain normal paraffins into isoparaffins by the PCP(s;s) steps at the elevated temperature.

5.1.6. Effect of Temperature on the Carbon Number Distribution of Hydrocarbon Classes

As the temperature in increased, the general trend in all the hydrocarbon classes is the decrease in the yield of heavier hydrocarbons together with an increase in the lighter ones [Figure 5-6 (a) to (i)]. At both 350 and 370 ^{o}C, the normal and isoparaffin yields show a peak at carbon number 5 [Figure 5-6 (b) and (c)] which is also reflected in the carbon number distribution of the total reactor effluents [Figure 5-6 (a)]. The peak around carbon number 25 in different hydrocarbon classes appears because of the corresponding peak in the feedstock. The heights of these peaks decrease (or the peaks completely vanish) due to a higher amount of cracking as the temperature is increased. The peak at carbon number 8-9 in the Figure 5-6 (a) comes from the corresponding peaks in the carbon number distribution of mononaphthenes [Figure 5-6 (d)], indicating a preferential cracking in the side chain of the mononaphthenes leaving 2-3 carbon atoms on the naphthenic ring. Similarly, in dinaphthenes [Figure 5-6 (e)], the peak is obtained at carbon number 13 leaving 3 carbon atoms on the dinaphthenic structure. The ring opening of these C_{13} dinaphthenes creates a slight peak at C_{13} in the carbon number distribution of mononaphthenes. Trinaphthenes [Figure 5-6 (f)] in the same way show a peak at carbon number 17 (=14+3), the ring opening of which creates a small peak at C_{17} in the carbon number distribution of dinaphthenes. The same reasoning is applicable to the C_{21} peak in the carbon number distribution of trinaphthenes. Monoaromatics, diaromatics and triaromatics [Figure 5-6 (g) to (i)] follow similar trends with peaks at C_9, C_{13} and C_{17} respectively, the height of these peaks does not increase with the increase in temperature because of the faster rate of hydrogenation of these aromatics at the increased temperature.

5.2. Effect of Pressure

To study the effect of pressure on the VGO conversion and product distribution, the simulations have been carried out at two different reactor total pressures: 150 bar and 170 bar; both at a reactor inlet temperature of 370 ^{o}C and a H_2 to hydrocarbon molar

ratio of 15.0. The VGO flow rate has been taken as 620 kmol/hr as in the previous simulations. The various simulation results are shown in Figure 5-7 to Figure 5-11 with solid lines corresponding to the simulations at 150 bar and the dotted lines at 170 bar.

Figure 5-7 (a) shows the temperature profiles of the solid and liquid phases along the reactor. As the pressure is increased from 150 to 170 bar, the concentration of hydrogen in the liquid phase increases which in turn increases the rate of hydrogenation of the aromatics and naphtheno-aromatics [eqn (3.41)]. The exothermic nature of these hydrogenation reactions leads to a faster temperature rise in each bed. The total temperature increase in the reactor at 170 bar is also increased to 63.8 ^{o}C against 58.8 ^{o}C at 150 bar.

The effect of reactor pressure on the conversion of VGO is the combined result of several competing phenomena: (i) As explained above, a higher pressure increases the rate of hydrogenation of aromatics, thus favoring their cracking and, therefore, the total VGO conversion. Higher aromatic saturation also increases the reactor temperature, further enhancing the VGO conversion. (ii) It can be seen from eqn (3.53) that the liquid phase concentration of hydrogen appears in the denominator of the rate expressions of the elementary steps belonging to group (a). Therefore, a higher liquid phase hydrogen concentration reduces the rate of PCP isomerization, acyclic β-scission, exo and endocyclic β-scission elementary steps, thereby reducing the VGO conversion with total pressure. (iii) A high reactor pressure increases the concentration of relatively lighter hydrocarbons in the liquid phase making them susceptible to secondary cracking. Increased amount of lighter species in the liquid phase causes a reduction in the liquid phase mole fraction of the heavier unconverted hydrocarbons leading to a reduction in their conversion. (iv) An increased liquid phase hydrogen concentration has a favorable effect on VGO conversion due to enhanced hydrogenation of coke resulting in improved catalytic actovity[67]. A high aromatic feedstock has a higher tendency for coke formation, therefore, an increased pressure will have more positive effect on conversion for aromatic feedstocks compared to the paraffinic ones.

As the model currently does not account for the deactivation of the catalyst due to coke formation, the simulations results of the effect of pressure on the conversion and overall product distribution is based on the first three phenomena only. It can be seen from Figure 5-7 (b) that with the increase in pressure, the total conversion has dropped by approximately 6% indicating the dominance of the (ii) and (iii) phenomena. High amounts of paraffins and naphthenes (~ 82 wt%) in the feed supports this behavior.

The increased hydrogen flux in the liquid phase [Figure 5-7 (c)] and reduced vaporization of hydrocarbons [Figure 5-7 (d)] are self explanatory in light of the increased reactor pressure.

5.2.1. Effect of Pressure on the Yields of Various Commercial Fractions

Reduced conversion resulted in roughly 2% increase in the yield of diesel with 2% and 4% decrease in the yield of light naphtha and heavy naphtha, respectively. The yield of kerosene and LPG remains almost constant [Figure 5-8(a)].

5.2.2. Effect of Pressure on the Yields of Various Hydrocarbon Classes

The main effect of pressure occurs on the aromatic and naphtheno-aromatic classes [Figure 5-8 (c), (d) and Figure 5-9 (a)] due to their increased rate of hydrogenation. The effect of pressure increase on these classes is similar to that of an increase in temperature, as discussed previously. Cyclization of the paraffins to form mononaphthenes depends on the inverse of the square of liquid phase hydrogen concentration [eqn (3.31)] causing a decrease in cyclization rates with increase in pressure. It can be seen from the decrease in the yield of mononaphthenes [Figure 5-8 (b)] in spite of faster hydrogenation of monoaromatics to mononaphthenes. The decreased rate of the ring opening and side chain cracking reactions causes slight increase in the yields of dinaphthenes, trinaphthenes and tetranaphthenes classes.

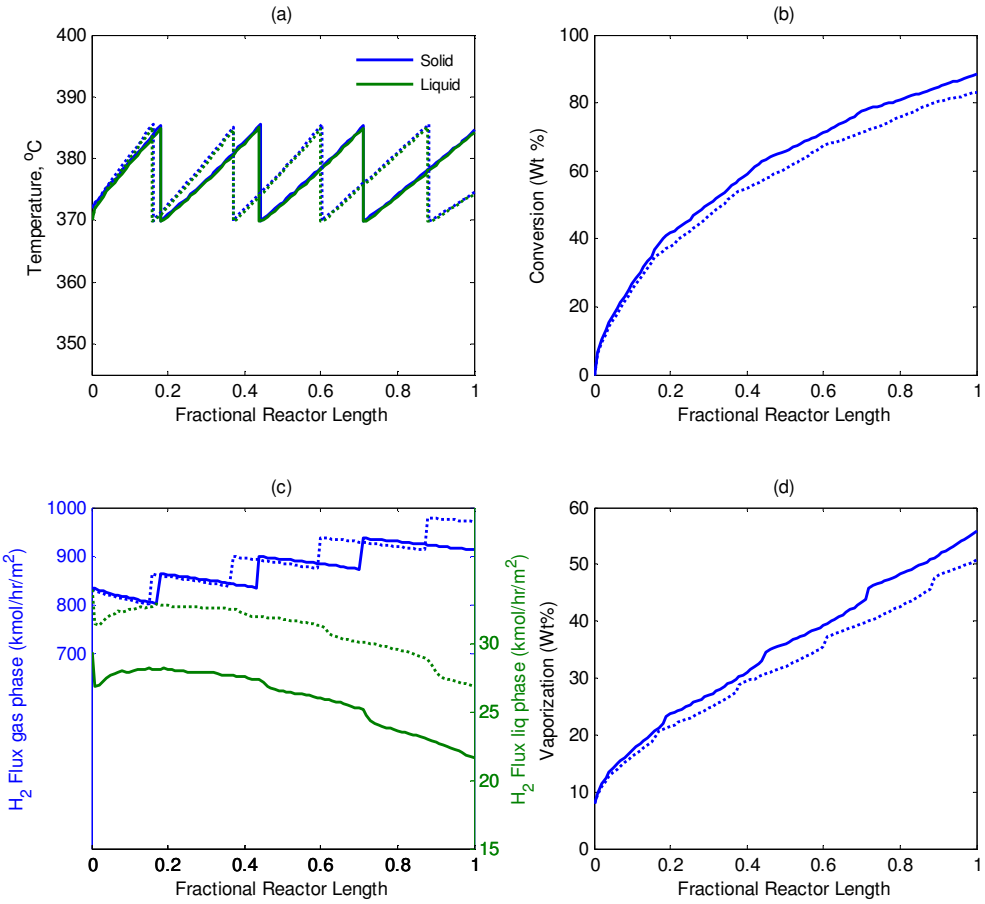

Figure 5-7. Effect of reactor pressure on the (a) Temperature profile of solid and liquid phases along the reactor beds. (b) Weight percent conversion of VGO. (c) Hydrogen flux in the gas and liquid phases along the reactor beds. (d) Weight percent vaporization of hydrocarbons along the reactor beds. (solid lines: 150 bar, dotted lines: 170 bar).

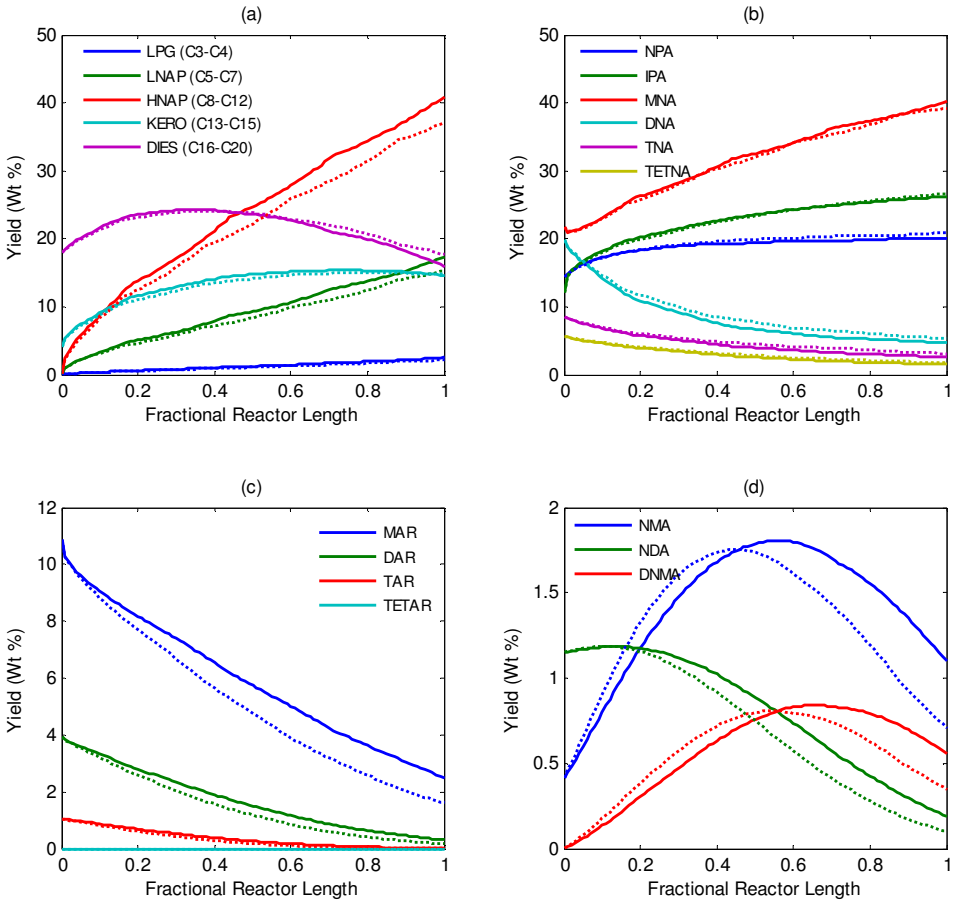

Figure 5-8. Effect of reactor pressure on the (a) Evolution of different commercial fractions. (b) Evolution of paraffins and one to four ring naphthenes. (c) Evolution of one to four ring aromatics. (d) Evolution of naphtheno-aromatics. (solid lines: 150 bar, dotted lines: 170 bar).

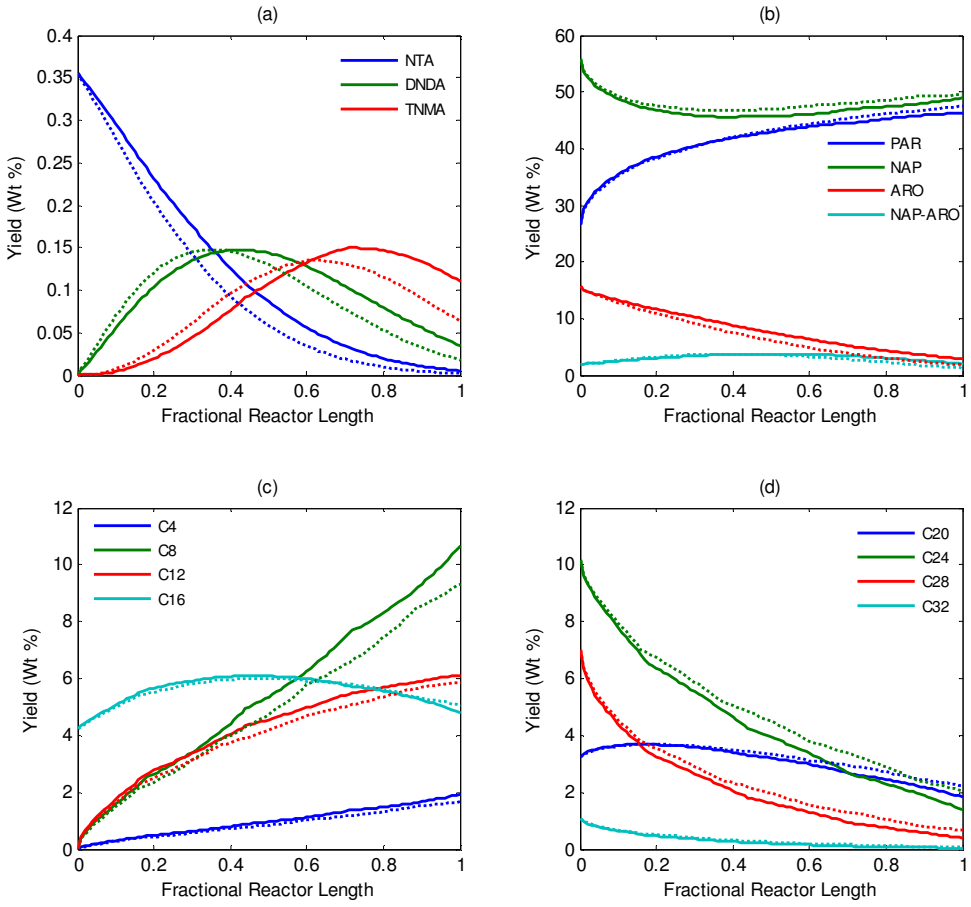

Figure 5-9. Effect of reactor pressure on the (a) Evolution of the naphtheno-aromatics. (b) Evolution of total paraffins, naphthenes, aromatics and naphtheno-aromatics. (c, d) Evolution of C_4 to C_{32} hydrocarbons. (solid lines: 150 bar, dotted lines: 170 bar).

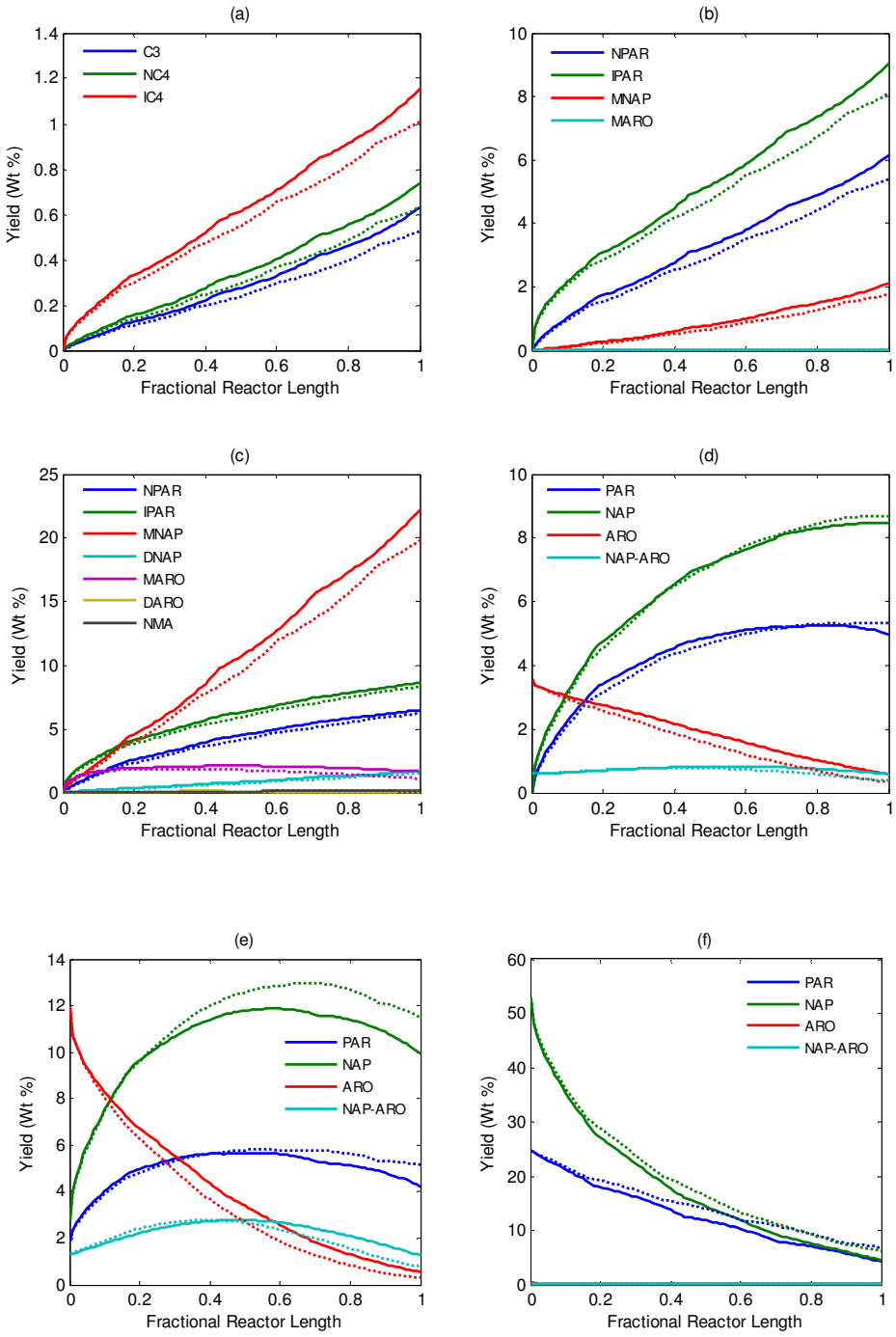

Figure 5-10. Effect of reactor pressure on the (a) Evolution of different components of LPG. (b) Evolution of different classes of light naphtha. (c) Evolution of different classes of heavy naphtha. (d) Evolution of different classes of kerosene. (e) Evolution of different classes of diesel. (f) Evolution of different classes of unconverted fraction. (solid lines: 150 bar, dotted lines: 170 bar).

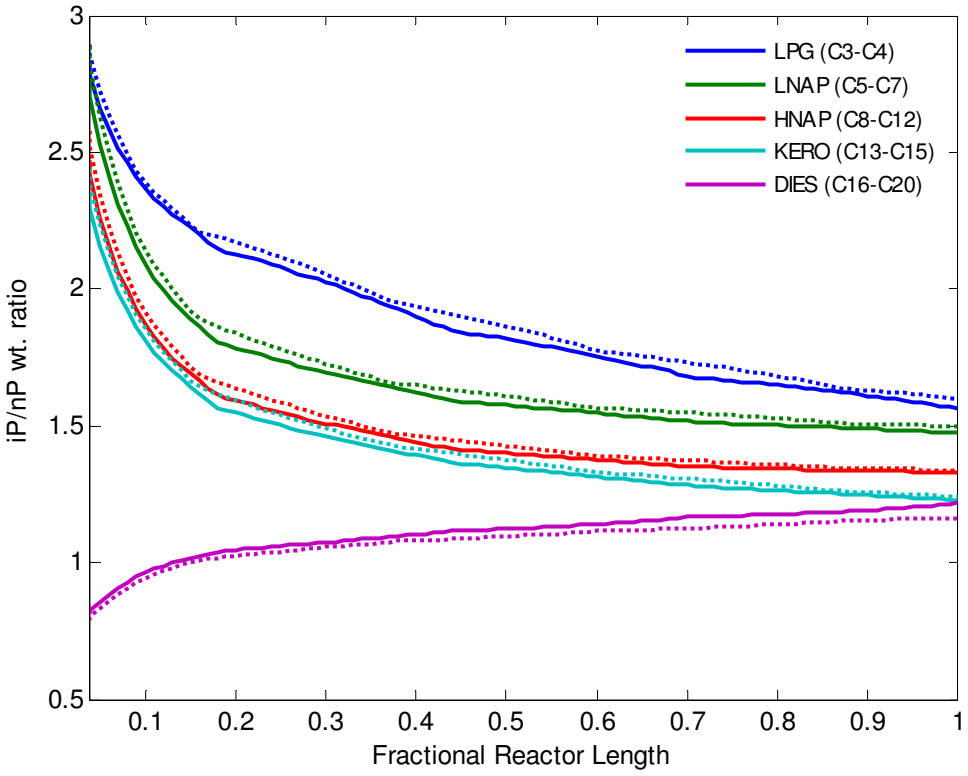

Figure 5-11. Effect of reactor pressure on the iso to normal paraffins ratio of different commercial fractions. (solid lines: 150 bar, dotted lines: 170 bar).

5.2.3. Effect of Pressure on the Yields of Hydrocarbons of Different Chain Length

Higher pressures lower the total conversion of VGO. The effect of the increase of total pressure on the hydrocarbons of different chain lengths is similar to that of a decrease in temperature. This similarity can be observed by comparing Figure 5-9 (c), (d) with Figure 5-3 (c), (d).

5.2.4. Effect of Pressure on the Yields of Individual Classes of Various Commercial Fractions

The various components of LPG and all the classes of light and heavy naphtha [Figure 5-10] are reduced due to the reduced conversion with the increase in pressure as all the components in this carbon number range are only produced by the hydrocracking reactions. Aromatics and naphtheno-aromatics in the kerosene and diesel fractions are decreased primarily because of more ring hydrogenation as reflected by the increase in the amount of naphthenes in these fractions. It can be seen in Figure 5-10 (e) that the increase in yield of naphthenes in diesel fraction is more than the total decrease in the yields of aromatics and naphtheno-aromatics. The difference is caused by a lower rate of cracking reactions of the diesel range naphthenic species which dominates after 70% length of the reactor at higher pressure as against 60% at the lower pressure. Slower cracking is also responsible for the increase of the paraffin yield in the kerosene, diesel and unconverted fractions.

5.2.5. Effect of Pressure on the Iso/Normal Paraffin Ratio

The effect of pressure on the final values of the iso/normal ratio for heavy naphtha and kerosene fractions is negligible [Figure 5-11]. The ratio has slightly increased for the LPG and light naphtha fraction and shows a decrease in the diesel fraction as the pressure is increased. As the rate coefficients of all the reactions in the model are independent of the total pressure and the rates of the all the elementary steps which can affect this ratio (except cyclization) vary in the same way (inversely proportional) with pressure, this effect can not be attributed to the change in relative rates of different

elementary steps with pressure. An explanation for this effect can possibly be found in the evolution of the ip/np ratio along the reactor itself. For all the fractions except diesel, this ratio decreases with reactor length, indicating the decrease in the ratio with increase in conversion. As the conversion is decreased with the increase in total pressure, the ip/np ratio shows some increase with pressure. The opposite is true in the case of diesel. For heavy naphtha, the ratio is independent of conversion in the last 25% of the reactor length justifying a negligible effect on its value with pressure.

5.3. Sensitivity of the Distribution of Subclasses in Various Classes

The typical composition of VGO is available at the detail given in Table 2-1 in which VGO composition is expressed in terms of the carbon number distribution of 16 molecular classes. This kind of VGO composition is converted into a more detailed composition in which each molecular class is divided into subclasses based on the number of methyl branches. All the simulations reported here are based on the following distribution:

Isoparaffins for each carbon number (for which minimum three methyl branches can exist) are considered to have 65 mole % monobranched, 25 mole % dibranched and 10 mole % tribranched isomers. In the classes with aromatic and naphthenic rings, a distribution of 20 mole %, 50 mole %, 20 mole % and 10 mole % has been assumed for the unbranched, monobranched, dibranched and tribranched isomers.

This section is dedicated to the study of the sensitivity of the isomer distribution on the conversion of VGO and the evolution of the isomers of a given class along the length of the reactor. The distribution mentioned above is referred as the base case. Two sets of simulations have been performed. In Set-I, only the distribution of isoparaffins has been altered while keeping the distribution of all other classes at the base values. In Set-II, the distribution of isoparaffins has been kept at the base value and that of all other classes is varied. The distribution of the isomers selected for different cases in Set-I and Set-II and the corresponding conversions of VGO obtained from the reactor simulations are shown

in Table 5-4 and Table 5-5. All the simulations reported in this section are performed at 350 ^{o}C, 150 bar and a H_2 to hydrocarbon molar ratio of 15.

Table 5-4. The distribution of isoparaffins selected for the simulations of Set I. (mole %).

	Monobranched	Dibranched	Tribranched	(Wt %) VGO Conversion
Base Case	65	25	10	56.7
Case 1	100	0	0	53.2
Case 2	0	100	0	62.4

Table 5-5. The distribution of isomers selected for the ring species for the simulations of Set II. (mole %).

	Unbranched	Monobranched	Dibranched	Tribranched	(Wt %) VGO Conversion
Base Case	20	50	20	10	59.8
Case 3	100	0	0	0	23.7
Case 4	0	100	0	0	54.5
Case 5	0	0	100	0	74.2

5.3.1. Analysis of the Distribution of Isoparaffins

The total amount of isoparaffins in the VGO feedstock is only 12.2 weight percent. Therefore, the effect of the change in the distribution of isoparaffins on VGO conversion while keeping the distribution of all other classes at the base values is relatively small, as seen from Table 5-4. It can be observed however that increasing the percentage of isomers with a higher degree of branching increases the total conversion as the number of pathways available for cracking steps increases with the increase in the number of methyl branches in the feedstock. Figure 5-12 shows the change in the mole percent composition of normal, monobranched, dibranched and tribranched isomers among the total paraffin fraction along the length of the reactor. It can be seen that the tribranched paraffins in the base case decrease very fast in the first 20% length of the reactor without any counter increase in the amount of dibranched isomers. This indicates the fast cracking of the tribranched paraffins. In both Case 1 and Case 2, the final composition of isomers approaches the base case values within 5 % range. The amount of isomers with different degrees of branching are approaching some steady state values in each case, however, it should be noted that these values are not the thermodynamic equilibrium values. If all the paraffinic isomers (NPA, MBP, DBP and TBP) of a given carbon number were able to reach thermodynamic equilibrium among them, the total amount of tribranched isomer fraction would have been the highest with decreasing amounts of dibranched, monobranched and normal paraffins, in that order. This can be explained qualitatively based on the increase in the number of isomers with increased number of methyl branches and a relatively less Gibbs free energy of formation of isomers with more methyl branches, particularly if the crowding of methyl branches is absent. Although the curves shown in Figure 5-12 represent the distribution of isomers for the entire carbon number range (C_3 to C_{33}) and not just for one particular carbon number, it can be said conclusively that the final distribution is very far from the thermodynamic equilibrium distribution as seen from maximum amount of monobranched isomers with very small amounts of di- and tribranched isomers. The deviation of the hydrocracking products from the thermodynamic equilibrium showing large amounts of monobranched

and smaller amounts of multibranched paraffins is well documented[34, 35] and is supported by these simulations. The above explanation also clarifies the need to divide the isoparaffins for a given carbon number into mono-, di-, and tribranched lumps, given the lack of thermodynamic equilibrium among them.

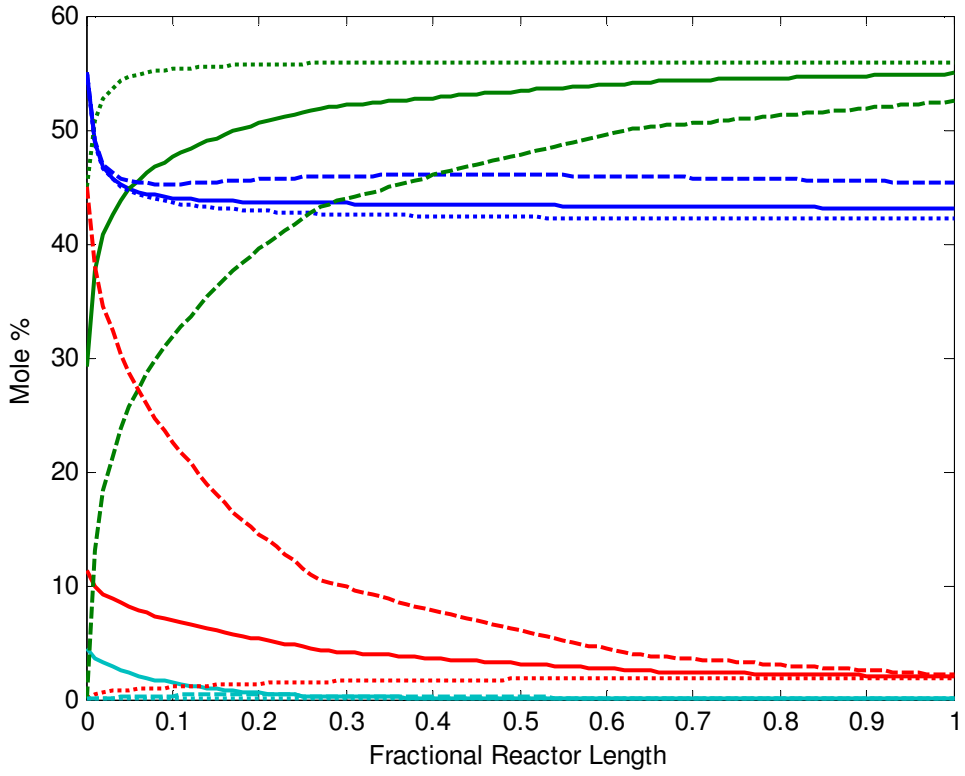

Figure 5-12. Molar composition of the normal, monobranched, dibranched and tribranched isomers among the total paraffins along the reactor length. (Blue: NPA. Green: MBP. Red: DBP. Cyan: TBP. Solid lines: Base Case. Dotted lines: Case-1. Dashed lines: Case-2.).

5.3.2. Analysis of the Distribution of Isomers in Ring-Containing Hydrocarbon Classes

In Set II simulations, the distribution of isoparaffins in the feedstock is maintained at their base values. Three different cases are compared with the base case to analyze the effect of the distribution of isomers with different number of methyl branches in the hydrocarbon classes containing one or more of naphthenic or aromatic rings (i.e., class 3 to 16 in Table 2-1. Case 3 simulation corresponds to a VGO feed composition in which 100 % of the isomers in each of classes 3 to 16 are assumed to be unbranched, i.e., not having any methyl branch anywhere on the ring or along the side chain. Case 4 and Case 4 assumed similarly the isomers to be 100% monobranched and 100 % dibranched, respectively. The comparison of the three cases with the base case is shown in Figure 5-13 to Figure 5-15.

Similar to the isoparaffins, increasing the isomers with more degree of branching increases the VGO conversion, however, the increase in conversion is substantial, unlike with isoparaffins, because of the large amount of ring containing species (73.5 wt %) in the VGO.

It can be seen from Figure 5-13 (Case 3) that for mononaphthenes and dinaphthenes classes [Figure (b) and (c)] unbranched fraction decreases quite rapidly to approach the base case composition with a similar increase in the monobranched isomer fraction. For the aromatics and naphtheno-monoaromatics, the rate at which the unbranched fraction decreases and monobranched fraction increases is very low and stays very far from the base case, even at the end of the reactor. This is probably because of the lower carbon number range (only up to C_{22} as against C_{33} for naphthenes) of these species in the VGO feedstock, [Table 5-2] as the global rate coefficient for *PCP* isomerization increases with the carbon number as can be deciphered from the lumping coefficient plots [Figure 3-5] for *PCP(s;s)* mode. Analogous behavior can be seen in Case 4 [Figure 5-14].

In Case 5, when the feedstock contains 100% dibranched isomers, 47% conversion takes place in only first 13% of the reactor with a sharp decrease in the amount of dibranched

isomers in each class [Figure 5-15]. This decrease is caused by the high rate of cracking of the dibranched isomers as well as to their sequential isomerization into the monobranched and unbranched isomers through PCP, seen by a rapid increase in the amount of monobranched and unbranched isomers approaching their base case values. The rapid increase in the monobranched isomers associated with the cracking of dibranched isomers can be explained by the fact that the total number of methyl branches in the products of β-scission is always one less than the number of methyl branches in the reactant, i.e., the two fragments obtained from the cracking of dibranched mononaphthenes (in the side chain) would have only one methyl branch in total.

Similar to the Set I simulation results for isoparaffins, it can be observed for ring containing species also that the final distribution of the hydrocracking products is very far from their thermodynamic equilibrium with respect to the isomers with different number of methyl branches, illustrating the requirement to have separate lumps for the four subclasses for each class per carbon number.

As a summary of this section, the VGO conversion is quite sensitive to the distribution of the isomers inside the classes. When the distribution is changed for the isomers of only one class, the change in the conversion is not very large, but the cumulative effect of the change in the isomer distribution of all the classes becomes significant. The conversion increases when the amount of isomers with more methyl branches is increased. The isomer distribution in the products converges to the similar values (within roughly 10% range) irrespective of the distribution of the isomers in the feedstock, especially at the high conversions. The final distribution of isomers in a class at the reactor exit is quite different from the corresponding thermodynamic equilibrium.

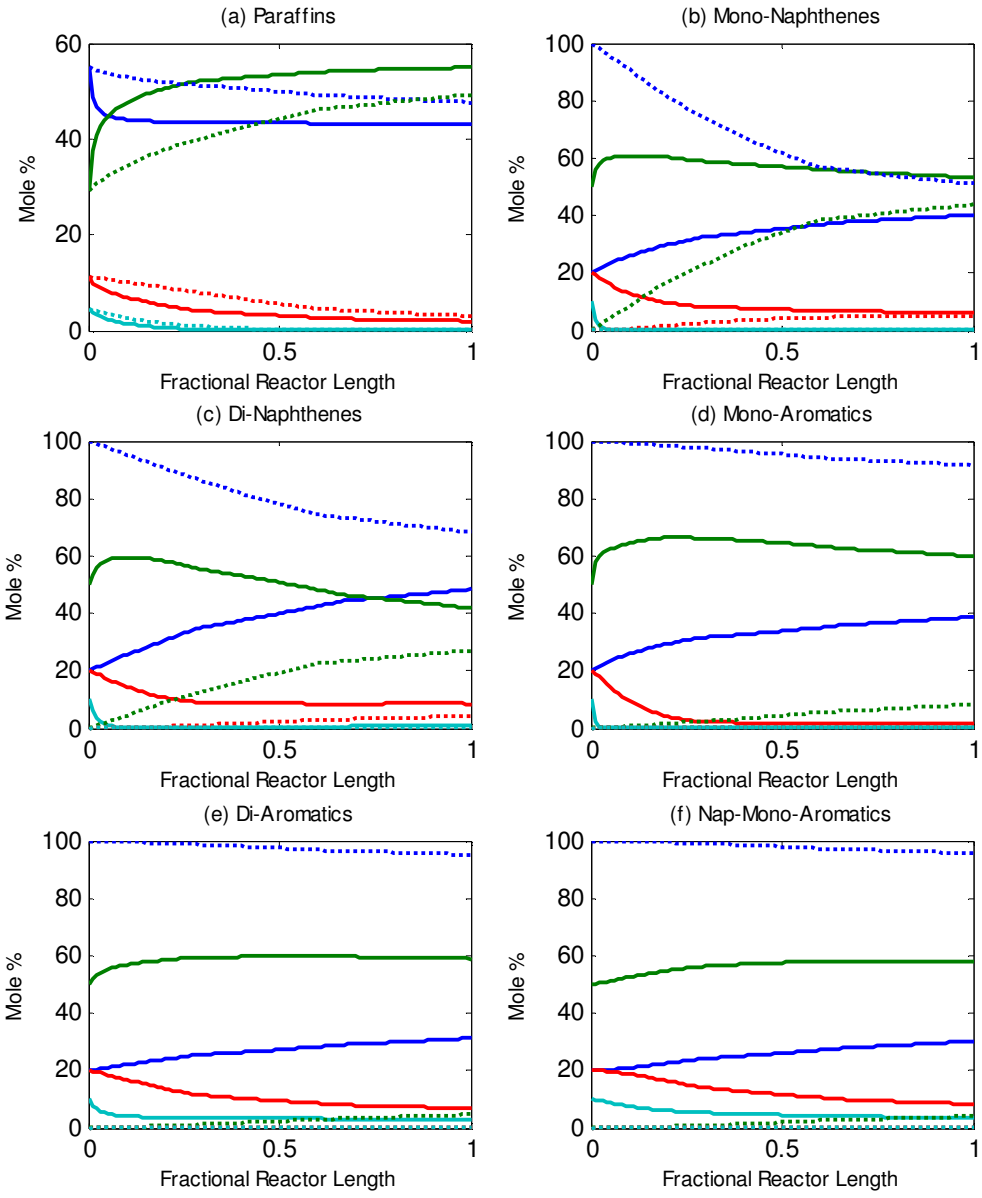

Figure 5-13. Molar composition of the unbranched, monobranched, dibranched and tribranched isomers for different hydrocarbon classes along the reactor length for case-3. (Blue: NPA. Green: MBP. Red: DBP. Cyan: TBP. Solid lines: Base Case. Dotted lines: Case 3.).

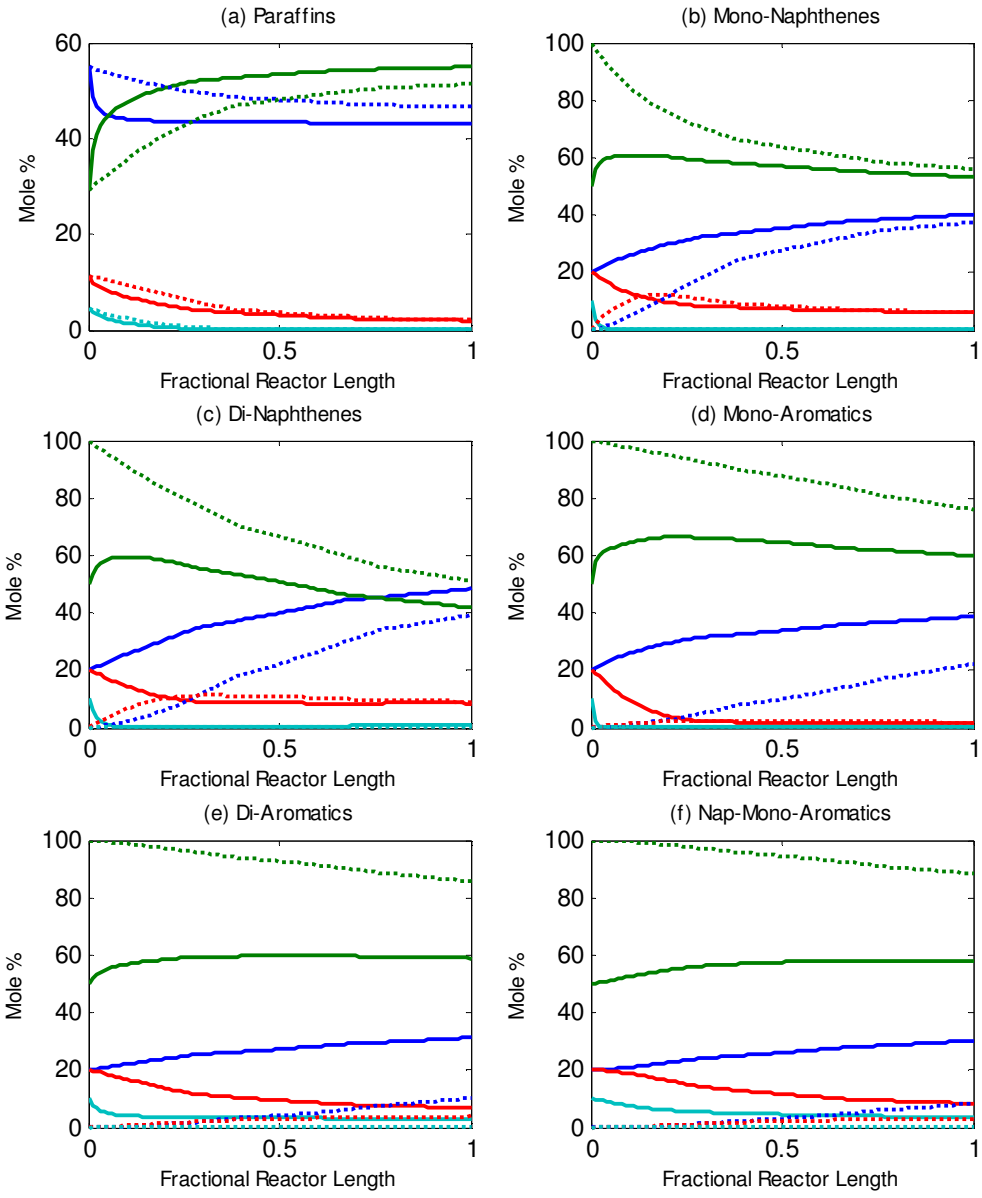

Figure 5-14. Molar composition of the unbranched, monobranched, dibranched and tribranched isomers for different hydrocarbon classes along the reactor length for case-4. (Blue: NPA. Green: MBP. Red: DBP. Cyan: TBP. Solid lines: Base Case. Dotted lines: Case 4.).

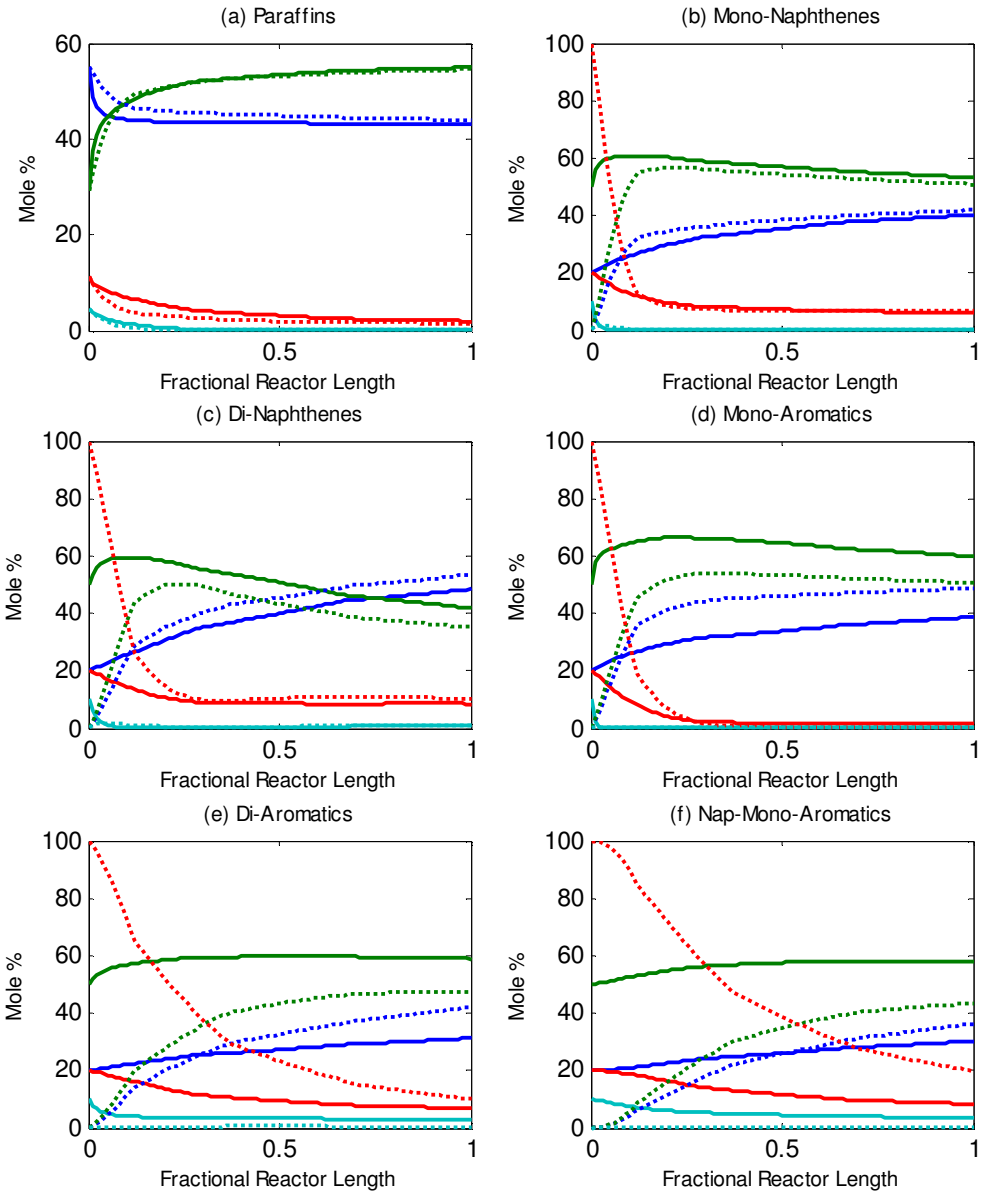

Figure 5-15. Molar composition of the unbranched, monobranched, dibranched and tribranched isomers for different hydrocarbon classes along the reactor length for case-5. (Blue: NPA. Green: MBP. Red: DBP. Cyan: TBP. Solid lines: Base Case. Dotted lines: Case 5.).

CHAPTER VI

KINETIC MODEL DEVELOPMENT FOR THE HYDROCRACKING OF PURE PARAFFINS

6.1. Introduction

Hydrocracking is a process of considerable flexibility and can be used for the conversion of a wide range of feedstocks into a variety of desired products.[3] In addition to the hydrocracking of vacuum gas oil (VGO) and other refinery residues, hydrocracking is also applied to crack the Fischer-Tropsch products for the production of middle distillate of very high quality.[93, 94] The synthetic diesel produced by this process has a cetane number of more than 74 with zero sulfur content.[95, 96] This has motivated the development of a detailed model for the hydrocracking of pure paraffins with a more fundamental approach than considered for the VGO hydrocracking in Chapters III to V.

Hydrocracking of paraffins is carried out on bifunctional catalysts with a metal function, generally provided by Pt to catalyze the dehydrogenation into olefins and an acid function catalyzing isomerization and cracking. The acid function is often provided by Y-zeolites because of their wider pore structure that minimizes the diffusion resistance for the bulky molecules of heavy feedstocks.

It has been shown in several studies[11, 17, 97] on hydroisomerization and hydrocracking of model compounds ranging from C_8 to C_{12} paraffins that on a well-balanced catalyst (i.e. having sufficient metal activity), hydrogenation/dehydrogenation steps are intrinsically much faster than the elementary steps taking place on the acid sites. As a result, the hydrogenation/dehydrogenation reactions attain quasi-equilibrium and the elementary steps on the acid sites are the rate determining steps, represented by 'Ac-rds'. Under these conditions, the concentration of a particular olefin intermediate depends only on the concentration of the corresponding saturated paraffin and monobranched feed isomers are the only primary products, whereas multibranched and cracked molecules are secondary products. The concentration of feed isomers is high and secondary

cracking is relatively limited. On the other hand, if the catalyst does not have sufficient metal activity to equilibrate the hydrogenation/dehydrogenation steps, the situation becomes considerably more complex. Under these so called 'non-ideal' hydrocracking conditions, the concentration of a particular olefin intermediate depends on the concentration of all the paraffins present in the reaction mixture.[98] When the rate determining steps shift from acidic sites to both the acid and metal sites of the catalyst (represented as 'Me-Ac-rds') multi-branched feed isomers and cracked products become primary products of hydrocracking. It also results in increased cracking selectivities and more secondary cracking. Degnan and Kennedy[98] studied this phenomenon by conducting experiments on n-heptane hydroisomerization on physical mixtures of beta zeolite and Pt/Al_2O_3 particles by varying the amount of metal containing component. They reported that the cracking vs. isomerization selectivity varies significantly with the metal loading up to a point beyond which the degree of isomerization is independent of the metal loading. They interpreted their results using a simplified dual-site model.

Debrabandere and Froment[99] studied the gas-phase hydrocracking of C_8 to C_{12} n-paraffins on a Pt/USY zeolite for a variety of operating conditions. For a catalyst with given metal to acid activity, high temperatures, low pressures and high hydrogen to hydrocarbon ratios shift the rate determining step from acidic sites to the metal sites of the catalyst. These effects are more pronounced when the reacting hydrocarbons have longer side chains. Thybaut et al.[100] explained this behavior in gas-phase hydrocracking of paraffins using a lumped reaction scheme and simplified analytical expressions.

In the work reported here, a detailed mechanistic kinetic model has been developed for the hydrocracking of heavy paraffins in which the rate determining step is assumed to occur on both acid and metal sites of the catalyst. The generalized nature of the model also makes it applicable to the specific case in which the hydrogenation/dehydrogenation steps are at equilibrium, which has been conventionally referred to as 'ideal hydrocracking' or 'Ac-rds'. Because of the fundamental nature of the rate parameters, this model can be used for the hydrocracking of mixtures of paraffins.

6.2. Kinetics of Hydrogenation/Dehydrogenation Reactions

Hydrogenation/dehydrogenation reactions are modeled using a molecular dehydrogenation mechanism and are represented by the following sequence of steps occurring on the metal sites:

$$P_i^{liq} \underset{(zeolite)}{\overset{sorption}{\rightleftharpoons}} P_i^{sorbed} \quad \left(K_{L,Pi}\right) \qquad \text{(i)}$$

$$P_i^{sorbed} + m \rightleftharpoons P_i m \quad \left(K_{C,Pi}\right) \qquad \text{(ii)}$$

$$P_i m + m \underset{kdh_{-ij}}{\overset{kdh_{ij}}{\rightleftharpoons}} O_{ij} m + H_2 m \quad \left(K_{DH,ij}^{ads}\right) \qquad \text{(iii)}$$

$$O_{ij} m \rightleftharpoons O_{ij}^{sorbed} + m \quad \left(K_{C,Oij}\right)^{-1} \qquad \text{(iv)}$$

$$O_{ij}^{sorbed} + H^+ \overset{pr/depr}{\rightleftharpoons} R_{ik}^+ \qquad \text{(v)}$$

$$R_{ik}^+ \xrightarrow{HS/MS/PCP} R_{il}^+ \qquad \text{(vi)}$$

$$R_{ik}^+ \xrightarrow{Cracking} R_{jm}^+ + O_{uv}^{sorbed} \qquad \text{(vii)}$$

$$H_2 m \rightleftharpoons H_2^{liq} + m \quad \left(K_{C,H_2}\right)^{-1} \qquad \text{(viii)}$$

$$O_{ij}^{sorbed} \underset{(zeolite)}{\overset{desorption}{\rightleftharpoons}} O_{ij}^{liq} \quad \left(K_{L,Oij}\right)^{-1} \qquad \text{(ix)}$$

Scheme 1. Reaction mechanism for metal and acid sites steps considered in the model

The elementary steps taking place on the acid sites have also been listed in Scheme 1. When the rate determining step of the hydrogenation/dehydrogenation sequence on the metal site is the surface dehydrogenation step, i.e., step (iii), the rate of formation of olefin O_{ij} is given by

$$r_{Oij,metal}^{Form} = \frac{kdh_{ij}\left(K_{C,Pi}\left[C_{Pi}\right] - \frac{K_{C,Oij}\left[C_{O_{ij}}\right]K_{C,H_2}C_{H_2}^{liq}}{K_{DHij}^{ads}}\right)c_m^2}{\left(1+\sum_i K_{C,Pi}\left[C_{Pi}\right]+\sum_{ij} K_{C,Oij}\left[C_{O_{ij}}\right]+K_{C,H_2}C_{H_2}^{liq}\right)^2} \tag{6.1}$$

The square brackets represent concentrations of the sorbed species in the zeolite pores. In a three-phase reactor operating in the trickle flow regime, it is assumed that the entire external catalyst surface is covered with a liquid film of hydrocarbons and the sorption of hydrocarbons into the pores of the zeolite proceeds from the liquid phase. It is further assumed that hydrogen is directly chemisorbed from the liquid phase onto the metal sites of the catalyst. The concentration of the sorbed species can be eliminated in terms of the observable liquid phase concentrations using the following expression:

$$\left[C_{Pi}\right] = \frac{H_{Pi}C_{Pi}^{liq}}{D_L} \tag{6.2}$$

in which Henry's coefficient for the sorption of paraffin P_i in the pores of the zeolite is given by

$$H_{Pi} = K_{L,Pi}c_{sat,Pi} \text{ and } D_L = \left[1+\sum_i K_{L,Pi}C_{Pi}^{liq}+\sum_{ij} K_{L,Oij}C_{Oij}^{liq}\right] \tag{6.3}$$

By using equation (6.2) and a similar eqn for olefins, eqn (6.1) can be written as

$$r_{Oij,metal}^{Form} = \frac{k_{dhij}\left[K_{C,Pi}H_{Pi}C_{Pi}^{liq} - \frac{K_{C,Oij}H_{Oij}C_{Oij}^{liq}K_{C,H2}C_{H_2}^{liq}}{K_{DH,ij}^{ads}}\right]c_m^2}{D_C^2 D_L} \tag{6.4}$$

$$\text{where } D_C = \left[1+\sum_i \frac{K_{C,Pi}H_{Pi}C_{Pi}^{liq}}{D_L}+\sum_{ij}\frac{K_{C,Oij}H_{Oij}C_{Oij}^{liq}}{D_L}+K_{C,H_2}C_{H_2}^{liq}\right] \tag{6.5}$$

The equilibrium constant for the overall dehydrogenation reaction in liquid phase, i.e., $K_{DH,ij}^{liq}$ can be expressed in terms of the equilibrium constant for the surface dehydrogenation step as

$$K_{DHij}^{liq} = \frac{K_{L,Pi} K_{C,Pi} K_{DHij}^{ads}}{K_{L,Oij} K_{C,Oij} K_{C,H_2}} \tag{6.6}$$

Considering that the difference in the saturated liquid molar volume of a paraffin and the corresponding olefin is negligible, the saturation concentration of paraffins in the pores of zeolite $c_{sat,Pi}$ can be assumed to be the same as that of the corresponding olefin $c_{sat,Oij}$. Eqns (6.4) and (6.6) can be combined to give the rate of formation of olefin O_{ij} on the metal sites as,

$$r_{Oij,metal}^{Form} = \frac{k_{dhij} K_{C,Pi} H_{Pi} \left[C_{Pi}^{liq} - \frac{C_{Oij}^{liq} C_{H_2}^{liq}}{K_{DH,ij}^{liq}} \right] c_m^2}{D_C^2 D_L} \tag{6.7}$$

6.3. Expressing $K_{DH,ij}^{liq}$ in Terms of the True Thermodynamic Equilibrium Coefficient

The true thermodynamic equilibrium coefficient K_{DH} for the dehydrogenation reaction $P_i = O_{ij} + H_2$ can be expressed in terms of the activities of the reactants and products as follows:

$$K_{DH} = \frac{\left(\hat{f}_{Oij} / f_{Oij}^o \right) \left(\hat{f}_{H2} / f_{H2}^o \right)}{\left(\hat{f}_{Pi} / f_{Pi}^o \right)} \tag{6.8}$$

Considering ideal gas at 1 atm *(=P_o)* to be the standard state for all the components, the liquid-phase fugacities of reacting species can be written as:

$$\hat{f}_{Pi} = x_{Pi} \gamma_{Pi} f_{Pi}^L(T, P) \tag{6.9}$$

$$\hat{f}_{Oij} = x_{Oij} \gamma_{Oij} f_{Oij}^L(T, P) \tag{6.10}$$

$$\hat{f}_{H2} = x_{H2} H_{H2}(T,P) \tag{6.11}$$

yielding

$$K_{DH} = \left(\frac{x_{Oij} x_{H2}}{x_{Pi}}\right)\left(\frac{\gamma_{Oij}}{\gamma_{Pi}}\right)\left(\frac{f_{Oij}^{L}(T,P)}{f_{Pi}^{L}(T,P)}\right)\left(\frac{K_{H_2}^{VLE}}{P_o}\right) \tag{6.12}$$

Therefore, the equilibrium coefficient relating the liquid-phase concentrations of reacting species can be expressed in terms of the 'true' gas-phase thermodynamic equilibrium coefficient by

$$K_{DH}^{liq} = \left(\frac{C_{oij}^{liq} C_{H2}^{liq}}{C_{Pi}^{liq}}\right) = K_{DH}\left(\frac{\gamma_{Pi}}{\gamma_{Oij}}\right)\left(\frac{f_{Pi}^{L}(T,P)}{f_{Oij}^{L}(T,P)}\right)\left(\frac{P_o}{K_{H_2}^{VLE}}\right) C_{total}^{liq} \tag{6.13}$$

It has been assumed that the ratio of the liquid phase fugacities of pure components and the ratio of activity coefficients of a paraffin and corresponding olefin are close to one, resulting in

$$K_{DH}^{liq} = K_{DH}\left(\frac{P_o}{K_{H_2}^{VLE}}\right) C_{total}^{liq} \tag{6.14}$$

The gas-phase equilibrium coefficient is calculated using Benson's group contribution method[65] and the Henry coefficient of hydrogen in the liquid phase is calculated using the Peng-Robinson equation of state[66].

6.4. Modeling of the Metal Site Rate Parameters

Eqn (6.7) contains the rate coefficients for the dehydrogenation reactions, k_{dhij}. For a particular paraffin molecule P_i, several dehydrogenation rate coefficients k_{dhij} may be required, depending upon the number and structure of the olefinic isomers O_{ij} produced from P_i. This leads to a large number of dehydrogenation rate coefficients, even for the hydrocracking of a simple paraffinic feedstock. For example, for n-decane, 411 hydrogenations / dehydrogenations are required to describe its hydrocracking at the fundamental level. The number of possible hydrogenations/dehydrogenations increases exponentially with the number of carbon atoms in the feedstock. The total number of

hydrogenations/dehydrogenations taking place in the hydrocracking of a feedstock with *n* carbon atoms in the heaviest molecule is obtained by the cumulative sum of all the olefinic isomers up to carbon number *n*. Given the large number of olefinic isomers and associated hydrogenation/dehydrogenations, it is obvious that some simplification is required to reduce the number of hydrogenation/dehydrogenation rate parameters. Baltanas et al.[101] considered one rate coefficient per carbon number in their model, leading to 9 independent rate coefficients for the hydrocracking of C_{16} and resulting in 18 temperature independent parameters, A and E. The number of these parameters keeps on increasing linearly with the carbon number of the feedstock. Given the highly non-linear nature of the kinetic model, it is obvious that the meaningful estimation of such a large number of parameters may be subject to considerable errors and would be practically impossible for heavier feedstocks. A more fundamental approach is required to model the rate coefficients for dehydrogenation reactions with a minimum number of truly independent parameters. The number of these independent parameters and their values should not change with the carbon number and composition of the feedstock. In the methodology proposed here, it is assumed that the activation energy for a particular dehydrogenation step depends on the ease with which the hydrogen atoms can be removed from two neighboring carbon atoms of a paraffin molecule. The energy required to remove a hydrogen atom depends on the nature of the parent carbon atom: primary, secondary or tertiary[102]. The activation energies for the dehydrogenation of paraffins would then depend on the location of the double bond in the product olefin, or in other words, on the nature of the carbon atoms forming the double bond in the olefin. Consequently, all the dehydrogenation rate coefficients can be modeled using five different activation energies depending upon the nature of the resulting double bonded carbon atoms, i.e., *(p-s), (p-t), (s-s), (s-t)* and *(t-t)*. A single value of the pre-exponential factor is used for all the dehydrogenation modes. Although the corresponding five fundamental rate coefficients are independent of the number of carbon atoms in the reactant, the 'effective' rate coefficient for the dehydrogenation of a particular paraffinic molecule increases with the number of carbon atoms. Figure 6-1 shows the relative

importance of the different modes of hydrogenation/dehydrogenation steps as a function of the carbon number. The percentage of *(s-s)* mode is highest and increases with the carbon number. The percentage of *(t-t)* mode is the lowest and decreases with the carbon number.

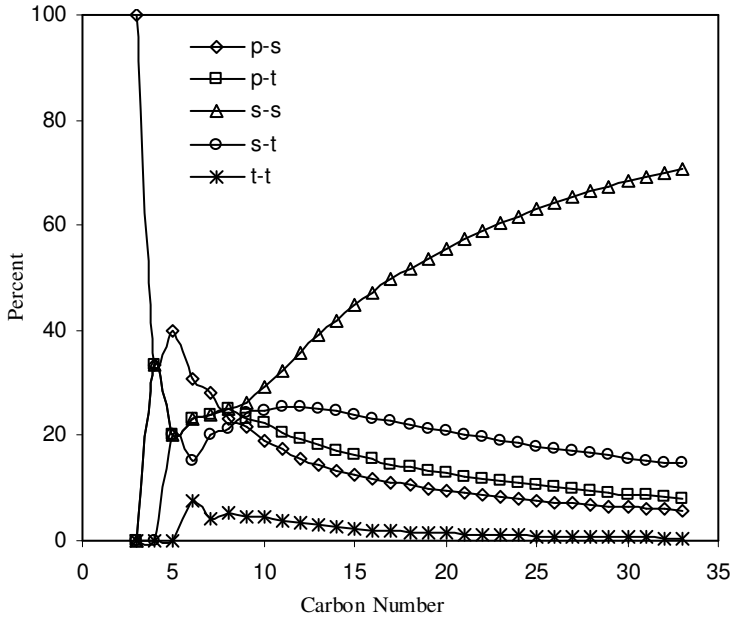

Figure 6-1. Importance of different dehydrogenation modes with respect to carbon number.

6.5. Modeling of the Acid Site Rate Parameters

The single-event concept[11, 36] has been applied to model the frequency factors for the acid site steps. Refer to Chapter III for the theory of single event kinetics. The activation energies of all these steps are modeled using the linear free-energy relationship of Evans-Polanyi[103]. The five different kinds of elementary steps in paraffins hydrocracking

namely, protonation/deprotonation, hydride shift, methyl shift, PCP and β- scission are named as five different 'types'. In the VGO hydrocracking model it was assumed that the energy level of a particular carbenium ion is determined only by its nature, i.e., secondary or tertiary. Therefore, it was generally considered that all the elementary steps of a particular type, in which a reactant carbenium ion of nature *m* is converted into a product carbenium ion of nature *n*, have the same value of activation energy (*m* and *n* can be *-s* or *–t*)*. As a result of this, for one type of elementary step, a total of four subtypes and consequently four different activation energies were used.

Considering that the energy of a carbenium ion depends only on its nature is equivalent to saying that the energy of carbenium ions depends only on the number of carbons in alpha position with respect to the positive charge, because all the secondary carbenium ions have two alpha carbons and the tertiary carbenium ions have three alpha carbons. It can be seen, however, that there is a significant difference in the energies of carbenium ions with the same carbon number and same nature, depending upon the possible amount of charge delocalization in the vicinity of the charge carrying carbon atom. Hence, the energy of carbenium ions of a particular carbon number not only depends on the number of alpha carbon atoms but also on their nature, although the latter effects are much weaker.

To eliminate the effects of the above assumption, the Evans-Polanyi relationship has been introduced into the single-event kinetic model for the hydrocracking of paraffins, as done by Park & Froment[74] for the simpler case of methanol to olefin (MTO) process and Martinis and Froment[73] for the alkylation of isobutane with butenes. The Evans-Polanyi approach requires the calculation of the heat of formation of every individual carbenium ion to get the heat of reactions of elementary steps. The activation energy of a particular step is then calculated by using the linear free energy relationship of Evans and Polanyi.

* From here on, all these steps will be referred to as belonging to one 'subtype'.

6.5.1. Evans-Polanyi Relationship

According to the Evans-Polanyi relationship, the activation energy varies linearly with the energy change associated with the elementary step as,

$$\begin{aligned} E &= E_o + \alpha(\Delta H_r^s) \qquad if\ \Delta H_r^s > 0 \\ E &= E_o + (1-\alpha)(\Delta H_r^s) \quad if\ \Delta H_r^s < 0 \end{aligned} \tag{6.15}$$

where α is the transfer coefficient and E_o is the intrinsic activation energy for the elementary steps of the given type. In the above equation, ΔH_r^s is the heat of reaction at the catalyst surface for the particular elementary step. Consequently, to model the activation energies of all the elementary steps of one type, only two independent parameters, E_o and α are required, provided the heat of individual elementary steps at the surface of the catalyst are available.

6.5.2. Rate Equations for the Acid Site Steps

Using the single-event approach and the Evans-Polanyi relationship, the rate of a PCP elementary step, e.g., $R_{ik}^+(m) \rightarrow R_{jl}^+(n)$ is given by

$$r_{pcp,(m;n)} = n_{e,pcp}\tilde{A}_{pcp} \exp\left(-\frac{E_{o,pcp} + \alpha_{pcp}^{'}\Delta H_r^s}{RT}\right)\left[C_{R_{ik}^+}\right] \tag{6.16}$$

$$\text{where } \alpha_{pcp}^{'} = \alpha_{pcp} \qquad if\ \Delta H_r^s > 0 \tag{6.17}$$

$$\text{and } \alpha_{pcp}^{'} = (1-\alpha_{pcp})\ \ if\ \Delta H_r^s < 0 \tag{6.18}$$

The concentration of surface carbenium ion, $\left[C_{R_{ik}^+}\right]$ is determined using the protonation equilibrium coefficient between the sorbed olefins and the surface carbenium ions. i.e.,

$$\left[C_{R_{ik}^+}\right] = K_{pr}\left[C_{Oij}\right]\left[H^+\right] \tag{6.19}$$

To get the value of the protonation equilibrium coefficient, the entropy of protonation ΔS_{pr}^s and the heat of protonation ΔH_{pr}^s at the surface are required. If the effect of the

structure of the reacting olefin and the product carbenium ion is accounted for using the single-event concept, a single value for the intrinsic entropy of protonation, $\Delta\hat{S}_{pr}$ would be sufficient to obtain the entropies of all the protonation steps. The heat of protonation is calculated from the heats of formation of the involved species according to

$$\Delta H^{s}_{pr} = \Delta H^{s}_{f}(R^{+}) - \Delta H^{s}_{f}(H^{+}) - \Delta H^{sorbed}_{f}(O) \tag{6.20}$$

In the above equation[‡], the superscript *s* refers to the surface species. In three phase hydrocracking, consideration of the 'effective' latent heat of the carbenium ion is required to get the heats of formation in the liquid phase from the gas phase heats of formation. The energy changes associated with the phase transition for a carbenium ion and olefin are shown in Figure 6-2. The heats of formation of surface carbenium ions are obtained by subtracting the heat of stabilization of these species from their liquid phase heats of formation. i.e.,

$$\Delta H^{s}_{f}(R^{+}) = \Delta H^{g}_{f}(R^{+}) - \Delta H_{vap}(R^{+}) - \Delta H_{stab}(R^{+}) \tag{6.21}$$

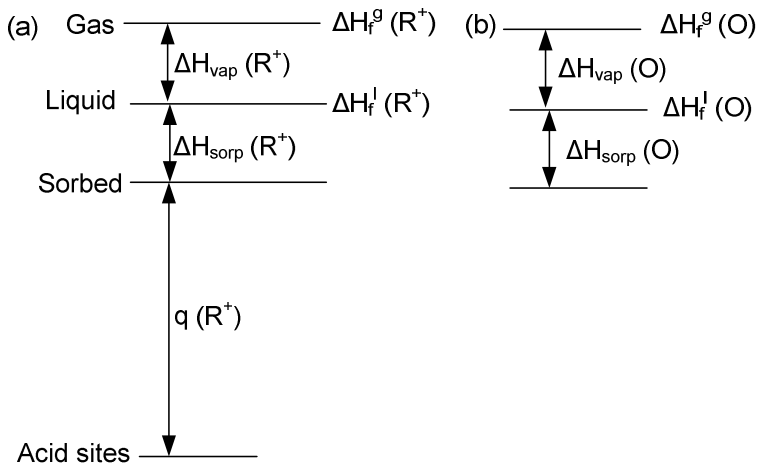

Figure 6-2. Energy changes associated with phase transition of (a) carbenium ion (b) olefin.

[‡] For the sake of simplicity, the subscripts of the olefins and carbenium ions have been dropped.

The heat of stabilization of carbenium ions $\Delta H_{stab}(R^+)$ can be written as the sum of the heat of sorption of carbenium ions from liquid phase into the zeolites pores $\Delta H_{sorp}(R^+)$ and the heat of chemisorption from sorbed phase to the surface $q(R^+)$ i.e.,

$$\Delta H_{stab}(R^+) = \Delta H_{sorp}(R^+) + q(R^+) \tag{6.22}$$

Dumesic et al.[72] considered a constant value for the energy of stabilization of carbenium ions, $q(R^+)$ regardless of the nature of the carbenium ion. Martinis and Froment[73] distinguished between the energy of stabilization of secondary and tertiary ions They also accounted for the effect of chain length on the stabilization energy. The latter effect, however, was found to be very small and has been neglected in the current model.

The stabilization of an olefin from the liquid phase to the zeolite pores involves only the heat of sorption $\Delta H_{sorp}(O)$ so that,

$$\Delta H_f^{sorbed}(O) = \Delta H_f^g(O) - \Delta H_{vap}(O) - \Delta H_{sorb}(O) \tag{6.23}$$

The heat of stabilization of a proton from the gas phase to the surface is represented by $q(H^+)$ so that,

$$\Delta H_f^s(H^+) = \Delta H_f^g(H^+) - q(H^+) \tag{6.24}$$

Substituting eqns (6.21), (6.22), (6.23), and (6.24) into eqn (6.20) and assuming that the latent heats of vaporization of an olefin and the corresponding carbenium ion are identical , the heat of protonation becomes:

$$\begin{aligned} \Delta H_{pr}^s = &\left[\Delta H_f^g(R^+) - \Delta H_f^g(H^+) - \Delta H_f^g(O)\right] + [q(H^+) - q(R^+)] \\ &- \left[\Delta H_{sorp}(R^+) - \Delta H_{sorp}(O)\right] \end{aligned} \tag{6.25}$$

The last bracket in eqn (6.25) is the difference in the heat of sorption of a carbenium ion and the corresponding olefin. For the same number of carbon atoms and the same skeleton structures of these two species, the difference in their heats of sorption is assumed to be negligible. The middle bracket is the difference in the heats of

chemisorption of a proton and the heat of chemisorption of a carbenium ion and is represented by $\Delta q(R^+)$ [74]. Depending upon the nature of the carbenium ion, it can have two values for a catalyst with given acid strength and can be written as $\Delta q(m)$, where *(m)* can be *(s)* for secondary or *(t)* for the tertiary ions. Eqn (6.25) is now written as

$$\Delta H^s_{pr} = \left[\Delta H^g_f(R^+) - \Delta H^g_f(H^+) - \Delta H^g_f(O)\right] + \Delta q(m) \tag{6.26}$$

The gas phase heat of formation of a proton is known to be 367.2 kcal/mol[72] at 298 K. The gas phase heats of formation of olefins at 298 K are obtained by using Benson's group contribution method. To obtain the gas phase heats of formation of carbenium ions at 298 K, a Benson like group contribution method has been developed. Experimental data on the heats of formation of a number of paraffinic carbenium ions have been taken from Lias et al.[71] Quantum chemical calculations have been performed using Gaussian 03 to obtain the heats of formation of the ions not available in the literature. G3 theory[104] has been used for ions having up to 5 carbon atoms and G3MP2[105] theory for ions with 6 carbon atoms. Secondary and tertiary ions are regressed separately because of the different amount of charge delocalization in the vicinity of the carbon atom carrying the positive charge.

To derive the heat of protonation at the reaction temperature T from the standard state temperature of 298 K, the difference in the heat capacities of the reactant and product species, ΔC_P^{rxn} is required. Given the similar skeleton structures of the reactant and product species, it is assumed that ΔC_P^{rxn} is negligible. Consequently, K_{pr} at the reaction temperature T can be given by applying the single-event approach as,

$$K_{pr} = \frac{\sigma_{gl}^{O_{ij}}}{\sigma_{gl}^{R^+_{ik}}} \exp\left(\frac{\Delta \hat{S}_{pr}}{R}\right) \exp\left(-\frac{\Delta H^s_{pr}}{RT}\right) \tag{6.27}$$

Eliminating ΔH^s_{pr} in terms of the gas phase heat of protonation ΔH^g_{pr} the following equation is obtained for the surface concentration of carbenium ions,

$$\left[C_{R_{ik}^{+}}\right]=\frac{\sigma_{gl}^{O_{ij}}}{\sigma_{gl}^{R_{ik}^{+}}}\exp\left(\frac{\Delta\hat{S}_{pr}}{R}\right)\exp\left(-\frac{\Delta H_{pr}^{g}+\Delta q(m)}{RT}\right)\left[C_{Oij}\right]\left[H^{+}\right] \tag{6.28}$$

Svoboda et al.[16] showed that in the hydrocracking of paraffins the total concentration of the carbenium ions is negligible with respect to the total concentration of the acidic sites. More recently, by taking typical values for the protonation equilibrium coefficients and concentration of sorbed olefins, Thybaut et al.[106] showed that at 506 K, the concentration of the carbenium ions is approximately $7.10\text{x}10^{-4}$ mol/kg$_{cat}$, to be compared with a total concentration of acid sites, which is typically of the order of 0.1-0.8 mol/kg$_{cat}$. Substituting the surface concentration of carbenium ions from eqn (6.28) into (6.16) and replacing $\left[H^{+}\right]$ by C_t, the rate of the PCP step can be written as,

$$r_{pcp(m;n)}=n_{e,pcp}\frac{\sigma_{gl}^{O_{ij}}}{\sigma_{gl}^{R_{ik}^{+}}}\tilde{A}_{pcp}C_t\exp\left(\frac{\Delta\hat{S}_{pr}}{R}\right)\exp\left(-\frac{\Delta H_{pr}^{g}+\Delta q(m)+E_{o,pcp}+\alpha_{pcp}^{'}\Delta H_{r}^{s}}{RT}\right)\left[C_{Oij}\right] \tag{6.29}$$

In the above equation, the heat of reaction of a PCP step is given by

$$\begin{aligned}\Delta H_r^s &= \Delta H_f^s(R_{jl}^{+})-\Delta H_f^s(R_{ik}^{+})\\ &=\left[\Delta H_f^g(R_{jl}^{+})-\Delta H_{vap}(R_{jl}^{+})-\Delta H_{sorp}(R_{jl}^{+})-q(R_{jl}^{+})\right]\\ &-\left[\Delta H_f^g(R_{ik}^{+})-\Delta H_{vap}(R_{ik}^{+})-\Delta H_{sorp}(R_{ik}^{+})-q(R_{ik}^{+})\right]\end{aligned} \tag{6.30}$$

Assuming the difference in the latent heat of vaporization and heat of sorption of the reactant and product carbenium ions to be negligible and adding and subtracting $q(H^{+})$ in the right hand side of equation (6.30), the heat of reaction of the PCP step can be written as,

$$\Delta H_r^s=\Delta H_r^g+\left[\Delta q(n)-\Delta q(m)\right] \tag{6.31}$$

where *n* and *m* represent the nature of the product and reactant carbenium ions, respectively. Substituting equation (6.31) into eqn (6.29) leads to,

$$r_{pcp(m;n)} = n_{e,pcp} \frac{\sigma_{gl}^{O_{ij}}}{\sigma_{gl}^{R_{ik}^{+}}} \tilde{A}_{pcp} C_t \exp\left(\frac{\Delta\hat{S}_{pr}}{R}\right) \exp\left(-\frac{E_{pcp(m;n)}^{comp}}{RT}\right) \left[C_{Oij}\right] \qquad (6.32)$$

$$\text{where } E_{pcp(m;n)}^{comp} = \Delta H_{pr}^{g} + \Delta q(m) + E_{o,pcp} + \alpha_{pcp}^{'} \left(\Delta H_{r}^{g} + \left[\Delta q(n) - \Delta q(m)\right]\right) \qquad (6.33)$$

is the composite activation energy for the PCP step. In eqn (6.32) the sorbed concentration of olefin is expressed by a Langmuir isotherm and is given by an equation analogous to eqn (6.2).

6.6. Late Thermodynamic Lumping of Components

Studies[97, 107, 108] on hydroisomerization and hydrocracking of model compounds from C_8 to C_{12} reveal, that the isomers of any carbon number fraction with a particular degree of branching reach thermodynamic equilibrium because the HS and MS steps are much faster as compared to the PCP steps. Therefore, all the isomers for a particular carbon number with a given degree of branching are placed in one lump with the distribution of isomers in the lump governed by thermodynamic equilibrium. With this late 'strict' or 'thermodynamic' lumping, the model requires four lumps/pure components per carbon number for paraffins and four lumps per carbon number for olefins. For paraffins, these lumps/pure components are designated as n-paraffins, mono-branched paraffins, di-branched paraffins and tri-branched paraffins and, similarly for olefins, n-olefins, mono-branched olefins, di-branched olefins, and tri-branched olefins. A n-paraffin, is obviously not a lump but a pure component. Based on the above late lumping scheme, the kinetic model for the hydrocracking of a paraffin mixture of up to C_{16} requires a total of 48 lumps/pure components for paraffins and 48 lumps (only C_3 will be a pure component in the case of olefins) for olefins.

6.7. Calculation of the Global Rate of Conversion of Lumps

The global rate of consumption of a particular paraffinic lump is the sum of the rates of consumption of all the isomers of that lump through dehydrogenation. Similarly, the rate of consumption of a particular olefinic lump is calculated by summing up the rate of

consumption of all the olefinic isomers of that lump through all the possible hydrogenation steps. To carry out these sums requires going through the entire set of computer generated hydrogenation/dehydrogenation steps, to calculate the equilibrium distribution of the isomers of every lump, and the thermodynamic equilibrium coefficients for all the hydrogenation /dehydrogenation steps. The global rate of conversion of the olefinic lumps through acid site elementary steps is obtained in the same way, but it also requires the heats of reaction for all the PCP and β-scission steps as well as the heats of protonation. This is computationally very demanding for heavy feedstocks, so that a systematic method was developed to calculate the so called 'lumping coefficients' for the steps on the metal and the acidic sites of the catalyst. Their values are pre-calculated at a number of temperature intervals and stored in the computer hard disk, to be used later in the parameter estimation and reactor simulations.

6.8. Lumping Coefficients for the Steps on the Metal Sites

Eqn (6.7) expresses the rate of formation of a particular olefin on the metal sites of the catalyst. This equation is used to calculate the net rate of formation of a particular paraffinic lump P_g, by summation over the rate of formation of every isomer P_i of this lump as,

$$R_{Pg,net}^{Form} = -\frac{K_{C,Pg} H_{Pg} c_m^2}{D_C^2 D_L}\left[\left(\sum_{q=1}^{5} k_{dh,q} LCP_{g,q}\right) C_{Pg}^{liq} - \left(\sum_{q=1}^{5} k_{dh,q} LCO_{g,q}\right) C_{Og}^{liq} C_{H_2}^{liq}\right] \quad (6.34)$$

In the above equation, q represents the index for the mode of dehydrogenation and g for lump number. $LCP_{g,q}$ is the Lumping Coefficient for the consumption of Paraffins of lump g through the q^{th} mode of dehydrogenation and $LCO_{g,q}$ is the Lumping Coefficient for the consumption of Olefins of lump g through the q^{th} mode of hydrogenation. The value of $LCP_{g,q}$ is calculated as

$$LCP_{g,q} = \sum_{i=1}^{\substack{paraffin \\ isomers}} n_{i,q}\, y_{Pi}^{eqm} \quad (6.35)$$

where the index *i* runs over all the paraffin isomers of lump *g*. Further, $n_{i,q}$ is the number of dehydrogenation reactions for the particular paraffin P_i through q^{th} mode and y_{Pi}^{eqm} is the equilibrium mole fraction of the isomer P_i in the lump *g*. Similarly, the value of $LCO_{g,q}$ is calculated as

$$LCO_{g,q} = \sum_{i=1}^{\substack{paraffin\\isomers}} \sum_{j=1}^{n_{i,q}} \frac{y_{Oij}^{eqm}}{K_{DH,ij}^{liq}} \tag{6.36}$$

with y_{Oij}^{eqm} as the equilibrium mole fraction of the olefin isomer O_{ij} in the lump O_g.

6.9. Lumping Coefficients for the Steps on the Acid Sites

Equation (6.32) gives the rate of a PCP elementary step in which an *m* type of carbenium ion is converted into an *n* type of carbenium ion. Since the protonation/deprotonation steps are assumed to be in pseudo-equilibrium, the rate of consumption/formation of carbenium ions would also be equal to the rate of consumption/formation of the corresponding olefinic species. Therefore, to get the global rate of conversion of an olefinic lump, *g*, into another olefinic lump, *h*, through PCP steps of subtype (*m;n*), a summation has to be carried out over the rate of all such steps, yielding

$$R_{pcp(m;n)}^{(g;h)} = \tilde{A}_{pcp} C_t \exp\left(\frac{\Delta \hat{S}_{pr}}{R}\right) \sum_{steps} \left[n_{e,pcp} \frac{\sigma_{gl}^{O_{ij}}}{\sigma_{gl}^{R_{ik}^+}} \exp\left(-\frac{E_{pcp(m;n)}^{comp}}{RT}\right) \left[C_{Oij}\right] \right] \tag{6.37}$$

It can be seen from eqn (6.33) that the composite activation energy involves the heat of protonation of the reacting olefin and heat of reaction of the corresponding elementary step so that the composite activation energies for different PCP *(m;n)* subtype of steps would be different.

To formulate the lumping coefficients for the acid site steps, the composite activation energy as given in eqn (6.33) is split into two parts. i.e.,

$$E_{pcp(m;n)}^{comp} = \left[E_{pcp(m;n)}\right]_1 + \left[E_{pcp(m;n)}\right]_2 \tag{6.38}$$

$$\text{where } \left[E_{pcp(m;n)}\right]_1 = \left[\Delta H_{pr}^{g} + \alpha_{pcp}^{'} \Delta H_{r}^{g}\right] \tag{6.39}$$

$$\text{and } \left[E_{pcp(m;n)}\right]_2 = \left[E_{o,pcp} + \Delta q(m) + \alpha_{pcp}^{'}\left(\Delta q(n) - \Delta q(m)\right)\right] \tag{6.40}$$

As stated above, the value of the terms in $\left[E_{pcp(m;n)}\right]_1$ is different for each elementary step and their evaluation requires the estimation of the heats of formation of individual carbenium ions and olefins. The terms in $\left[E_{pcp(m;n)}\right]_2$, on the other hand, depend only on the nature of the reactant and product carbenium ions and are identical for all the PCP *(m;n)* subtype of steps. By splitting the composite activation energy in this way and taking $\left[E_{pcp(m;n)}\right]_2$ out of the summation, eqn (6.37) can be written as,

$$R_{pcp(m;n)}^{(g;h)} = \tilde{A}_{pcp} C_t \exp\left(\frac{\Delta \hat{S}_{pr}}{R}\right) \exp\left(-\frac{\left[E_{pcp(m;n)}\right]_2}{RT}\right) \sum_{steps} \left[n_{e,pcp} \frac{\sigma_{gl}^{O_{ij}}}{\sigma_{gl}^{R_{ik}^{+}}} \exp\left(-\frac{\left[E_{pcp(m;n)}\right]_1}{RT}\right) \left[C_{Oij}\right] \right] \tag{6.41}$$

Expressing the concentration of the olefin isomer O_{ij} in terms of the concentration of the olefinic lump *g* by using its equilibrium mole fraction y_{Oij}^{eqm}, the global rate of conversion of the olefinic lump *g* into lump *h* by PCP *(m;n)* subtype of steps can be written as:

$$R_{pcp(m;n)}^{(g;h)} = LC_{pcp(m;n)}^{(g;h)} \tilde{A}_{pcp} C_t \exp\left(\frac{\Delta \hat{S}_{pr}}{R}\right) \exp\left(-\frac{\left[E_{pcp(m;n)}\right]_2}{RT}\right) \left[C_g\right] \tag{6.42}$$

where $LC_{pcp(m;n)}^{(g;h)}$ is the corresponding lumping coefficient given by,

$$LC_{pcp(m;n)}^{(g;h)} = \sum_{steps} \left[n_{e,pcp} \frac{\sigma_{gl}^{O_{ij}}}{\sigma_{gl}^{R_{ik}^{+}}} \exp\left(-\frac{\left[E_{pcp(m;n)}\right]_1}{RT}\right) y_{Oij}^{eqm} \right] \tag{6.43}$$

A similar approach is applied to formulate the rate of consumption/formation of a lump through cracking steps. The lumping coefficients for PCP/cracking are functions of α_{pcp}, α_{cr}, and temperature and do not depend on any other model parameter.

In eqn (6.42), the concentration of the olefinic lump g in the sorbed phase is eliminated in favor of its concentration in the liquid phase so that,

$$R_{pcp(m;n)}^{(g;h)} = LC_{pcp(m;n)}^{(g;h)} \tilde{A}_{pcp} C_t \exp\left(\frac{\Delta \hat{S}_{pr}}{R}\right) \exp\left(-\frac{\left[E_{pcp(m;n)}\right]_2}{RT}\right) \frac{H_{Og} C_{Og}^{liq}}{D_L} \tag{6.44}$$

Given the form of the rate expressions in eqn (6.44), the separate estimation of the single-event frequency factor for PCP/cracking and the entropy of protonation is not possible. Therefore, composite single-event frequency factors for PCP and cracking steps are defined as,

$$\tilde{A}_{pcp}^{comp} = \tilde{A}_{pcp} C_t \exp\left(\frac{\Delta \hat{S}_{pr}}{R}\right) \tag{6.45}$$

$$\tilde{A}_{cr}^{comp} = \tilde{A}_{cr} C_t \exp\left(\frac{\Delta \hat{S}_{pr}}{R}\right) \tag{6.46}$$

Introducing these composite frequency factors, eqn (6.44) becomes after rearranging:

$$R_{pcp(m;n)}^{(g;h)} = LC_{pcp(m;n)}^{(g;h)} \tilde{A}_{pcp}^{comp} \left(\frac{H_{Og}}{D_L}\right) \exp\left(-\frac{\left[E_{pcp(m;n)}\right]_2}{RT}\right) C_{Og}^{liq} \tag{6.47}$$

6.10. Net Rate of Formation of Paraffinic and Olefinic Lumps

A paraffinic lump/pure component can only be consumed or produced on the metal sites of the catalyst. Therefore, the net rate of formation of a paraffinic lump P_g is directly given by eqn (6.34). Olefinic lumps, on the other hand are produced/consumed on both the metal and acid sites. The rate of formation of a particular olefinic lump O_g on the metal sites is given by the negative of the rate of formation of the corresponding paraffinic lump P_g, i.e.,

$$R_{Og,metal}^{Form} = -R_{Pg,metal}^{Form} \tag{6.48}$$

The rate of formation of an olefinic lump O_g on the acid sites is obtained by summing up the rate of formation of this lump from all the other olefinic lumps by PCP/cracking steps. The net rate of formation of lump O_g is then given by

$$R_{Og,net}^{Form} = R_{Og,metal}^{Form} + R_{Og,acid}^{Form} \tag{6.49}$$

$$\text{where } R_{Og,acid}^{Form} = \sum_{i=1}^{N_{lumps}} \sum_{(m;n)} R_{pcp(m;n)/cr(m;n)}^{(i;g)} \tag{6.50}$$

The summation over *(m;n)* implies summation over all the four subtypes namely, *(s;s),(s;t),(t;s)* and *(t;t)* of PCP and cracking steps.

The rate of formation of hydrogen is written as the sum of the rate of formation of olefins from the hydrogenation/dehydrogenation reactions on metal sites, i.e.,

$$R_{H_2,net}^{Form} = -\sum_{i=1}^{N_{lumps}} R_{Pi,net}^{Form} \tag{6.51}$$

6.11. Reactor Model for Three-Phase Hydrocracking

Similar to the continuity equations developed in Chapter IV for the hydrocracking of VGO, continuity equations are written for the gas phase paraffinic components/lumps and hydrogen as

$$\frac{1}{\Omega}\frac{dF_{Pg}^{gas}}{dz} = -k_{O,Pg}a_v\left(\frac{C_{Pg}^{gas}}{K_{Pg}^{C,eqm}} - C_{Pg}^{liq}\right) \quad g = 1,2,.....N_{lumps} \tag{6.52}$$

The continuity equations for paraffinic components in the liquid phase also take into account the net rate of formation of component/lump g along with the gas-liquid flux term,

$$\frac{1}{\Omega}\frac{dF_{Pg}^{liq}}{dz} = k_{O,Pg}a_v\left(\frac{C_{Pg}^{gas}}{K_{Pg}^{C,eqm}} - C_{Pg}^{liq}\right) + R_{Pg,net}^{Form} \quad g = 1,2,.....N_{lumps} \tag{6.53}$$

As the equilibrium coefficient for the dehydrogenation of paraffins is of the order of 10^{-4}-10^{-5} and the reactor is operated under high hydrogen partial pressures, the

concentration of olefins are several orders of magnitude smaller than the corresponding paraffins. Therefore it has been assumed that the olefinic components exist only in the liquid phase. Consequently, the continuity equations for olefinic lumps/components do not contain the mass-transfer term, i.e.,

$$\frac{1}{\Omega}\frac{dF_{Og}^{liq}}{dz} = R_{Og,net}^{Form} \quad g = 1,2,.....N_{lumps} \tag{6.54}$$

For three-phase hydrocracking of n-hexadecane, a total of 48 lumps/pure components for paraffins and the same number of lumps/components for olefins is required. As a result, the model consists of 97 (= 48+48+1) continuity equations for the liquid phase components and 49 (= 48+1) continuity equations for the gas-phase components, including hydrogen. The set of ordinary differential equations defined above is solved for the initial conditions given by the feed composition:

$$F_{Pg}^{gas}\Big|_{z=0} = F_{Pg,o}^{gas}$$
$$F_{Pg}^{liq}\Big|_{z=0} = F_{Pg,o}^{liq}$$
$$F_{Og}^{liq}\Big|_{z=0} = 0$$
$$g = 1,2,.....N_{lumps}$$

Approximate analytical solutions have been obtained to see that the difference in the eigen values of ODEs for a paraffin and corresponding olefin are of the order of k_{dh}/K_{dh}^{eqm}. Such a large difference in the eigen values leads to a stiff set of ODEs which has to be integrated using backward differentiation formula (BDF), e. g. Gear's method.

6.12. Model Degeneration into Equilibrated (de)Hydrogenation Case

The above approach automatically allows the model to also predict the product distribution for a catalyst which has sufficient metal activity, i.e., when the hydrogenation/dehydrogenation reactions are equilibrated. When the ratio of rate coefficients of acid site steps (PCP/cracking) to the rate coefficients of dehydrogenation steps tends to zero, the set of ODE representing the continuity equations for the liquid

phase paraffins and olefins degenerates into the set of ODEs given by eqn (6.55) and algebraic equations given by eqn (6.56),

$$\frac{1}{\Omega}\frac{dF_{Pg}^{liq}}{dz} = k_{O,Pg}a_v\left(\frac{C_{Pg}^{gas}}{K_{Pg}^{C,eqm}} - C_{Pg}^{liq}\right) + R_{Og,acid}^{Form} \quad g = 1,2,.....N_{lumps} \tag{6.55}$$

$$K_{DH(Pg\Leftrightarrow Og)}^{app} = \left(\frac{C_{Og}^{liq}C_{H_2}^{liq}}{C_{Pg}^{liq}}\right) \; g = 1,2,.....N_{lumps} \tag{6.56}$$

The above set of algebraic equations relates the liquid phase concentration of any paraffinic lump P_g and the corresponding olefinic lump O_g through the apparent dehydrogenation equilibrium coefficient K_{DH}^{app}. K_{DH}^{app} gives the average value of the dehydrogenation equilibrium coefficient for the dehydrogenation of lump P_g into lump O_g through all possible isomers and is related to the individual dehydrogenation equilibrium coefficients by,

$$K_{DH(Pg\Leftrightarrow Og)}^{app} = \frac{\left(\sum_{q=1}^{5}\sum_{i=1}^{paraffin\ isomers} n_{i,q}y_{Pi}^{eqm}\right)}{\left(\sum_{i=1}^{paraffin\ isomers}\sum_{j=1}\frac{y_{Oij}^{eqm}}{K_{DH,ij}^{liq}}\right)} \tag{6.57}$$

6.13. Estimation of the Model Parameters

The model parameters are estimated from the isothermal experimental data on three-phase hydrocracking of n-hexadecane in a tubular reactor. The parameters involved in the model are divided into four categories:

6.13.1. Rate Parameters for the Metal Site Steps

As discussed earlier, to model the hydrogenation/dehydrogenation reactions, five activation energies for five different modes of dehydrogenation and one frequency factor is required.

6.13.2. Rate Parameters for Acid Site Elementary Steps

The lumping coefficients for the acid site steps are functions of the Evan-Polanyi parameters α_{pcp} and α_{cr} and therefore, simultaneous estimation of these two parameters along with other model parameters requires the recalculation of the lumping coefficients at each iteration during the parameters estimation. As the value of alpha should lie between 0 and 1, the recalculation of lumping coefficients at every iteration has been avoided by calculating them once at several pairs of alpha at an interval of 0.1 and estimating the remaining model parameters at these different pairs of alpha, maintaining them constant. The pair of alpha corresponding to the best set of parameters has been retained as final.

To find out the actual number of independent parameters that can be determined from experimental data, eqn (6.40) is written for all the four subtypes of PCP steps. i.e.,

$$\begin{aligned}
\left[E_{pcp(s;s)}\right]_2 &= E_{o,pcp} + \Delta q(s) \\
\left[E_{pcp(s;t)}\right]_2 &= E_{o,pcp} + \Delta q(s) + \alpha'_{pcp}\left(\Delta q(t) - \Delta q(s)\right) \\
\left[E_{pcp(t;s)}\right]_2 &= E_{o,pcp} + \Delta q(t) + \alpha'_{pcp}\left(\Delta q(s) - \Delta q(t)\right) \\
\left[E_{pcp(t;t)}\right]_2 &= E_{o,pcp} + \Delta q(t)
\end{aligned} \tag{6.58}$$

Defining $E'_{o,pcp} = E_{o,pcp} + \Delta q(s)$ and $\Delta q(t;s) = \Delta q(t) - \Delta q(s)$ the above equations can be written as,

$$\begin{aligned}
\left[E_{pcp(s;s)}\right]_2 &= E'_{o,pcp} \\
\left[E_{pcp(s;t)}\right]_2 &= E'_{o,pcp} + \alpha'_{pcp}\Delta q(t;s) \\
\left[E_{pcp(t;s)}\right]_2 &= E'_{o,pcp} + (1-\alpha'_{pcp})\Delta q(t;s) \\
\left[E_{pcp(t;t)}\right]_2 &= E'_{o,pcp} + \Delta q(t;s)
\end{aligned} \tag{6.59}$$

In the same way, $E'_{o,cr} = E_{o,cr} + \Delta q(s)$ is defined for the cracking steps and equations analogous to (6.59) are written for the cracking steps. It can be seen from the above transformation of parameters that for constant values of alpha, the four original parameters used in eqn (6.58), i.e., $E_{o,pcp}$, $E_{o,cr}$, $\Delta q(t)$ and $\Delta q(s)$ are not mutually independent. Only three re-parameterized entities defined as $E'_{o,pcp}$, $E'_{o,cr}$ and $\Delta q(t;s)$ are mutually independent parameters regarding the acid site activation energies that can be determined from the experimental data. Apart from these three parameters two composite single-event frequency factors $\tilde{A}^{comp}_{pcp}$ and $\tilde{A}^{comp}_{cr}$ are also independent parameters for the acid site steps.

6.13.3. Parameters for Sorption in Zeolite Pores

From the experiments[76] on the adsorption of alkane molecules up to carbon number 16, it was found that the Henry coefficients of alkanes of different chain length in non-polar n-octane mobile phase are almost identical at high liquid densities and increases slightly with carbon number at relatively lower liquid densities. Moreover, Henry coefficients in the liquid phase have been found to be very weak functions of temperature meaning a relatively small heat of sorption, in contrast to the high heat of sorption in the gas phase[109]. Therefore, in the hydrocracking of pure paraffins, only one temperature independent Henry coefficient has been used irrespective of the chain length and degree of branching of the molecules. The Langmuir coefficient for sorption $K_{L,Pg}$ for a paraffinic lump g is obtained as the ratio of the Henry coefficient and the saturation concentration of lump g, $c_{sat,g}$. Because of the existence of liquid like densities of hydrocarbons inside the zeolite pores, the saturation concentration of a lump is obtained by dividing the pore volume of the zeolite by the saturated molar volume of lump g in the liquid phase[70], i.e.,

$$c_{sat,g} = \frac{v_{pore}}{v^{liq}_{sat,g}} \tag{6.60}$$

Because of very high correlation in the sorption equilibrium coefficients and the kinetic rate parameters, the Henry coefficients for the olefins have been assumed to be the same as those of the paraffins.

6.13.4. Parameters for Chemisorption on Metal Sites

The independent estimation of the chemisorption parameters was found to be difficult because the form of the rate expression leads to a high correlation between the chemisorption equilibrium coefficient, Henry coefficient and rate coefficient for dehydrogenation. The chemisorption equilibrium coefficient for a particular paraffinic and olefinic lump at the metal sites were initially assumed to be equal and a function of carbon number represented by a relationship analogous to that given by Denayer[109] for the gas phase sorption of paraffins in zeolite pores. However, from the initial parameter estimation, the carbon number dependency came out to be very weak. Moreover, the denominator term D_c for chemisorption was close to unity. Consequently, it was assumed that the chemisorption equilibrium coefficients are small and independent of the carbon number. This allowed coupling the entropy and heat of chemisorption for paraffins and olefins along with the pre-exponential factor and activation energies of dehydrogenation, respectively.

Summarizing, the model contains a total of 14 temperature and feedstock composition independent parameters whose values were estimated from the experimental data by minimizing the sum of squares of the residuals between the experimental and model predicted responses using the Levenberg-Marquardt optimization algorithm.

$$S(\beta) = \sum_{i=1}^{nresp} \sum_{j=1}^{nobs} \left[y_{ij}^{exp} - y_{ij}^{cal} \right]^2 \tag{6.61}$$

In the absence of replicate experimental data no weighting factors are used. 34 responses representing the molar flow rates of normal paraffins and iso-paraffins, the total conversion and isomerization yield of n-hexadecane, and the C_4/C_{12} molar ratio are used per set of experimental data. The distribution of mono-branched and multi-branched

isomers for a given carbon number was available only from C_6 to C_9 and this information has also been used in the parameter estimation. For a particular Pt/USY catalyst (Cat-I) experimental data was available at a total pressure of 35 atm., at two temperatures, 300 ^oC and 320 ^oC, and molar H_2/HC ratio of 6.0 to 11.0. The parameters related to the acid sites have been found to satisfy the rules of carbenium ions chemistry. The ratio of the composite single-event frequency factor for β-scission to that of PCP is in agreement with the values reported earlier[17, 72]. The estimated parameters lead to effective activation energies of PCP and β-scission which are close, resulting in the selectivity vs. conversion behavior with respect to temperature observed by Steijns et al.[97] for the Ac-rds case. The five effective activation energies for dehydrogenation on the metal sites are of the order of 80 kJ/mol.

The product distribution obtained by using the parameters for Cat-I is shown in Figure 6-3 to Figure 6-5. The agreement between the experimental and calculated conversions, the distribution of cracked products as well as the percentage of isomers for the entire product range of C_3 to C_{13} is very good. The percentage of isomers in the cracked products increases with the carbon number. The skewed product distribution of Figure 6-4 reveals a significant amount of secondary cracking. For this catalyst, a single-event

kinetic model with rate determining step only on the acidic sites predicted a much smaller amount of secondary cracking and a poorer fit of the experimental data.

The single-event kinetic models previously developed for the hydrocracking of paraffins are based on four rate coefficients per type of elementary step, namely *k(s;s), k(s;t), k(t;s)* and *k(t;t)*. It was found in previous work that such a model consistently over-predicted the yields of C_3 and C_4 products. One of the reasons for this behavior is the inability of these models to distinguish among the rate coefficient of cracking steps in which a C_3/C_4 product is formed from those in which both the cracked products are larger than C_4. Because of the lesser degree of charge distribution, the heats of formation of 2-propyl and s-butyl carbenium ions are relatively higher than those of the larger secondary ions whose stability is slightly increased due to the presence of a larger number of β-carbons with respect to the positive charge. The implementation of the Evans-Polanyi relationship in the current model accounts for such subtle differences in the stability of ions and accordingly assigns a higher activation energy to the cracking steps in which a C_3 or C_4 ions is formed, resulting in an improved fit of the experimental data.

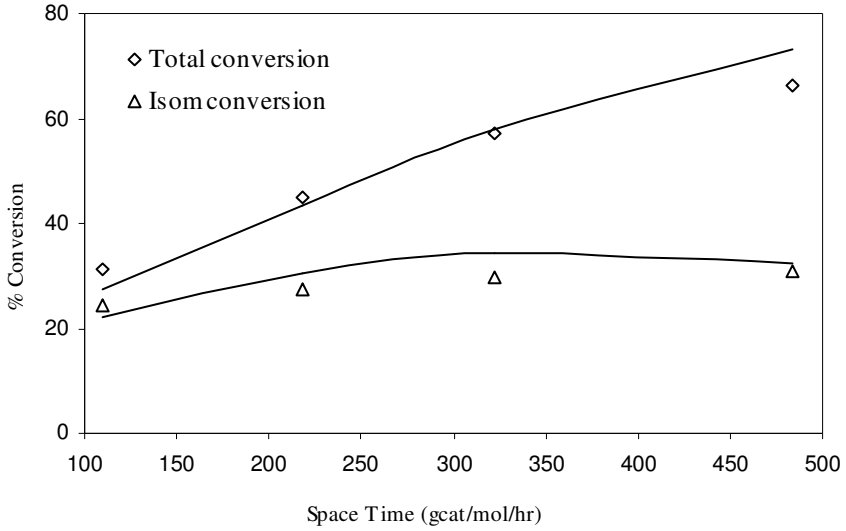

Figure 6-3. Total and isomerization conversion of nC_{16} as a function of space time at T = 300 ^{o}C, P = 35 Bar and H_2/HC ratio = 11.0. (Points: experimental, lines: predicted).

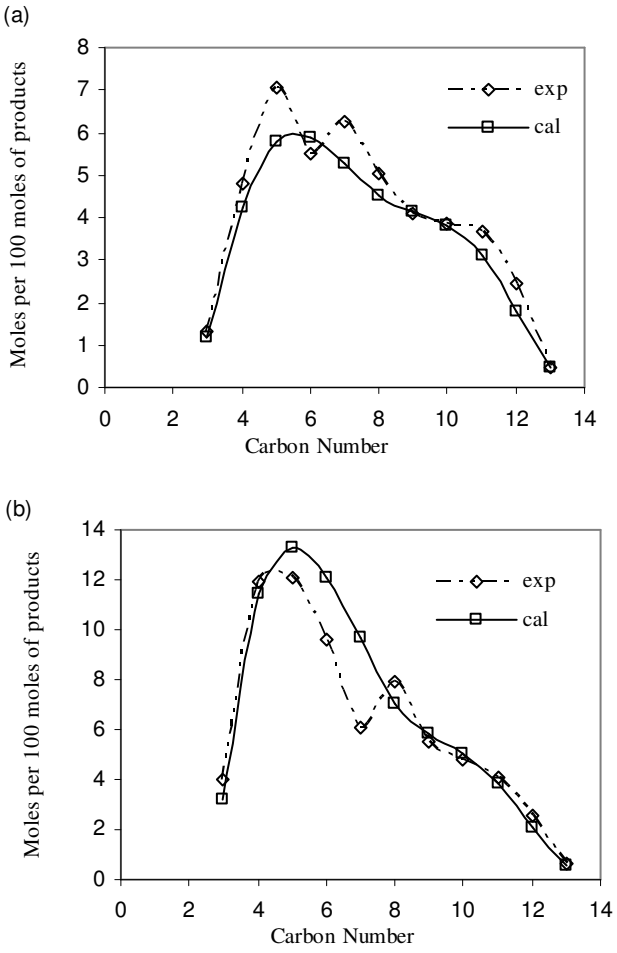

Figure 6-4. Carbon number distribution of cracked products in the hydrocracking of nC_{16}. (a) T = 300 ^{o}C, P = 35 Bar, H_2/HC ratio = 11.0 and total conversion = 57 % (b) T = 320 ^{o}C, P = 35 Bar, H_2/HC ratio = 11.0 and total conversion = 78 %.

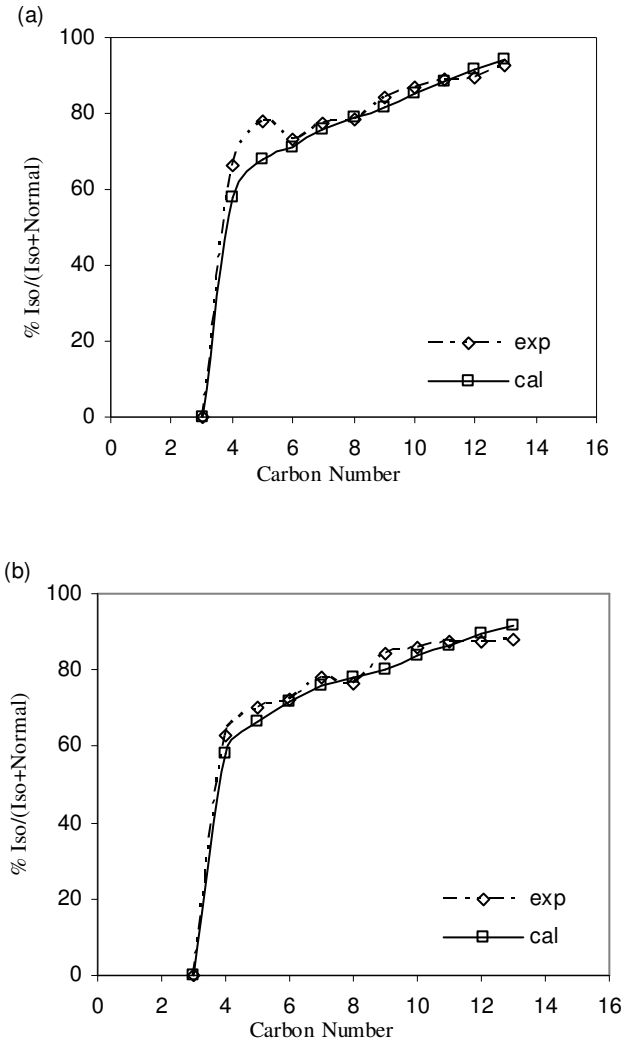

Figure 6-5. Percentage of isomers per carbon number in the hydrocracking of nC_{16} (a) T = 300 ^{o}C, P = 35 Bar, H_2/HC ratio = 11.0 and total conversion = 57 % (b) T = 320 ^{o}C, P = 35 Bar, H_2/HC ratio = 11.0 and total conversion = 78 %.

6.14. Approach to (De)Hydrogenation Equilibrium

Depending upon the relative metal/acid activity of the catalyst, the hydrogenation/dehydrogenation steps do not necessarily attain equilibrium. The initial cracking selectivity, S_o can be used as a measure to quantify the 'approach to (de)hydrogenation equilibrium' because S_o would be zero when the hydrogenation/dehydrogenation steps are at equilibrium and it would increase as the deviation of these steps from the equilibrium increases. It was observed, however, that the deviation in the value of S_o is not very sensitive with respect to the relative metal/acid activity of the catalyst. To quantify the approach to equilibrium, a new variable $\Psi_g = \frac{\left(C_{Og}^{liq} C_{H_2}^{liq} / C_{Pg}^{liq}\right)}{K_{DH(Pg \Leftrightarrow Og)}^{app}}$ has been defined for a particular lump g. To compare the approach to (de)hydrogenation equilibrium for different catalysts, the value of Ψ at zero conversion for the reacting normal paraffin (i.e., $\Psi_{o,feed}$) has been found to be useful. When the catalyst has sufficient metal activity to bring the hydrogenation/dehydrogenation steps to equilibrium, the value of Ψ for all the lumps equals unity. With a catalyst having a relatively weaker metal/acid activity, the value of Ψ for different lumps deviates from unity. For example, in the hydrocracking of nC_{16} the value of Ψ for the feed molecule decreases from unity as the relative metal/acid activity decreases, whereas for all other lumps, Ψ becomes greater than unity. A weak metal function is not able to dehydrogenate the paraffinic feed nC_{16} fast enough (i.e., compared to the rate at which the corresponding olefinic nC_{16} lump is consumed on the acid sites) to bring the concentration of olefinic nC_{16} lump at its equilibrium value, resulting in a value of Ψ smaller than 1. At the same time, a weak metal function is not able to hydrogenate the branched olefinic isomers of C_{16} and the olefinic products formed on the acid sites fast enough (compared to the rate they are produced on the acid sites) to reduce their concentration to the corresponding (de)hydrogenation equilibrium concentration. Consequently, these olefins attain a steady state at concentrations higher than their equilibrium concentrations, resulting in Ψ larger than unity. The deviation

from unity increases as the relative metal/acid activity decreases. Here it should be noticed that in the hydrocracking of paraffin mixtures, the value of Ψ for the heaviest paraffin should be used for quantifying the approach to equilibrium, as the other reacting paraffins would also be formed by the cracking of the heaviest paraffin, and therefore the value of Ψ for them may actually be larger than unity.

The value of $\Psi_{o,feed}$ obtained from the reactor simulations depends on the values of the model parameters, which in turn depend on the relative metal/acid activity of a particular catalyst, the reactor operating temperature, total pressure and H_2/HC ratio. In three-phase hydrocracking, the effect of total pressure and H_2/HC ratio on $\Psi_{o,feed}$ is much smaller than that of temperature.

The value of $\Psi_{o,nC16}$ obtained from the simulations for Cat-I is 0.774 at 300 ^oC and 0.571 at 320 ^oC indicating that higher temperatures lead to larger deviation from the equilibrated hydrogenation/dehydrogenation steps. Similar conclusions have been arrived at in previous experimental studies[35, 99]. These results point to higher 'effective' activation energies of acid site steps compared to the 'effective' activation energies of the metal site steps.

6.15. Application of the Model to Heavy Paraffins and Different Catalysts

The model has been used to simulate the three-phase hydrocracking of heavy paraffins ranging from C_{16} to C_{32} over a number of operating conditions. To study the effect of the relative metal/acid activity of the catalyst on the product distribution, two new set of parameters (Set-II and Set-III) have been derived from Set-I, which was obtained from the experimental data on Cat-I. Set-II has been obtained from Set-I by decreasing the composite frequency factor for dehydrogenation by 50% and increasing the composite frequency factors for PCP and β-scission by 35%, while keeping all other parameters unchanged. Set-II, therefore, corresponds to a hypothetical catalyst Cat-II, having a relatively lower metal/acid activity than Cat-I. The composite frequency factors for PCP and β-scission in Set-III (corresponding to a hypothetical catalyst Cat-III) were chosen at

30% of the corresponding values in Set-I. The Ac-rds case can be considered as the asymptotic behavior of the Me-Ac-rds with respect to the relative metal/acid activity of the catalyst, and therefore a large number has been taken for the composite frequency factor for dehydrogenation for Cat-III so that it corresponds to Ac-rds case. It should be mentioned that the possibility of direct isomerization and hydrogenolysis of paraffins on the metal sites of the catalyst has not been considered in the current study.

6.15.1. Effect of Relative Metal/Acid Activity of the Catalyst

The effect of the relative metal/acid activities on product distribution is illustrated in Figure 6-6 to Figure 6-11 for the hydrocracking of nC_{32} at 375 ^{o}C, 150 bar and a H_2/HC molar ratio of 11.0. Figure 6-6 and Figure 6-7 show the evolution of C_{32} isomers with different degrees of branching vs. the total conversion. Figure 6-6 corresponds to Cat-III resulting in $\Psi_{o,nC32} = 0.99$. The well-known Ac-rds behavior can be seen from the initial slopes of the curves indicating mono-branched paraffins to be the primary products and di-branched and tri-branched products formed sequentially from the mono-branched paraffins. Figure 6-7 corresponds to Cat-II resulting in $\Psi_{o,nC32} = 0.40$, representing a significant deviation from the equilibrated hydrogenation/dehydrogenation steps. In contrast to Figure 6-6, di-branched and tri-branched isomers are not really secondary products but are formed directly from nC_{32}. The appearance of the multi-branched isomers of the feed as the primary products can be used as a possible criterion to identify the lack of metal activity of the catalyst in an experimental study. Alvarez et. al[110] using catalysts having different metal/acid activities observed this phenomenon in the hydrocracking of n-decane. When the *intrinsic* hydrogenation/dehydrogenation rates are comparable or smaller than the *intrinsic* rates of acid sites PCP steps, di-branched and tri-branched olefinic isomers of the feed are produced from the mono-branched olefinic isomers at a rate faster than that at which mono-branched olefinic isomers could be hydrogenated into mono-branched paraffins. Consequently, all the mono-, di- and tri-branched olefinic isomers are hydrogenated almost simultaneously, exhibiting a non-zero initial selectivity for multi-branched isomers. An analogous behavior for cracking

can be observed in Figure 6-8 showing the isomerization selectivity as a function of total conversion for the above mentioned three catalysts. The initial isomerization selectivity for Cat-III (i.e., Ac-rds) is unity, while that for Cat-I and Cat-II (i.e., Me-Ac-rds), 0.95 and 0.82 respectively, indicating that normal paraffins are directly cracked into smaller products, even before their isomerization into the branched paraffins could take place. The explanation for this behavior is the same as described for the direct appearance of multi-branched feed isomers and has been observed experimentally.[110, 111]

Figure 6-9 and Figure 6-10 show the moles of cracked products formed per 100 moles of C_{32} cracked. Figure 6-9 corresponds to the hydrocracking on Cat-III, resulting in $\Psi_{o,nC32} = 0.99$ and Figure 6-10 corresponds to Cat-I for which $\Psi_{o,nC32}$ is 0.67. It can be observed that secondary cracking takes place even in Ac-rds hydrocracking (Cat-III), however, in Me-Ac-rds (Cat-I) the amount of secondary cracking is significantly higher for comparable values of the total conversion. This is because at the same operating conditions, the concentrations of cracked olefins for Cat-I are higher than those on Cat-III due to their lower rates of hydrogenation. This leads to higher concentrations of the corresponding carbenium ions as the protonation/deprotonation steps maintain pseudo-equilibrium with the olefins. The existence of higher concentrations of the carbenium ions of cracked products increases their rate of cracking compared to Ac-rds hydrocracking, resulting in increased secondary cracking.

At the same time, the lower metal/acid activity of Cat-I leads to higher concentrations of the branched C_{32} carbenium ions as compared to Cat-III. This increases the rate of cracking of the branched isomers, resulting in a lower isomerization conversion. This is shown in Figure 6-11 in which the isomerization conversion is plotted against the total conversion for the three catalysts. For Cat-III, the maximum isomerization conversion is 46.7 % as compared to 24.3 % for Cat-II for which the value of $\Psi_{o,nC32}$ is 0.4. This behavior has been observed in several experimental studies.[99, 112]

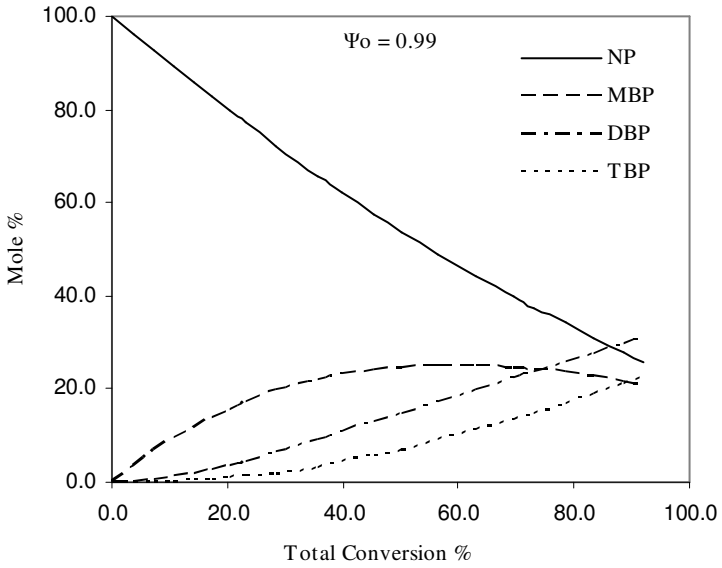

Figure 6-6. Evolution of the isomers of different degrees of branching for the hydrocracking of nC_{32} corresponding to equilibrated (de)hydrogenation condition (Ac-rds case).

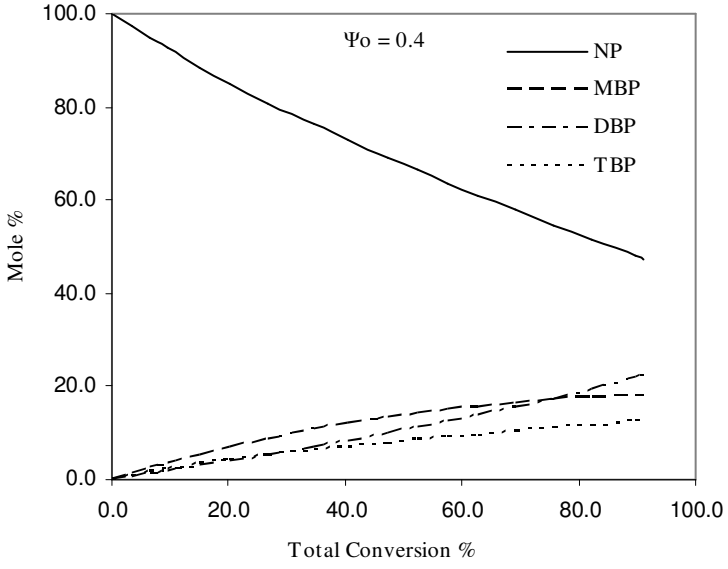

Figure 6-7. Evolution of the isomers of different degrees of branching for the hydrocracking of nC_{32} corresponding to non-equilibrated (de)hydrogenation condition (Me-Ac-rds case).

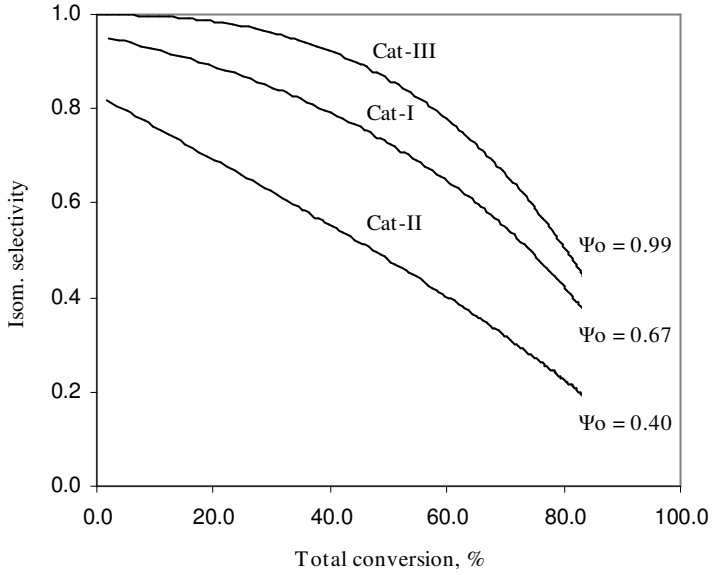

Figure 6-8. Effect of relative metal/acid activity on initial isomerization selectivity in nC_{32} hydrocracking.

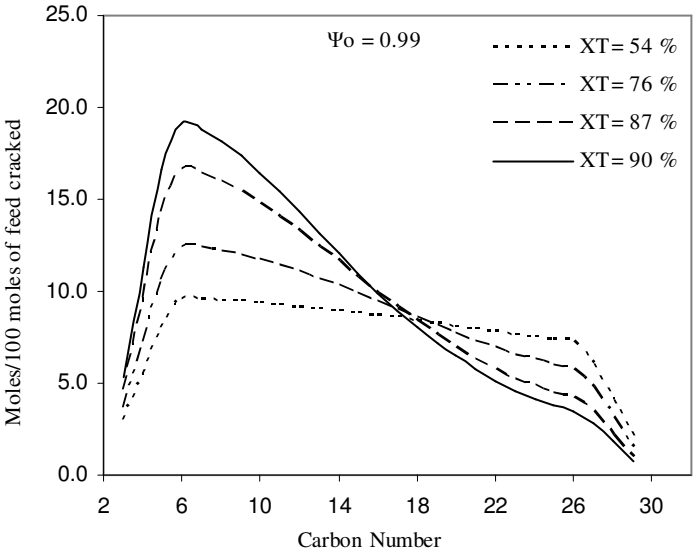

Figure 6-9. Simulated distribution of cracked products for Ac-rds case at various total conversions for the hydrocracking of nC_{32}.

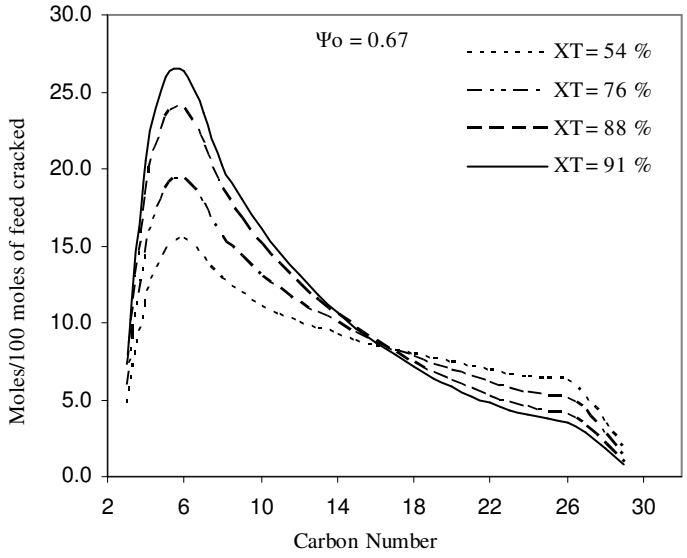

Figure 6-10. Simulated distribution of cracked products for Me-Ac-rds case at various total conversions for the hydrocracking of $nC_{32.}$

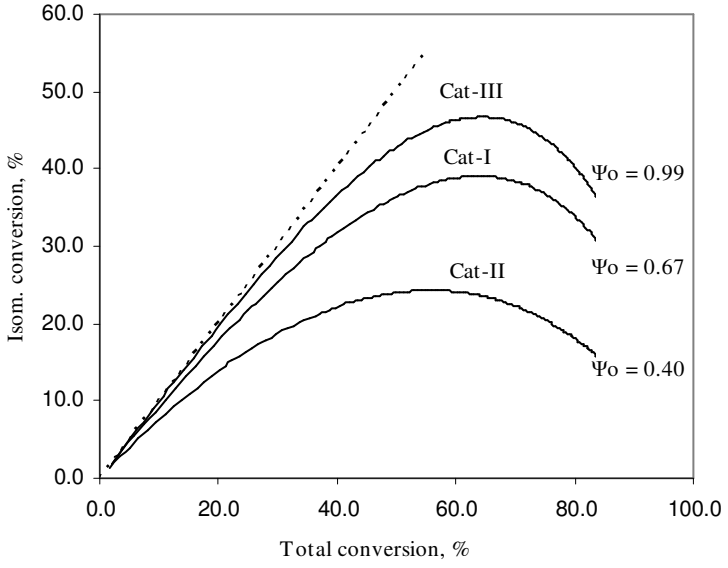

Figure 6-11. Influence of the relative metal/acid activity on the maximum isomerization conversion for the hydrocracking of $nC_{32.}$

6.15.2. Effect of Temperature

Figure 6-12 shows the isomerization conversion plotted against total conversion for the hydrocracking of nC_{32} on Cat-II at a total pressure of 150 bar, H_2/HC molar ratio of 11.0 and three different temperatures. It can be seen that the maximum isomerization conversion (or yield) decreases when the temperature is increased. The decrease in the maximum isomerization yields as well as in the values of $\Psi_{o,nC32}$ show that the deviation from the equilibrated hydrogenation/dehydrogenation steps increases with temperature. This phenomenon has been observed experimentally[99] and can be attributed to higher 'effective' activation energies of acid site steps than the 'effective' activation energies of metal site steps. The 'effective' activation energies of acid site steps include the heat of sorption in the zeolite pores, heat of chemisorption on the metal sites, heat of protonation of olefins and the 'intrinsic' activation energies of the acid site steps. Similarly, the 'effective' activation energies for metal site steps include the heat of sorption in the zeolite pores, heat of chemisorption on the metal sites, and the 'intrinsic' activation energies of dehydrogenation steps.

When the catalyst has sufficient metal activity to achieve hydrogenation/dehydrogenation equilibrium (i.e., $\Psi_{o,nC32}=1.0$) at the highest temperature, the value of $\Psi_{o,nC32}$ remains 1.0 at all lower temperatures. In that case the decrease in the maximum isomerization conversion with an increase in temperature would be significantly lower or negligible, attributed entirely to the differences in the effective activation energies of PCP and cracking steps, in contrast to a catalyst with weak metal/acid activity. No experimental data could be found documenting this behavior for the three-phase hydrocracking of long chain paraffin like C_{32} on a so-called 'well-balanced' catalyst. Experiments on gas-phase hydrocracking of C_8 to C_{12} paraffins on well-balanced catalysts show a unique curve i.e., independent of temperature.[97]

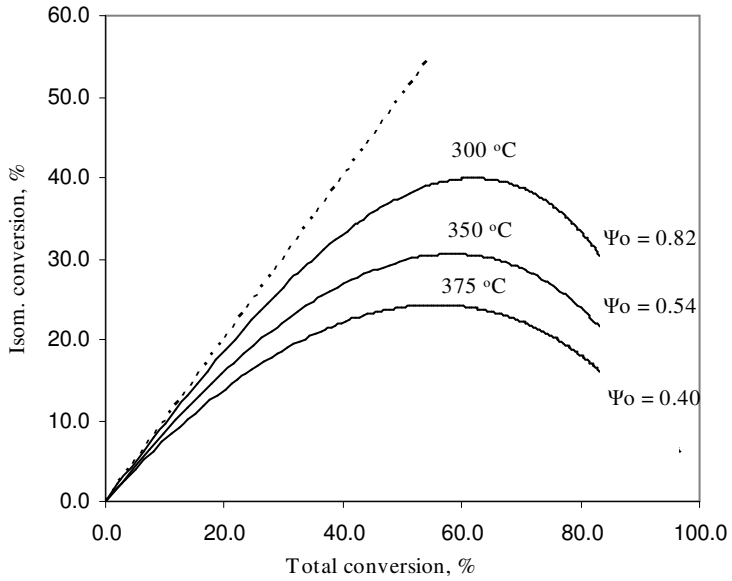

Figure 6-12. Influence of temperature on the maximum isomerization conversion for the hydrocracking of nC_{32} over Cat-II.

6.15.3. Effect of Total Pressure and H_2/HC Molar Ratio

The effect of total pressure at a constant temperature of 375 ^oC and H_2/HC molar ratio of 11.0 has been simulated for three-phase hydrocracking of nC_{32}. Figure 6-13 shows that the increase in the total pressure does not change the value of $\Psi_{o,nC32}$ for Ac-rds case (i.e., Cat-III). For Cat-I and II, the values of $\Psi_{o,nC32}$ increase with total pressure, indicating that over a catalyst with insufficient metal activity, an increase in the total pressure brings the hydrogenation/dehydrogenations steps closer to equilibrium. The shift is more pronounced over a catalyst with a lower metal/acid activity.

Figure 6-14 shows the effect of total pressure on the total conversion, isomerization conversion, and the secondary cracking for Cat-I. Secondary cracking is represented by the moles of cracked products formed per 100 moles of feed cracked. The behavior of Figure 6-14 can be explained as follows. In three-phase hydrocracking the reaction rates

are governed by the liquid phase concentrations (or fugacities) of hydrocarbons and hydrogen. With the increase in total pressure, liquid phase fugacity of hydrogen increases significantly with only negligible increase in the fugacity of hydrocarbons. Increased hydrogen fugacity decreases the 'intrinsic' rate of dehydrogenation of the feed paraffin and therefore, the total conversion. A higher liquid phase fugacity of hydrogen increases the rate of hydrogenation of the olefinic isomers of the feed and of the olefins produced by cracking, so that an increased total pressure favors the isomerization conversion but decreases the secondary cracking. These trends correspond to an increase of $\Psi_{o,nC32}$ with total pressure.

In three-phase hydrocracking at constant temperature and total pressure, change in the H_2/HC ratio has negligible effect on the liquid phase fugacities of hydrogen and hydrocarbons and alters primarily the rate of mass-transfer of these species between the gas and liquid phases. Therefore, it has small effect on the total conversion of paraffinic feedstocks provided there are no mass transfer limitations. A higher H_2/HC ratio, on the other hand, provides more driving force to the lighter cracked products to escape from the liquid phase into the gas phase leading to a decrease in secondary cracking.

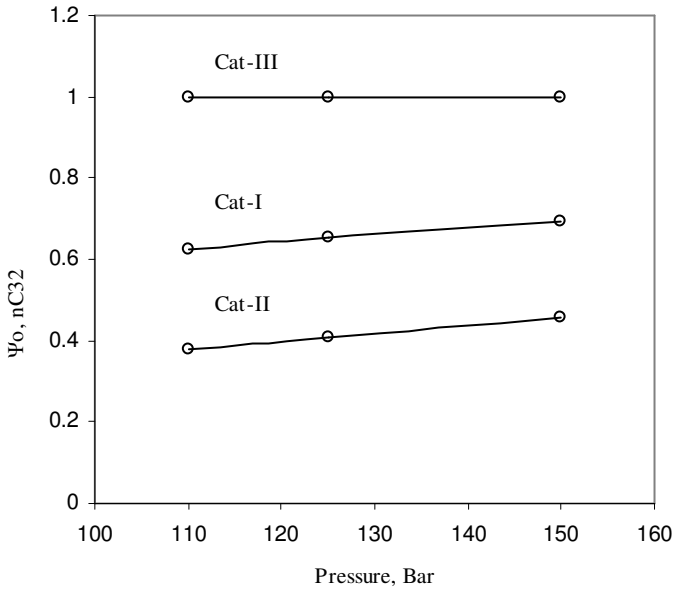

Figure 6-13. Effect of total pressure on the value of $\Psi_{o,nC32}$ at T=375 ^{o}C and R=11 for the hydrocracking of nC_{32} over different catalysts.

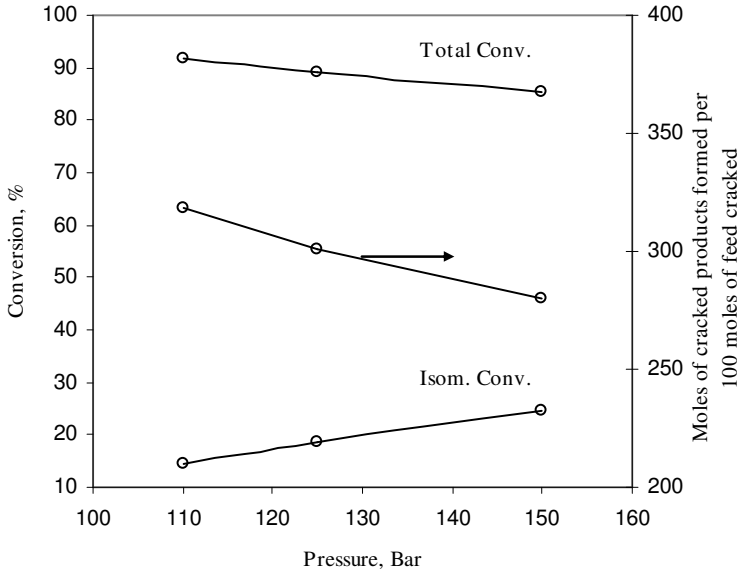

Figure 6-14. Effect of total pressure on the total conversion, isomerization conversion and secondary cracking at T=375 ^{o}C and R=11 for the hydrocracking of nC_{32} over Cat-I.

6.15.4. Effect of Feed Chain Length

Figure 6-15 shows the effect of the chain length on the total conversion and secondary cracking. With chain length, reactivity of paraffins increases because of the increase in the available reaction pathways resulting in higher conversions. The chain length of primary cracking products formed from a long chain hydrocarbon is likely to be longer than those formed from short chain hydrocarbons, making them more susceptible to further cracking and thus leading to increased secondary cracking.

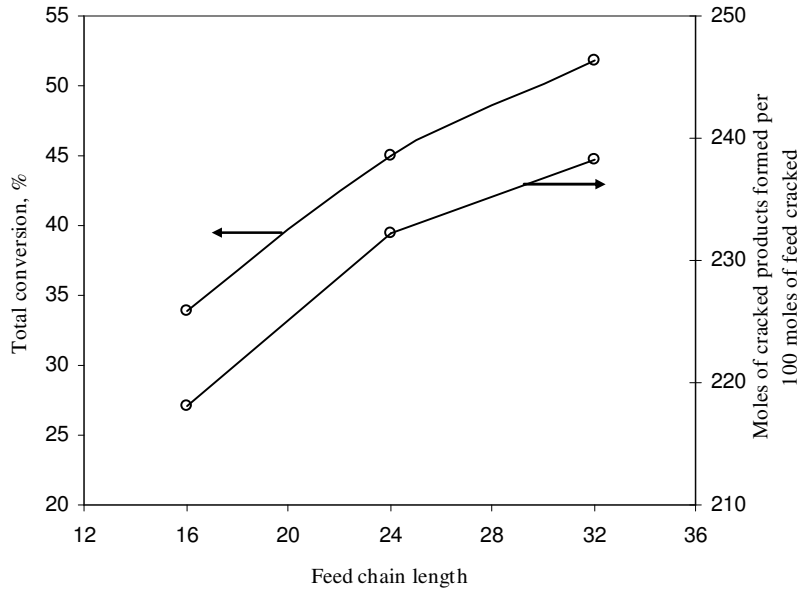

Figure 6-15. Effect of chain length on the total conversion and secondary cracking expressed as the moles of cracked products formed per 100 moles of feed cracked at 375 ^{o}C, 150 bar and H_2/HC molar ratio of 11.0 for a given space time over Cat-I.

CHAPTER VII

CONCLUSIONS

This research is focused on the development of mechanistic kinetic models for the hydrocracking of complex feedstocks of industrial relevance. Two separate models are developed, one for the hydrocracking of vacuum gas oils and the other for the hydrocracking of long chain paraffins. Because of the complex structures of the molecules present in a typical vacuum gas oil and the gigantic reaction network, some simplifying assumptions are made in the hydrocracking model of vacuum gas oil. In the hydrocracking model of paraffin feeds, on the other hand, the modeling approach adopted for VGO has been extended to an even more detailed and fundamental level which allowed to investigate the effect of the relative strength of the metal/acid activity of the hydrocracking catalyst on the hydrocracking product distribution.

Both models are developed using an exhaustive network of elementary steps, generated by a computer algorithm. The elementary steps occurring on the acid sites of the catalyst are based on the underlying carbenium ion chemistry of the hydrocracking process. The reaction network for the saturation of aromatic species is based on the sequential hydrogenation of the aromatic rings.

In the VGO hydrocracking model, it is assumed that the dehydrogenation/hydrogenation reactions preceding/following the acid site transformations attain quasi-equilibrium, so that the elementary steps on the acid sites are considered to be the rate determining steps. The frequency factors for these steps are modeled using the single event concept and the activation energies are based on the nature of the reactant and the product carbenium ions. This leads to a tractable number of model parameters in spite of a very large number of steps actually considered in the model. The number of activation energies required in the model has been further reduced by identifying the similarity in the structural transformation in the acyclic, exocyclic and endocyclic β-scission steps.

An investigation of the available experimental data on the hydrocracking of VGO revealed that the amount of mono-ring species found in the hydrocracking products was significantly higher than what could be formed by the opening of the multi-ring species. This suggested the importance of the cyclization of paraffins in the formation of mono-ring naphthenes. A reaction mechanism proceeding through diolefinic species has been proposed in this work to model the rate of the cyclization steps. A significant increase in the rate of cyclization with temperature has been reported in the literature. It is supported by this mechanism, as shown from the reactor simulations.

To model the equilibrium coefficients of the protonation steps, a new hypothesis has been proposed in this work which eliminates the involvement of the reference olefins, practiced previously. This hypothesis has been corroborated by calculating the true values of the lumping coefficients using the gas phase heats of formation of carbenium ions and comparing them with the lumping coefficients calculated with the existing and proposed methods.

As the reactions on zeolite catalysts occur through the reactants sorbed in the zeolite pores, the kinetic model have been developed to account for the sorption of hydrocarbons belonging to different classes from the liquid phase to the zeolite pores. As reported in the literature, the reactivity of bulky molecules decreases with molecular size on the zeolite catalysts due to their reduced probability to enter the pores. The current modeling approach allows to account for the reduced reactivity of the bulky molecules by using the smaller values of their sorption equilibrium coefficients.

The model for the hydrocracking of VGO explicitly considers the strong competitive chemisorption of aromatic/polyaromatic species on the acid sites of the catalyst to account for the influence of the aromatic content of the feedstock on the rates of acid site transformations. The values of the protonation equilibrium coefficients required to calculate the acid site coverage have been estimated from the gas-phase proton affinities of the aromatics and their heats of stabilization from gas phase to acid sites. The entropic part of the protonation equilibrium coefficients has been estimated using statistical thermodynamics.

The increase in the hydrogenation reactivity of aromatics with the number of aromatic and saturated rings is well known from the experimental literature. This increase in the reactivity is caused both by the higher chemisorption coefficients of polyaromatics on the metal sites as well as the higher values of their *intrinsic* hydrogenation rate coefficients. The current model accounts for both these important aspects to model the rate of aromatic hydrogenation reactions at a fundamental level.

The total number of molecular species considered in this model is of the order of 1 million. It was not possible to write a continuity equation for each individual species because of the mathematical problems that would arise during the integration of such a large number of ordinary differential equations as well as the limitations of the current analytical techniques for the identification of individual molecules in the heavy petroleum mixtures. Therefore, a 'strict' lumping strategy has been devised which is based on the attainment of thermodynamic equilibrium among the isomers placed in each lump. This approach leads to 1266 pure components/lumps to be used in this model. Although a lumping of components is employed in the model, the global rates of conversion among the lumps are calculated by accounting for the contribution of all the reactions of every component present in a lump. The concentration profiles of all these lumps and hydrogen are obtained in the gas and liquid phases along the reactor by integrating 2534 ordinary differential equations. An ordinary differential equation for the temperature profile of the gas/liquid phases and an algebraic equation for the calculation of the temperature of the catalyst at each axial position in the reactor are solved simultaneously with the 2534 mass balance equations. The model has been used to estimate the parameters from the experimental data on VGO hydrocracking.

A variety of simulations have been performed in this work using the estimated parameters to analyze the effect of operating conditions on the product distribution. The model is capable of providing the product distribution at any level of detail desired by the user. For example, the evolution of various commercial fractions, the evolution of various hydrocarbon classes, the evolution of paraffins, naphthenes and aromatics in each commercial fraction, the evolution of each hydrocarbon class in a commercial

fraction, the evolution of the carbon number distribution of each class as well as each commercial fraction and so on. The effect of temperature and pressure on the product distribution predicted by the model is supported by the information available in the open literature. The effect of the distribution of the isomers with different degree of branching in a class on the reactivity of vacuum gas oil has also been studied, showing the increase in the VGO conversion with an increase in the content of isomers with higher number of methyl branches. The simulations carried out in this study reveal the deviation of the isomer distribution from the corresponding thermodynamic distribution, confirming the published experimental data.

The potential of the model for commercial applications is clear considering the wealth of information it produces compared to the available models based on lumps mainly defined by their physical properties. For example, the prediction of the yield of aromatics in the hydrocracking products is very important to the refining industry considering the growing environmental regulations imposed by federal agencies. Apart from that, the properties of the products obtained from the hydrocracking process are significantly affected by their aromatic content, e.g., aromatics improve the quality of the gasoline fraction by enhancing its octane number, while they deteriorate the quality of kerosene and diesel in terms of their smoke point and cetane number. Therefore, the accurate prediction of the amount and composition of aromatics in various commercial fractions and the effect of operating conditions on their yields as predicted by the present model can be extremely valuable to the refiners.

The hydrogen consumption for different feedstocks and the knowledge of the temperature increase during hydrocracking reactions are also very important parameters for the hydrocracker operators. The conventional lumped models obtain the amount of hydrogen consumption using the average C/H ratios of the feed and products, whereas the total heat generated is calculated by taking a constant value for the heat evolved per mole of hydrogen consumed. The current model considers a detailed reaction network for the hydrogenation of mono- and multiring aromatics which allows the prediction of precise values for of hydrogen consumption, depending on the aromatic content and

composition of the feed, as well as on the conversion level. The detailed energy balance based on the heats of formation of all the reacting species along with the heat effects associated with the vaporization of lighter hydrocarbons formed during the cracking reactions permits the model to accurately predict the temperature profile along the reactor. This kind of information can be efficiently used for the optimization of commercial plants with respect to the operating conditions as well as the efficient selection of the feedstock for a desired product slate.

The other contribution of this research is the development of a *generalized* mechanistic kinetic model for the hydroisomerization and hydrocracking of long chain paraffins. Unlike the assumption made in the VGO model, this model considers the dehydrogenation/hydrogenation reactions preceding/following the acid site transformations also to be rate determining like some of the elementary steps occurring on the acid sites of the catalyst. This enables the model to simulate hydrocracking on catalysts with low metal activity. The activation energies of acid site steps in this model are obtained by the use of the Evans-Polanyi relationship. Quantum chemical calculations have been performed to obtain the energies of the gas phase carbenium ions. These are used to develop a group contribution method for the faster estimation of heats of formation of all the carbenium ions. This model contains 14 independent parameters which are invariant with respect to the carbon number of the feedstock and the reactor operating conditions. These parameters have been estimated from experimental data on the hydrocracking of n-hexadecane. A new parameter $\Psi_{o,feed}$ is introduced in this model which quantifies the approach of the hydrogenation/dehydrogenation steps to the corresponding equilibrium. The effects of the metal activity, of temperature, pressure and H_2/HC ratio on the product distribution and on the shift in the rate determining step have been investigated. The model has potential application for selecting the optimum operating conditions in the hydrocracking of mixtures of paraffins as encountered in Fisher-Tropsch waxes, now produced starting from natural gas, and for a more efficient selection of the catalyst.

7.1. Recommendations for the Future Work

Similar to the approach taken for the hydrocracking of pure paraffins, the VGO model can also be built considering the rate determining steps to be both on metal and acid sites of the catalysts. A firm ground work has been laid down in this research to model the rate coefficients of the metal site dehydrogenation/hydrogenation reactions of paraffinic species which can be extended to the ring species present in VGO.

Another important development in the VGO model is the implementation of the Evans-Polanyi relationship for the modeling of activation energies. This requires the energies of the carbenium ions with complex naphthenic and aromatic structures. Calculation of the energies of these species, although computationally expensive, can be carried out considering the ever increasing processor speeds. Uncertainties in the energies of such species using currently available *ab initio* theories, however, need to be addressed in this effort. Similar to the acid site steps, the modeling of the activation energies of the metal site rate coefficients using the Evans-Polanyi relationship in the two-site rate determining VGO model would also be a significant theoretical development.

The current model does not account for the deactivation of the catalyst due to coke deposition. Although the rate of coking in hydrocracking is very low because of the high hydrogen pressures, the prediction of the decrease of the catalyst activity with run time and the knowledge of the rate of temperature increase required to maintain the conversion levels are of great importance to the refining industry. Modeling of the rate of coke formation using a fundamental approach as advanced in the current model would be highly recommended. At the same time, addition of the hydrodesulfurization and hydrodenitrification reactions to the current reaction network would be of great practical importance. The deleterious effect of the organic nitrogen on the acidic sites of the catalyst also needs to be considered.

The need for reliable kinetic models with high predictive capabilities for such kind of complex processes is ubiquitous in the oil industry. Development of such models is possible only through fundamental mechanistic approaches which require a detailed

composition of the feedstock. As discussed in this dissertation, to obtain this type of detailed feedstock composition is very difficult, practically impossible, in a typical refinery. This opens up the avenues for the development of theoretical approaches that can predict the detailed feedstock composition from a partial analysis, which is generally available in the oil industry. Integration of such techniques with the detailed mechanistic models as developed in this work would consummate the current research.

NOMENCLATURE

a_v = Gas-liquid interfacial area, [m_i^2/m_r^3]

a_{LS} = Liquid-solid interfacial area, [m_i^2/m_r^3]

$\tilde{A}_\omega$ = Single event frequency factor for ω type of elementary steps, [1/hr]

$\tilde{A}_\omega^{comp}$ = Composite single event frequency factor for ω type of steps, [kmol/kg_{cat}/hr]

c_m = Total concentration of the metal sites, [kmol/kg_{cat}]

$c_{sat,Pi}$ = Sat. concentration of paraffin P_i in the zeolite pore, [kmol/kg_{cat}]

C_{P,H_2}^{gas} = Gas phase heat capacity of hydrogen, [kJ/mol/K]

$C_{P,Sg}^{gas}$ = Gas phase heat capacity of lump S_g, [kJ/mol/K]

$C_{P,Sg}^{liq}$ = Liquid phase heat capacity of lump S_g, [kJ/mol/K]

C_{total}^{gas} = Total concentration of the gas phase, [kmol/m^3]

C_{total}^{liq} = Total concentration of the liquid phase, [kmol/m^3]

C_t = Total concentration of the acid sites, [kmol/kg_{cat}]

$C_{H_2}^{liq}$ = Concentration of hydrogen in the liquid phase, [kmol/m^3]

C_{Pi}^{liq} = Concentration of paraffin P_i in the liquid phase, [kmol/m^3]

C_{Si}^{liq} = Concentration of species S_i in the liquid phase, [kmol/m^3]

C_{Sg}^{liq} = Concentration of lump S_g in the liquid phase, [kmol/m^3]

C_{Sg}^{gas} = Concentration of lump S_g in the gas phase, [kmol/m^3]

$[C_{Pi}]$ = Concentration of sorbed paraffin, [kmol/kg_{cat}]

$\left[C_{Oij}\right]$ = Concentration of sorbed olefins, [kmol/kg_{cat}]

$\left[C_{R_{ik}^+}\right]$ = Concentration of surface carbenium ions R_{ik}^+, [kmol/kg_{cat}]

$E_{o,k}$ = Intrinsic activation energy for elementary steps of type *k*, [kJ/mol]

$E_{\omega(m;n)}$ = Activation energy for the steps of $\omega(m;n)$ subtype, [kJ/mol]

$E_{\omega(m;n)}^{comp}$ = Composite activation energy for the steps of $\omega(m;n)$ subtype, [kJ/mol]

$\hat{f}_i$ = Partial fugacity of component *i* at reaction temperature and pressure, [bar]

f_i^o = Fugacity of pure component *i* at standard state conditions, [bar]

F_{Sg}^{gas} = Gas phase flow rate of lump S_g, [kmol/hr]

F_{Sg}^{liq} = Liquid phase flow rate of lump S_g, [kmol/hr]

$F_{H_2,quench}$ = Molar flow rate of the hydrogen stream for quench, [kmol/hr]

h = Planck's constant, [kJ.hr]

h_{LS} = Solid-liquid heat transfer coefficient, [kJ/m^2/K/hr]

$\Delta H_{exo-\beta}$ = Heat of the exocyclic β-scission elementary steps, [kJ/mol]

$\Delta H_{acyc-\beta}$ = Heat of the acyclic β-scission elementary steps, [kJ/mol]

$\Delta H_f^g(i)$ = Heat of formation of specie *i* in the gas phase, [kJ/mol]

$\Delta H_f^s(i)$ = Heat of formation of species *i* at the surface, [kJ/mol]

$\Delta H_{f,g}^{liq}$ = Heat of formation of lump S_g in the liquid phase, [kJ/mol]

$\Delta H_f^{sorbed}(O)$ = Heat of formation of olefin in the sorbed phase, [kJ/mol]

$\Delta H_{vap}(i)$ = Latent heat of vaporization of species *i*, [kJ/mol]

$\Delta H_{stab}(R^+)$ = Heat of stabilization of carbenium ion, R^+ from liquid phase to the surface, [kJ/mol]

$\Delta H_{sorp}(i)$ = Heat of sorption of specie *i* from liquid phase to the sorbed phase, [kJ/mol]

$\Delta H_{pr(S_{Oij} \rightleftarrows m)}$ = Enthalpy of protonation of olefinic species S_{Oij}

$\left[H^+\right]$ = Concentration of vacant acid sites, [kmol/kg_{cat}]

H_{Si} = Henry coefficient for the sorption of paraffin S_i, [m^3/kg_{cat}]

k_B = Bolztman's constant, [kJ/molecule/^oC]

$\tilde{k}_{\omega(m;n)}$ = Single event rate coefficient for the elementary step of type $\omega(m;n)$, [1/sec]

$k_{O,Sg}$ = Overall mass transfer coefficient for lump S_g, [m_i/hr]

k_G = Gas phase mass transfer coefficient, [m_i/hr]

k_L = Liquid phase mass transfer coefficient, [m_i/hr]

kdh_{ij} = Dehydrogenation rate coefficient, [kg_{cat}/kmol/hr]

$k_{hyd,3H_2}^{comp}$ = Composite rate coefficient for the hydrogenation of monoaromatics, [(kmol/kg_{cat}/hr)(m^3/kmol)^3]

$K_{H_2}^{VLE}$ = Vapor liquid equilibrium coefficient for hydrogen, [dimensionless]

$K_{Sg}^{C,VLE}$ = Concentration based vapor liquid equilibrium coefficient for lump S_g, [dimensionless]

K_{C,H_2} = Chemisorption equilibrium coefficient for hydrogen at the metal site, [m^3/kmol]

$K_{C,Pi}$ = Chemisorption equilibrium coefficient of paraffin P_i at the metal site, [kg_{cat}/kmol]

$K_{DH,ij}^{ads}$ = Dehydrogenation equilibrium coefficient at the metal site, [dimensionless]

$K_{DH,ij}^{liq}$ = Equilibrium coefficient for the overall dehydrogenation reaction in the liquid phase, [kmol/m^3]

$K_{DH(Si \rightleftarrows S_{Oij})}^{liq}$ = Equilibrium coefficient for the given overall dehydrogenation reaction in the liquid phase, [kmol/m^3]

$K_{L,Pi}$ = Sorption equilibrium coefficient of paraffin P_i in the zeolite pore, [m^3/kmol]

K_{pr} = protonation/deprotonation equilibrium coefficient, [dimensionless]

n_e = Number of single-events, [dimensionless]

N_{lumps} = Total number of lumps/pure components, [dimensionless]

N_{sat_lumps} = Number of saturated lumps/pure components, [dimensionless]

N_{aro_lumps} = Number of aromatic lumps/pure components, [dimensionless]

N_{Sg} = Molar flux of lump S_g from gas phase to liquid phase, [kmol/hr/m$_i^2$]

$q(m)$ = Heat of stabilization of m type of carbenium ion, from sorbed phase to the surface, [kJ/mol]

$\Delta q(m)$ = Relative heat of stabilization of a proton with respect to an m type of paraffinic carbenium ion, [kJ/mol]

$\Delta q(z,m)$ = Relative heat of stabilization of a proton with respect to an m type of carbenium ion of class Z, [kJ/mol]

R = Universal gas constant, [kJ/mol/K]

$R_{\omega(m;n)}^{(g;h)}$ = Global rate of conversion of lump g into lump h through $\omega(m;n)$ type of elementary steps, [kmol/kg$_{cat}$/hr]

$R_{Pg,metal}^{Form}$ = Rate of formation of paraffin lump P_g on metal sites, [kmol/kg_{cat}/hr]

$R_{Og,metal}^{Form}$ = Rate of formation of Olefin lump O_g on metal sites, [kmol/kg_{cat}/hr]

$R_{Og,acid}^{Form}$ = Rate of formation of Olefin lump O_g on acid sites, [kmol/kg_{cat}/hr]

$R_{Sg,net}^{Form}$ = Net rate of formation of lump S_g on acid sites, [kmol/m_r^3/hr]

$[S_i]$ = Sorbed concentration of species S_i in the zeolite pores, [kmol/kg_{cat}]

$\left[S_{Rik}^{+}\right]$ = Concentration of surface carbenium ions S_{Rik}^{+}, [kmol/kg_{cat}]

$\Delta\hat{S}_{pr}$ = Intrinsic entropy of protonation, [kJ/mol/K]

S_t = Entropy corresponding to three translational degrees of freedom, [kJ/mol/K]

T^{liq} = Liquid phase temperature, [K]

T^{solid} = Solid phase temperature, [K]

T_{H_2} = Temperature of the hydrogen stream used for quench, [K]

T_{in} = Bed inlet temperature, [K]

T_{out} = Bed outlet temperature, [K]

v_{pore} = Micro-pore volume in the zeolite, [m^3/kg_{cat}]

$v_{sat,g}^{liq}$ = Saturated liquid phase volume of lump g, [m^3/kmol]

W_{C20+}^{feed} = Weight of C_{20+} hydrocarbons in the feed, [kg]

W_{C20+}^{prod} = Weight of C_{20+} hydrocarbons in the products, [kg]

W_{C20+}^{feed} = Weight of C_{20+} hydrocarbons in the feed, [kg]

x_i = Mole fraction of component *i* in the liquid phase, [dimensionless]

X = weight percent conversion of VGO

y_{Pi}^{eqm} = Equilibrium mole fraction of paraffin i in the corresponding lump, [dimensionless]

y_{Oij}^{eqm} = Equilibrium mole fraction of olefin ij in the corresponding lump, [dimensionless]

z = Axial length along the reactor, [m_r]

Greek symbols

α_k = Transfer function for elementary steps of type k

γ_i = Activity coefficient of component i in the liquid phase, [dimensionless]

Ω = Reactor cross-sectional area, [m_r^2]

λ_{Sg} = Latent heat of vaporization of lump S_g, [kJ/mol]

Ψ = Parameter for quantifying approach to equilibrium, [dimensionless]

σ_{EXT} = External rotational symmetry number, [dimensionless]

σ_{INT} = Internal rotational symmetry number, [dimensionless]

σ_{gl}^{i} = Global symmetry number of species i, [dimensionless]

REFERENCES

(1) Algelt, K. H.; Boduszynski, M. M., *Composition and Analysis of Heavy Petroleum Fractions*. Marcel Dekker, Inc.: New York, 1994.

(2) Snyder, L. R., Nitrogen and Oxygen Compound Types in Petroleum - Total Analysis of a 400-700 Degrees F Distillate from a California Crude Oil. *Analytical Chemistry* **1969,** *41*, (2), 314-320.

(3) Scherzer, J.; Gruia, A. J., *Hydrocracking Science and Technology*. Marcel Dekker, Inc.: New York, 1996.

(4) Weekman, V. W.; Nace, D. M., Kinetics of Catalytic Cracking Selectivity in Fixed, Moving, and Fluid Bed Reactors. *AIChE Journal* **1970,** *16*, (3), 397-404.

(5) Jacob, S. M.; Gross, B.; Voltz, S. E.; Weekman, V. W., Lumping and Reaction Scheme for Catalytic Cracking. *AIChE Journal* **1976,** *22*, (4), 701-713.

(6) Stangela.B. E., Kinetic-Model for Prediction of Hydrocracker Yields. *Industrial & Engineering Chemistry Process Design and Development* **1974,** *13*, (1), 71-76.

(7) Laxminarasimhan, C. S.; Verma, R. P.; Ramachandran, P. A., Continuous lumping model for simulation of hydrocracking. *AIChE Journal* **1996,** *42*, (9), 2645-2653.

(8) Liguras, D. K.; Allen, D. T., Structural Models for Catalytic Cracking. 1. Model-Compound Reactions. *Industrial & Engineering Chemistry Research* **1989,** *28*, (6), 665-673.

(9) Liguras, D. K.; Allen, D. T., Structural Models for Catalytic Cracking. 2. Reactions of Simulated Oil Mixtures. *Industrial & Engineering Chemistry Research* **1989,** *28*, (6), 674-683.

(10) Quann, R. J.; Jaffe, S. B., Structure-Oriented Lumping - Describing the Chemistry of Complex Hydrocarbon Mixtures. *Industrial & Engineering Chemistry Research* **1992,** *31*, (11), 2483-2497.

(11) Baltanas, M. A.; Vanraemdonck, K. K.; Froment, G. F.; Mohedas, S. R., Fundamental Kinetic Modeling of Hydroisomerization and Hydrocracking on Noble-Metal-Loaded Faujasites. 1. Rate Parameters for Hydroisomerization. *Industrial & Engineering Chemistry Research* **1989,** *28*, (7), 899-910.

(12) Vynckier, E.; Froment, G. F., *Modeling of the Kinetics of Complex Porcesses Based upon Elementary Steps.* Elsevier Science Publishers BV: Amsterdam, The Netherlands, 1991; Vol. 131.

(13) Clymans, P. J.; Froment, G. F., Computer-Generation of Reaction Paths and Rate-Equations in the Thermal-Cracking of Normal and Branched Paraffins. *Computers & Chemical Engineering* **1984,** *8*, (2), 137-142.

(14) Hillewaert, L. P.; Dierickx, J. L.; Froment, G. F., Computer-Generation of Reaction Schemes and Rate-Equations for Thermal-Cracking. *AIChE Journal* **1988,** *34*, (1), 17-24.

(15) Feng, W.; Vynckier, E.; Froment, G. F., Single-Event Kinetics of Catalytic Cracking. *Industrial & Engineering Chemistry Research* **1993,** *32*, (12), 2997-3005.

(16) Svoboda, G. D.; Vynckier, E.; Debrabandere, B.; Froment, G. F., Single-Event Rate Parameters for Paraffin Hydrocracking Oil a Pt/Us-Y Zeolite. *Industrial & Engineering Chemistry Research* **1995,** *34*, (11), 3793-3800.

(17) Martens, G. G.; Marin, G. B.; Martens, J. A.; Jacobs, P. A.; Baroni, G. V., A Fundamental Kinetic Model for Hydrocracking of C-8 to C-12 Alkanes on Pt/US-Y Zeolites. *Journal of Catalysis* **2000,** *195*, (2), 253-267.

(18) Park, T. P.; Froment, G. F., Kinetic Modeling of the Methanol to Olefins Process. 1. Model Formulation. *Ind. Eng. Chem. Res.* **2001,** *40*, 4172-4186.

(19) Martinis, J. M.; Froment, G. F., Alkylation on Solid Acids. Part 2. Single-Event Kinetic Modeling. *Ind. Eng. Chem. Res.* **2006,** *45*, 954-967.

(20) Egan, C. J.; White, R. J.; Langlois, G. E., Selective Hydrocracking of C9-Alkylcyclohexanes to C12-Alkylcyclohexanes on Acidic Catalysts - Evidence for Paring Reaction. *Journal of the American Chemical Society* **1962,** *84*, (7), 1204-1215.

(21) Baltanas, M. A.; Froment, G. F., Computer-Generation of Reaction Networks and Calculation of Product Distributions in the Hydroisomerization and Hydrocracking of Paraffins on Pt-Containing Bifunctional Catalysts. *Computers & Chemical Engineering* **1985,** *9*, (1), 71-81.

(22) Govindhakannan, J. Modeling of a Hydrogenated Vacuum Gas Oil Hydrocracker. Ph.D. Dissertation, Texas Tech. University, Lubbock TX, 2003.

(23) Miller, R. L.; Ettre, L. S.; Johansen, N. G., Quantitative-Analysis of Hydrocarbons by Structural Group Type in Gasolines and Distillates. 3. Combined Use of Liquid and Gas-Chromatography. *Journal of Chromatography* **1983,** *264*, (1), 19-32.

(24) Miller, R. L.; Ettre, L. S.; Johansen, N. G., Quantitative-Analysis of Hydrocarbons by Structural Group Type in Gasolines and Distillates. 2. Liquid-Chromatography. *Journal of Chromatography* **1983,** *259*, (3), 393-412.

(25) Johansen, N. G.; Ettre, L. S.; Miller, R. L., Quantitative-Analysis of Hydrocarbons by Structural Group Type in Gasolines and Distillates. 1. Gas-Chromatography. *Journal of Chromatography* **1983,** *256*, (3), 393-417.

(26) Szakasits, J. J.; Robinson, R. E., Hydrocarbon Type Determination of Naphthas and Catalytically Reformed Products by Automated Multidimensional Gas-Chromatography. *Analytical Chemistry* **1991,** *63*, (2), 114-120.

(27) Boduszynski, M. M., Characterization of Heavy Crude Components. *Abstracts of Papers of the American Chemical Society* **1985,** *190*, (SEP), 78-88.

(28) Boduszynski, M. M., Composition of Heavy Petroleums. 2. Molecular Characterization. *Energy & Fuels* **1988,** *2*, (5), 597-613.

(29) Allen, D. T., Structural Models of Catalytic Cracking Chemistry. *Abstracts of Papers of the American Chemical Society* **1991,** *201*, 27-35.

(30) Neurock, M.; Nigam, A.; Trauth, D.; Klein, M. T., Molecular Representation of Complex Hydrocarbon Feedstocks through Efficient Characterization and Stochastic Algorithms. *Chemical Engineering Science* **1994,** *49*, (24A), 4153-4177.

(31) Trauth, D. M.; Stark, S. M.; Petti, T. F.; Neurock, M.; Klein, M. T., Representation of the Molecular-Structure of Petroleum Resid through Characterization and Monte-Carlo Modeling. *Energy & Fuels* **1994,** *8*, (3), 576-580.

(32) Hudebine, D.; Verstraete, J. J., Molecular Reconstruction of LCO Gasoils from Overall Petroleum Analyses. *Chemical Engineering Science* **2004,** *59*, (22-23), 4755-4763.

(33) Aye, M. M. S.; Zhang, N., A Novel Methodology in Transforming Bulk Properties of Refining Streams into Molecular Information. *Chemical Engineering Science* **2005,** *60*, (23), 6702-6717.

(34) Vansina, H.; Baltanas, M. A.; Froment, G. F., Hydroisomerization and Hydrocracking. 4. Product Distribution from N-Octane and 2,2,4-Trimethylpentane. *Industrial & Engineering Chemistry Product Research and Development* **1983,** *22*, (4), 526-531.

(35) Schulz, H. F.; Weitkamp, J. H., Zeolite Catalysts - Hydrocracking and Hydroisomerization of N-Dodecane. *Industrial & Engineering Chemistry Product Research and Development* **1972,** *11*, (1), 46-53.

(36) Froment, G. F., Single Event Kinetic Modeling of Complex Catalytic Processes. *Catalysis Reviews-Science and Engineering* **2005,** *47*, (1), 83-124.

(37) Eyring, H., The Activated Complex and the Absolute Rate of Chemical Reactions. *Chemical Reviews* **1935,** *17*, (1), 65-77.

(38) Girgis, M. J.; Gates, B. C., Reactivities, Reaction Networks, and Kinetics in High-Pressure Catalytic Hydroprocessing. *Industrial & Engineering Chemistry Research* **1991,** *30*, (9), 2021-2058.

(39) Lin, S. D.; Vannice, M. A., Hydrogenation of Aromatic-Hydrocarbons over Supported Pt Catalysts. 1. Benzene Hydrogenation. *Journal of Catalysis* **1993,** *143*, (2), 539-553.

(40) Lin, S. D.; Vannice, M. A., Hydrogenation of Aromatic-Hydrocarbons over Supported Pt Catalysts. 2. Toluene Hydrogenation. *Journal of Catalysis* **1993,** *143*, (2), 554-562.

(41) Lin, S. D.; Vannice, M. A., Hydrogenation of Aromatic-Hydrocarbons over Supported Pt Catalysts. 3. Reaction Models for Metal-Surfaces and Acidic Sites on Oxide Supports. *Journal of Catalysis* **1993,** *143*, (2), 563-572.

(42) Lin, S. D.; Vannice, M. A.; Herrmann, J. M.; Wang, D.; Apestequia, C.; Duprez, D.; Figueras, F.; Conner, W. C.; Kiperman, S. L.; Hall, W. K.; Blackmond, D. G.; Grunert, W.; Butt, J. B.; Schulz, H., Toluene Hydrogenation over Supported Platinum Catalysts. *Studies in Surface Science and Catalysis* **1993,** *75*, 861-874.

(43) Girgis, M. J.; Gates, B. C., Catalytic Hydroprocessing of Simulated Heavy Coal Liquids. 2. Reaction Networks of Aromatic-Hydrocarbons and Sulfur and Oxygen Heterocyclic-Compounds. *Industrial & Engineering Chemistry Research* **1994,** *33*, (10), 2301-2313.

(44) Girgis, M. J.; Gates, B. C., Catalytic Hydroprocessing of Simulated Heavy Coal Liquids. 1. Reactivities of Aromatic-Hydrocarbons and Sulfur and Oxygen Heterocyclic-Compounds. *Industrial & Engineering Chemistry Research* **1994,** *33*, (5), 1098-1106.

(45) Klein, M. T.; Korre, S. C.; Read, C. J.; Russell, C. L., Hydrocracking of Model Polynuclear Aromatics - Pathways, Kinetics, and Structure Reactivity Correlations. *Abstracts of Papers of the American Chemical Society* **1993,** *205*, 43-51.

(46) Korre, S. C.; Klein, M. T., Development of Temperature-Independent Quantitative Structure/Reactivity Relationships for Metal- and Acid-Catalyzed Reactions. *Catalysis Today* **1996,** *31*, (1-2), 79-91.

(47) Korre, S. C.; Klein, M. T.; Quann, R. J., Effect of Temperature on Quantitative Structure-Reactivity Correlations for Hydrocracking Polynuclear Aromatics. *Abstracts of Papers of the American Chemical Society* **1995,** *210*, 120-128.

(48) Korre, S. C.; Klein, M. T.; Quann, R. J., Polynuclear Aromatic-Hydrocarbons Hydrogenation. 1. Experimental Reaction Pathways and Kinetics. *Industrial & Engineering Chemistry Research* **1995,** *34*, (1), 101-117.

(49) Korre, S. C.; Klein, M. T.; Quann, R. J., Hydrocracking of Polynuclear Aromatic Hydrocarbons. Development of Rate Laws Through Inhibition Studies. *Industrial & Engineering Chemistry Research* **1997,** *36*, (6), 2041-2050.

(50) Korre, S. C.; Neurock, M.; Klein, M. T.; Quann, R. J., Hydrogenation of Polynuclear Aromatic-Hydrocarbons. 2. Quantitative Structure-Reactivity Correlations. *Chemical Engineering Science* **1994,** *49*, (24A), 4191-4210.

(51) Rahier, H.; Denayer, J. F.; Van Mele, B., Low-Temperature Synthesized Aluminosilicate Glasses - Part IV - Modulated DSC Study on the Effect of Particle Size of Metakaolinite on the Production of Inorganic Polymer Glasses. *Journal of Materials Science* **2003,** *38*, (14), 3131-3136.

(52) Rautanen, P. A.; Aittamaa, J. R.; Krause, A. O. I., Liquid Phase Hydrogenation of Tetralin on Ni/Al-2 O-3. *Chemical Engineering Science* **2001,** *56*, (4), 1247-1254.

(53) Rautanen, P. A.; Aittamaa, J. R.; Krause, K. O. I., Solvent Effect in Liquid-Phase Hydrogenation of Toluene. *Industrial & Engineering Chemistry Research* **2000,** *39*, (11), 4032-4039.

(54) Rautanen, P. A.; Lylykangas, M. S.; Aittamaa, J. R.; Krause, A. O. I., Liquid-Phase Hydrogenation of Naphthalene and Tetralin on Ni/Al2O3: Kinetic Modeling. *Industrial & Engineering Chemistry Research* **2002,** *41*, (24), 5966-5975.

(55) Lylykangas, M. S.; Rautanen, P. A.; Krause, A. O. I., Liquid-Phase Hydrogenation Kinetics of Multicomponent Axomatic Mixtures on Ni/Al2O3. *Industrial & Engineering Chemistry Research* **2002,** *41*, (23), 5632-5639.

(56) Lylykangas, M. S.; Rautanen, P. A.; Krause, A. O. I., Hydrogenation and Deactivation Kinetics in the Liquid-Phase Hydrogenation of Isooctenes on Pt/Al2O3. *Industrial & Engineering Chemistry Research* **2004,** *43*, (7), 1641-1648.

(57) Singh, U. K.; Vannice, M. A., Kinetics of Liquid-Phase Hydrogenation Reactions over Supported Metal Catalysts - A Review. *Applied Catalysis A-General* **2001,** *213*, (1), 1-24.

(58) Singh, U. K.; Vannice, M. A., Kinetics of Liquid-Phase Hydrogenation Reactions over Supported Metal Catalyst - A Review. *Applied Catalysis A-General* **2003,** *255*, (2), 361-361.

(59) Stanislaus, A.; Cooper, B. H., Aromatic Hydrogenation Catalysis - A Review. *Catalysis Reviews-Science and Engineering* **1994,** *36*, (1), 75-123.

(60) Aben, P. C.; Platteeu, J. C.; Stoutham, B., Hydrogenation of Benzene over Supported Plantinum, Palladium and Nickel Catalysts. *Recueil Des Travaux Chimiques Des Pays-Bas* **1970,** *89*, (5), 449-455.

(61) Vanmeerten, R. Z. C.; Coenen, J. W. E., Gas-Phase Benzene Hydrogenation on a Nickel-Silica Catalyst. 1. Experimental-Data and Phenomenological Description. *Journal of Catalysis* **1975,** *37*, (1), 37-43.

(62) Chou, P.; Vannice, M. A., Benzene Hydrogenation over Supported and Unsupported Palladium. 1. Kinetic-Behavior. *Journal of Catalysis* **1987,** *107*, (1), 129-139.

(63) Chou, P.; Vannice, M. A., Benzene Hydrogenation over Supported and Unsupported Palladium. 2. Reaction Model. *Journal of Catalysis* **1987,** *107*, (1), 140-153.

(64) Singh, U. K.; Vannice, M. A., Kinetic and Thermodynamic Analysis of Liquid-Phase Benzene Hydrogenation. *AIChE Journal* **1999,** *45*, (5), 1059-1071.

(65) Cohen, N.; Benson, S. W., Estimation of Heats of Formation of Organic-Compounds by Additivity Methods. *Chemical Reviews* **1993,** *93*, (7), 2419-2438.

(66) Peng, D.; Robinson, D. B., New 2-Constant Equation of State. *Industrial & Engineering Chemistry Fundamentals* **1976,** *15*, (1), 59-64.

(67) Dufresne, P.; Bigeard, P. H.; Billon, A., New Developments in Hydrocracking: Low Pressure High-Conversion Hydrocracking. *Catalysis Today* **1987,** *1*, (4), 367-384.

(68) Melis, S.; Erby, L.; Sassu, L.; Baratti, R., A Model for the Hydrogenation of Aromatic Compounds During Gasoil Hydroprocessing. *Chemical Engineering Science* **2004,** *59*, (22-23), 5671-5677.

(69) Lavopa, V.; Satterfield, C. N., Poisoning of Thiophene Hydrodesulfurization by Nitrogen-Compounds. *Journal of Catalysis* **1988,** *110*, (2), 375-387.

(70) Martens, G. G.; Marin, G. B., Kinetics for Hydrocracking Based on Structural Classes: Model Development and Application. *AIChE Journal* **2001,** *47*, (7), 1607-1622.

(71) Hunter, E. P. L.; Lias, S. G., Evaluated Gas Phase Basicities and Proton Affinities of Molecules: An Update. *Journal of Physical and Chemical Reference Data* **1998,** *27*, (3), 413-656.

(72) Dumesic, J. A.; Rudd, D. F.; Aparicio, L. M.; Rekoske, J. E.; Trevino, A. A., *The Microkinetics of Hetrogeneous Catalysis*. American Chemical Society: Washington, DC, 1993.

(73) Martinis, J. M.; Froment, G. F., Alkylation on solid acids. Part 2. Single-Event Kinetic Modeling. *Industrial & Engineering Chemistry Research* **2006,** *45*, (3), 954-967.

(74) Park, T. Y.; Froment, G. F., Kinetic Modeling of the Methanol to Olefins Process. 1. Model Formulation. *Industrial & Engineering Chemistry Research* **2001,** *40*, (20), 4172-4186.

(75) Park, T. Y.; Froment, G. F., Kinetic Modeling of the Methanol to Olefins Process. 2. Experimental Results, Model Discrimination, and Parameter Estimation. *Industrial & Engineering Chemistry Research* **2001,** *40*, (20), 4187-4196.

(76) Denayer, J. F.; Bouyermaouen, A.; Baron, G. V., Adsorption of Alkanes and Other Organic Molecules in Liquid Phase and in the Dense Vapor Phase: Influence of Polarity, Zeolite Topology, and External Fluid Density and Pressure. *Industrial & Engineering Chemistry Research* **1998,** *37*, (9), 3691-3698.

(77) Froment, G. F.; Depauw, G. A.; Vanrysselberghe, V., Kinetic Modeling and Reactor Simulation in Hydrodesulfurization of Oil Fractions. *Industrial & Engineering Chemistry Research* **1994,** *33*, (12), 2975-2988.

(78) Sato, Y.; Hirose, H.; Takahashi, F.; Toda, M., *First Pacific Chemical Engineering Congress* **1972**, 187-195.

(79) Reiss, L. P., Cocurrent Gas-Liquid Contacting in Packed Columns. *Industrial & Engineering Chemistry Process Design and Development* **1967,** *6*, (4), 486-499.

(80) Charpentier, J. C., Recent Progress in Gas-Liquid Mass Transfer in Packed Beds. *Chem. Eng. Journal* **1976,** *11*, 161-171.

(81) Whitaker, S., Forced Convection Heat Transfer Correlations or Flow in Pipes, Past Flat Plates, Single Cylinders, Single Spheres, and for Flow in Packed Beds and Tube Bundles. *AIChE J.* **1972,** *18*, (2), 361-371.

(82) Poling, B. E.; Prausnitz, J. M.; O'Connell, J. P., *The Properties and Gases and Liquids*. Fifth ed.; McGraw-Hill: New York, 2001.

(83) Twu, C. H., Internally Consistent Correlation for Predicting Liquid Viscosities of Petroleum Fractions. *Industrial & Engineering Chemistry Process Design and Development* **1985,** *24*, (4), 1287-1293.

(84) Macknick, A. B.; Prausnitz, J. M., Vapor-Pressures of Heavy Liquid Hydrocarbons by a Group-Contribution Method. *Industrial & Engineering Chemistry Fundamentals* **1979,** *18*, (4), 348-351.

(85) Garvin, J., Determine Liquid Specific Heat for Organic Compounds. *Chemical Engineering Progress* **2002,** *98*, (5), 48-50.

(86) Martens, G. G.; Thybaut, J. W.; Marin, G. B., Single-Event Rate Parameters for the Hydrocracking of Cycloalkanes on Pt/US-Y Zeolites. *Industrial & Engineering Chemistry Research* **2001,** *40*, (8), 1832-1844.

(87) Pacheco, M. A.; Dassori, C. G., Hydrocracking: An Improved Kinetic Model and Reactor Modeling. *Chemical Engineering Communications* **2002,** *189*, (12), 1684-1704.

(88) Moustafa, T. M.; Froment, G. F., Kinetic Modeling of Coke Formation and Deactivation in the Catalytic Cracking of Vacuum Gas Oil. *Industrial & Engineering Chemistry Research* **2003,** *42*, (1), 14-25.

(89) Weismantel, G. E., *Petroleum Processing Handbook*. Marcel Dekker: New York, 1992.

(90) Filimono.Va; Rogov, S. P.; Osipov, L. N.; Agafonov, A. V.; Perezhig.Iy; Popov, A. A.; Khavkin, V. A., Rates of Reaction of Individual Groups of Hydrocarbons in Hydrocracking. *International Chemical Engineering* **1972,** *12*, (1), 21-26.

(91) Sullivan, R. F.; Meyer, J. A., Catalyst Effects on Yields and Product Properties in Hydrocracking. *ACS Symposium Series* **1975**, *20*, 28-51.

(92) Bourne, K. H.; Bennett, R. N., Hydrocracking for Middle Distillates - Study of Process Reactions and Corresponding Product Yields and Qualities. *Abstracts of Papers of the American Chemical Society* 1972, *164*, G45-G62.

(93) Böhringer, W.; Kotsiopoulos, A.; Fletcher, J. C., Selective Fischer-Tropsch Wax Hydrocracking Opportunity for Improvement of Overall Gas-to-Liquids Processing. Paper presented at the International R&D Forum on Oil, Gas and Petrochemicals, Kuala Lumpur, Malaysia, 2004.

(94) Schweitzer, J. M.; Galtier, P.; Schweich, D., A Single Events Kinetic Model for the Hydrocracking of Paraffins in a Three-Phase Reactor. *Chemical Engineering Science* **1999,** *54*, (13-14), 2441-2452.

(95) Fox, J. M., The Different Catalytic Routes for Methane Valorization - An Assessment of Processes for Liquid Fuels. *Catalysis Reviews-Science and Engineering* **1993,** *35*, (2), 169-212.

(96) Gregor, J. H., Fischer-Tropsch Products as Liquid Fuels or Chemicals - An Economic-Evaluation. *Catalysis Letters* **1991,** *7*, (1-4), 317-331.

(97) Steijns, M.; Froment, G. F., Hydroisomerization and Hydrocracking. 3. Kinetic-Analysis of Rate Data for Normal-Decane and Normal-Dodecane. *Industrial & Engineering Chemistry Product Research and Development* **1981,** *20*, (4), 660-668.

(98) Degnan, T. F.; Kennedy, C. R., Impact of Catalyst Acid Metal Balance in Hydroisomerization of Normal Paraffins. *AIChE Journal* 1993, *39*, (4), 607-614.

(99) Debrabandere, B.; Froment, G. F., Influence of the Hydrocarbon Chain Length on the Kinetics of the Hydroisomerization and Hydrocracking of n-Paraffins. In *Hydrotreatment and Hydrocracking of Oil Fractions*, Froment, G. F.; Delmon, B.; Grange, P.` eds., Elsevier: Amsterdam, 1997.

(100) Thybaut, J. W.; Narasimhan, C. S. L.; Denayer, J. F.; Baron, G. V.; Jacobs, P. A.; Martens, J. A.; Marin, G. B., Acid-Metal Balance of a Hydrocracking Catalyst: Ideal Versus Nonideal Behavior. *Industrial & Engineering Chemistry Research* **2005,** *44*, (14), 5159-5169.

(101) Chavarria, J. C.; Ramirez, J.; Gonzalez, H.; Baltanas, M. A., Modelling of n-Hexadecane Hydroisomerization and Hydrocracking Reactions on a Mo/H Beta-Alumina Bi-functional Catalyst, Using the Single Event Concept. *Catalysis Today* **2004,** *98*, (1-2), 235-242.

(102) Pines, H., *The Chemistry of Catalytic Hydrocarbon Conversions*. Academic Press Inc.: New York, 1981.

(103) Evans, M. G.; Polanyi, M., Inertia and Driving Force of Chemical Reactions. *Transactions of the Faraday Society* **1938,** *34*, (1), 0011-0023.

(104) Curtiss, L. A.; Raghavachari, K.; Redfern, P. C.; Rassolov, V.; Pople, J. A., Gaussian-3 (G3) Theory for Molecules Containing First and Second-Row Atoms. *Journal of Chemical Physics* **1998,** *109*, (18), 7764-7776.

(105) Curtiss, L. A.; Raghavachari, K.; Redfern, P. C.; Pople, J. A., Assessment of Gaussian-3 and Density Functional Theories for a Larger Experimental Test Set. *Journal of Chemical Physics* **2000,** *112*, (17), 7374-7383.

(106) Thybaut, J. W.; Marin, G. B.; Baron, G. V.; Jacobs, P. A.; Martens, J. A., Alkene Protonation Enthalpy Determination from Fundamental Kinetic Modeling of Alkane Hydroconversion on Pt/H-(US)Y-Zeolite. *Journal of Catalysis* **2001,** *202*, (2), 324-339.

(107) Martens, G.; Froment, G. F., Kinetic Modeling of Paraffins Hydrocracking Based upon Elementary Steps and the Single Event Concept. In *Reaction Kinetics and the*

Development of Catalytic Processes, Froment, G. F.; Waugh, K. C. eds., Elsevier: Amsterdam, 1999.

(108) Martens, J. A.; Tialen, M.; Jacobs, P. A., Attempts to Rationalize the Distribution of Hydrocracked Products. III. Mechanistic Aspects of Isomerization and Hydrocracking of Branched Alkanes on Ideal Bifunctional Large-Pore Zeolite Catalysts. *Catalysis Today* **1987,** *1*, 435-453.

(109) Denayer, J. F.; Baron, G. V.; Souverijns, W.; Martens, J. A.; Jacobs, P. A., Hydrocracking of n-Alkane Mixtures on Pt/H-Y Zeolite: Chain Length Dependence of the Adsorption and the Kinetic Constants. *Industrial & Engineering Chemistry Research* **1997,** *36*, (8), 3242-3247.

(110) Alvarez, F.; Ribeiro, F. R.; Perot, G.; Thomazeau, C.; Guisnet, M., Hydroisomerization and Hydrocracking of Alkanes - Influence of the Balance Between Acid and Hydrogenating Functions on the Transformation of n-Decane on PtHY Catalysts. *Journal of Catalysis* **1996,** *162*, (2), 179-189.

(111) Guisnet, M.; Alvarez, F.; Giannetto, G.; Perot, G., Hydroisomerization and Hydrocracking of n-Heptane on the Zeolites. Effect of the Porosity and of the Distribution of Metallic and Acid Sites. *Catalysis Today* **1987,** *1*, 415-426.

(112) Kuznetsov, P. N., Study of n-Octane Hydrocracking and Hydroisomerization over Pt/HY Zeolites Using the Reactors of Different Configurations. *Journal of Catalysis* **2003,** *218*, (1), 12-23.

VITA

Hans Kumar was born in Shamli, India on April 20, 1979. He received a Bachelor of Engineering degree in chemical engineering from the Indian Institute of Technology, Roorkee, India in July 2000. Then he worked as a process engineer at the Process Design and Development Division of Engineers India Limited, New Delhi, India from July 2000 to July 2002. He joined the graduate program in the Department of Chemical Engineering, Texas A&M University in August 2002 and obtained his Master of Science degree in chemical engineering in August 2004 and Doctor of Philosophy degree in chemical engineering in December 2006. He can be contacted through email hansgupta@gmail.com or through his parents at his permanent address:

Hans Kumar
c/o Kuldeeep Gupta
H.No:108, Kaka Nagar
Shamli - 247776
U. P. (India)
Phone: (91)-1398-257416